IOWA STATE UNIVERSITY
Digital Repository

Retrospective Theses and Dissertations

Iowa State University Capstones, Theses and Dissertations

1984

Synthesis and characterization of octahedral zirconium iodide clusters containing interstitial atoms

Jerome David Smith
Iowa State University

Follow this and additional works at: https://lib.dr.iastate.edu/rtd

 Part of the Inorganic Chemistry Commons

Recommended Citation
Smith, Jerome David, "Synthesis and characterization of octahedral zirconium iodide clusters containing interstitial atoms " (1984). *Retrospective Theses and Dissertations*. 8218.
https://lib.dr.iastate.edu/rtd/8218

This Dissertation is brought to you for free and open access by the Iowa State University Capstones, Theses and Dissertations at Iowa State University Digital Repository. It has been accepted for inclusion in Retrospective Theses and Dissertations by an authorized administrator of Iowa State University Digital Repository. For more information, please contact digirep@iastate.edu.

www.manaraa.com

INFORMATION TO USERS

This reproduction was made from a copy of a document sent to us for microfilming. While the most advanced technology has been used to photograph and reproduce this document, the quality of the reproduction is heavily dependent upon the quality of the material submitted.

The following explanation of techniques is provided to help clarify markings or notations which may appear on this reproduction.

1. The sign or "target" for pages apparently lacking from the document photographed is "Missing Page(s)". If it was possible to obtain the missing page(s) or section, they are spliced into the film along with adjacent pages. This may have necessitated cutting through an image and duplicating adjacent pages to assure complete continuity.

2. When an image on the film is obliterated with a round black mark, it is an indication of either blurred copy because of movement during exposure, duplicate copy, or copyrighted materials that should not have been filmed. For blurred pages, a good image of the page can be found in the adjacent frame. If copyrighted materials were deleted, a target note will appear listing the pages in the adjacent frame.

3. When a map, drawing or chart, etc., is part of the material being photographed, a definite method of "sectioning" the material has been followed. It is customary to begin filming at the upper left hand corner of a large sheet and to continue from left to right in equal sections with small overlaps. If necessary, sectioning is continued again—beginning below the first row and continuing on until complete.

4. For illustrations that cannot be satisfactorily reproduced by xerographic means, photographic prints can be purchased at additional cost and inserted into your xerographic copy. These prints are available upon request from the Dissertations Customer Services Department.

5. Some pages in any document may have indistinct print. In all cases the best available copy has been filmed.

University Microfilms International
300 N. Zeeb Road
Ann Arbor, MI 48106

8505872

Smith, Jerome David

SYNTHESIS AND CHARACTERIZATION OF OCTAHEDRAL ZIRCONIUM IODIDE CLUSTERS CONTAINING INTERSTITIAL ATOMS

Iowa State University PH.D. 1984

University Microfilms International 300 N. Zeeb Road, Ann Arbor, MI 48106

PLEASE NOTE:

In all cases this material has been filmed in the best possible way from the available copy. Problems encountered with this document have been identified here with a check mark ✓.

1. Glossy photographs or pages ✓
2. Colored illustrations, paper or print _____
3. Photographs with dark background _____
4. Illustrations are poor copy _____
5. Pages with black marks, not original copy _____
6. Print shows through as there is text on both sides of page _____
7. Indistinct, broken or small print on several pages ✓
8. Print exceeds margin requirements _____
9. Tightly bound copy with print lost in spine _____
10. Computer printout pages with indistinct print _____
11. Page(s) _____ lacking when material received, and not available from school or author.
12. Page(s) _____ seem to be missing in numbering only as text follows.
13. Two pages numbered _____. Text follows.
14. Curling and wrinkled pages _____
15. Other _____

University Microfilms International

Synthesis and characterization of octahedral zirconium iodide clusters containing interstitial atoms

by

Jerome David Smith

A Dissertation Submitted to the
Graduate Faculty in Partial Fulfillment of the
Requirements for the Degree of
DOCTOR OF PHILOSOPHY

Department: Chemistry
Major: Inorganic Chemistry

Approved:

Signature was redacted for privacy.

In Charge of Major Work

Signature was redacted for privacy.

For the Major Department

Signature was redacted for privacy.

For the Graduate College

Iowa State University
Ames, Iowa

1984

TABLE OF CONTENTS

INTRODUCTION

In the past decade, synthetic studies to determine the composition, structures, and properties of reduced zirconium iodides have been prompted by the clear relationship between the presence of fission product iodine and the occurrence of stress-corrosion-cracking (SCC) of zirconium fuel cladding in water-cooled reactors.[1] The possible involvement of the abundant fission product cesium has also led to the study of reduced phases in the ternary CsI-ZrI_4-Zr system.[2] The numerous reduced phases that have been found all exhibit Zr-Zr bonding in one form or another. ZrI_3 contains one-dimensional linear zirconium chains,[3] although the nature of the Zr-Zr bonding is not clear. The two forms of diiodide, α,β-ZrI_2, are distorted CdI_2-type structures in which the zirconium atoms are displaced from their 'ideal' octahedral environment to form one-dimensional zig-zag chains.[4] In the reduced ternary phase $Cs_3Zr_2I_9$, $Zr_2I_9^{3-}$ face-sharing bioctahedra are found.[5] The zirconium atoms again are displaced from 'ideal' octahedral iodine coordination by formation of a Zr-Zr bond through the shared face.

Prior to this work, two reduced phases were also reported that contained octahedral Zr_6I_{12} clusters. The first of these phases was initially synthesized by Daake[6] as a few black gems growing on the surface of zirconium strips in binary reactions of ZrI_4 and excess zirconium at 750-850°C for 1-2 weeks. Daake hypothesized the cluster-containing nature of these gems and subsequently they were structurally characterized by Guthrie and reported as Zr_6I_{12}.[7]

Later, Guthrie synthesized a second phase that contains Zr_6I_{12} clusters, $CsZr_6I_{14}$,[8] by reacting CsI, ZrI_4, and excess zirconium at between 800 and 900°C for 4 to to 6 weeks. The material was again characterized by single crystal X-ray diffraction, but low yields prevented attempts to further characterize this material.

Such clusters are not new inasmuch as the synthesis and structures of several reduced group V halides containing M_6X_{12} cluster have been known for some time. The clusters in these group V materials can be found as isolated $M_6X_{12}X_6^{n-}$ units or linked together through the sharing of halides in at least two ways resulting in the stoichiometries M_6X_{14} and M_6X_{15}.[9-11] In all these compounds, between 14 and 16 electrons fill seven or eight bonding orbitals derived from metal d orbitals that are not heavily involved in metal-halide bonding. The number of electrons available for metal-metal bonding is obtained by assuming that the halide valence band is filled and at considerably lower energy than the orbitals derived from the metal d orbitals. For example, Ta_6I_{14} has 6 x 5 - 14 = 16 electrons available for metal-metal bonding and there are 15 such electrons in Ta_6Cl_{15}. This bonding scheme has found support in some theoretical considerations.[12-14]

In the past few years, M_6X_{12} clusters in halides of metals further to the left in the periodic table (including zirconium) have been reported.[7,8,15] Many of these compounds were also obtained in low yields from binary reactions. The compounds appear to contain as few as 9 to 12 electrons per cluster for metal-metal bonding, 12 and 11 for the Zr_6I_{12} and $CsZr_6I_{14}$ clusters above. In addition to compounds where the

clusters are found as isolated units, many binary phases have been synthesized and characterized that contain octahedra condensed together to form one-dimensional chains and two-dimensional double sheets of metal atoms.[16,17]

Except for the delocalized electrons involved in metal-metal bonding, the centers of these octahedra were believed to be empty. Indeed, the word 'cluster' to describe groups of bonded metal atoms was coined as a preference to the term 'cage' because of the empty nature of these units.[16] The clusters in some of these reduced halides, especially for compounds that were synthesized in high yield, are still believed to be empty. However, the inclusion of small nonmetals in the centers of metal clusters has been recently reported for a number of reduced metal halides that contain either isolated clusters or clusters in the condensed arrays noted above. The first well-characterized example of a nonmetal in the center of an octahedral cluster was the compound $Nb_6I_{11}H$.[19] Reports of other examples of hydrogen in metal-metal bonded arrays have more recently appeared, i.e., $CsNb_6I_{11}H$[20] and $ZrXH_x$.[21]

The first well-characterized example of a second period nonmetal in such an array was reported by Seaverson, who found that oxygen occupied tetrahedral sites between the double metal layers of $ZrClO_{0.4}$.[22] Other examples followed rapidly. Warkentin and coworkers reported a number of rare earth metal halides that contained carbon, nitrogen, and dicarbon units in the centers of metal-metal bonded clusters.[23,24] It was also found that carbon could be included in the octahedral interstices between the double metal layers of the yttrium or scandium monohalide structure

to give compounds of the composition Y_2Cl_2C and Sc_2Cl_2C.[25] Ziebarth later expanded this area of synthesis by showing that carbon, nitrogen, and boron could be included in zirconium monohalides to give isostructural materials.[26] Hwu has very recently shown that such interstitial phases are also present in the Sc-Cl system, e.g., $Sc_7Cl_{10}C_2$.[27]

This sudden rush of compounds that contain interstitial atoms precipitated the close inspection of previously reported materials prepared in low yield and showing signs of the inclusion of small nonmetals. Among these are the compound $CsZr_6I_{14}$.[6]

There were several hints that $CsZr_6I_{14}$ might contain an interstitial atom.[2] First among these was an anomaly that appeared in the final electron density difference maps of single crystal X-ray studies. A residual peak (Z = 4-5) was found in the center of the zirconium octahedron. At the time this structure was reported, possibilities cited for the cause of this peak included an interstitial atom or errors in the X-ray diffraction data collected. A second hint was the observation of a range of cell volumes obtained for different preparations of this phase. Because of this difference in cell volumes, single crystals from two separate preparations of $CsZr_6I_{14}$ were studied by X-ray diffraction. The average Zr-Zr bond distances of these structures were found to be significantly different, providing a third clue that something was amiss. Not only were the Zr-Zr bonds of different length in these two structures, they were also significantly longer than those found in the structure reported as Zr_6I_{12}, though the numbers of electrons involved in Zr-Zr bonding in these two phases differ by only one electron.

Because of these anomalies, research was begun in an attempt to more fully understand reduced zirconium iodide clusters. The results of that research are reported here. The phase that was reported as '$CsZr_6I_{14}$'[6] has been found to actually or potentially be one of a number of materials all of which contain atoms in the centers of the zirconium clusters. The chemical diversity of the interstitial atoms that have successfully been included is indeed surprising and includes C, B, Si, and Al. Reactions that were conducted in conjunction with those directly related to the '$CsZr_6I_{14}$' problem demonstrated that some alkali metal atoms could alternatively occupy the centers of the zirconium octahedra in such compounds as $Zr_6I_{14}K$. Further reactions demonstrated that the material reported as 'Zr_6I_{12}'[7,8] is actually $Zr_6I_{12}C$. The isostructural phase $Zr_6I_{12}B$ was also prepared.

The number of isostructural phases that have been prepared and structurally characterized allows a careful examination of factors that have a pronounced effect on the degree of metal-metal bonding of these materials. It is hoped that the reader will gain some appreciation of these factors, and that this work may provide some insight and guidance for further synthetic study.

EXPERIMENTAL

Materials

Zirconium tetraiodide was prepared from the elements by combining I_2 (Baker, sublimed) with a 10-20% excess of zirconium metal in a 25 mm o.d. fused silica tube 25 cm in length. The tube was then evacuated with a forepump and sealed. The reaction tube was placed at a slight incline in a two-zone furnace. The lower end of the furnace was maintained at 200°C and provides an iodine reservoir. The zirconium metal remained in the higher end of the tube that is heated to 500°C. The reddish-brown ZrI_4, as it formed, sublimed away from the Zr metal and was deposited in the region between the two temperature zones. The reaction proceeded smoothly and was usually complete in 6 to 12 hours. Some care must be exercised when conducting this reaction to prevent a plug of the product from totally blocking the reaction tube. Typically, 40 g of ZrI_4 was obtained in a single reaction of this type. The crude product was purified by multiple sublimations under dynamic vacuum in a Pyrex tube equipped with a coarse frit. The vacuum system should have a $N_2(\ell)$ cooled trap attached between the sublimation and the pumping system. The final product was stored in sealed glass ampoules until use and was not opened except in inert (N_2, Ar) atmospheres, because of its hygroscopic nature.

Analytical-reagent-grade alkali metal iodides (CsI, RbI, KI, and NaI) were dried at low temperatures (100°C) under vacuum and then distilled in a fused silica tube before use. The iodides were stored in

sealed glass ampoules outside the dry box, or in glass vials with tightly fitting plastic stoppers inside the nitrogen-filled dry box where reaction vessels were usually loaded.

Lithium iodide (anhydrous, reagent grade) was very carefully dehydrated under vacuum by slow heating before being distilled in a fused silica jacket. LiI was stored in sealed glass ampoules, wrapped with aluminum foil for protection from light, until they were required in the dry box.

Reactor grade zirconium metal, cold-rolled to between 12 and 20 mil, was obtained from F. Schmidt of the Ames Laboratory. The metal was cut into strips suitable for reactions and was cleaned with a solution of 45% conc. HNO_3, 10% conc. HF, and 45% H_2O. Some care must be exercised in cleaning strips to avoid too strong a reaction with the cleaning solution that tends to leave a dark coating on the metal. The strips were rinsed with distilled H_2O immediately to remove the cleaning solution, and were subsequently rinsed with acetone and finally air dried.

To prepare powdered zirconium, strips were carefully hydrogenated in a fused silica jacketed Mo boat at 750°C until hydrogen uptake ceased (P_{H_2} = 1 atm). The ZrH_x which resulted was taken into the dry box, then ground in a clean diamond mortar and pestle until it passed through a 100 mesh screen. The powder was subsequently reloaded into the Mo boat, placed in the silica jacket and slowly dehydrogenated by allowing the vacuum system to go below discharge before the temperature of the furnace was raised an additional 50°C. This stepwise process was

continued until the system was below discharge at 700°C, above which the metal powder sinters badly. The metal was then ground in the mortar until it passed through the 100 mesh screen. The lattice parameters of this metal powder obtained from Guinier diffraction patterns are within 3σ of the reported values of Zr metal,[28] indicating a fairly low level of impurities, espcially carbon, nitrogen, oxygen, or hydrogen.

Spectroscopic grade graphite powder (National brand, Union Carbide) obtained from E. DeKalb of Ames Laboratory and 99% ^{13}C enriched graphite (MSD ISOTOPES, Lot 664-I) were degassed at 850°C for a few hours under dynamic vacuum. The graphite was then stored in tightly-stoppered vials in the dry box.

National Bureau of Standards silicon (SRM-640) was used as received, both as an X-ray diffraction reference and for the small amounts of silicon required for syntheses.

Aluminum triiodide was prepared from the elements in a Pyrex container at 200°C and was sublimed twice under vacuum before use. Sealed glass ampoules were used to store the product.

Boron (Alpha, 95%, 325 mesh, amorphous) was surreptitiously obtained by R. Ziebarth's brother from a freshman chemistry lab at the University of Wisconsin. High purity boron was obtained from Dr. R. N. Shelton of Ames Laboratory. The lattice parameters of samples made from these two different sources did not differ significantly, though the amorphous boron gave more complete reactions, presumably because of its much higher surface area.

Zirconium nitride iodide was prepared by passing ammonia over ZrI_4 according to descriptions in the literature.[29]

Zirconium dioxide was obtained from R. Ziebarth. It had been made by precipitating zirconium hydroxide by addition of aqueous ammonia to aqueous solutions of $ZrOCl_2 \cdot 8H_2O$. The hydroxide was then rinsed with copious amounts of water to free it of any residual chloride before being dehydrated at 400°C. The ZrO_2 was subsequently heated to 850°C under oxygen to ensure full oxidation. Atomic emission spectroscopy (AES) later showed that this ZrO_2 was contaminated with about 2000 ppm silicon, which may have been present in the $ZrOCl_2 \cdot 8H_2O$ or may have come from the ammonia.

Zirconium diiodide was prepared in large yield by reacting ZrI_4 with excess zirconium metal strips at 750°C for a week.[30] The reaction products were found to coat the surface of the strips and thus to limit the completion of the reaction. Hence, the product was scraped from the strips and was re-equilibrated with fresh zirconium two or three times at the conditions above until no ZrI_3 was found visually or in the powder pattern of the product.

General Synthetic Techniques

The syntheses of reduced halides of early transition and rare earth metals are complicated by properties characteristic of the reactants, the products, or both. Foremost of these troublesome properties is their air-sensitive nature. The zirconium iodide system is no exception. ZrI_4 is quite hygroscopic, liberating HI immediately after exposure to

moisture in the air and turning from reddish brown to white after only a few minutes. At elevated temperatures, oxygen reacts directly with ZrI_4, resulting in ZrO_2 and I_2. ZrI_3 also reacts rather rapidly with moisture in the air, though not as rapidly as ZrI_4. Other reduced zirconium iodides react more slowly with components of the atmosphere and often hours or even days are required to observe changes in the appearance of the solid. For some time, it was thought[2] that the black gems that are typical of the cluster-containing products synthesized here did not react with the atmosphere because no visible change was evident after they were left standing for days in open petri dishes on the bench. But crystals mounted after such treatment give rather smeary X-ray diffraction patterns (spots, lines), probably the result of slow reaction with moisture in the air.

In principle, the manner in which this sensitivity is overcome is quite simple. Reactants and products are kept at all times in environments free of moisture and oxygen. In practice, many techniques have been developed by a number of contributors in an attempt to achieve, as far as possible, this ideal.

Reactants are prepared in Pyrex or fused silica containers in either inert atmospheres (He or Ar), or in vacuum. Dry boxes, previously described,[30] have been devised for use in the preparation and purification of reactants, for loading reactions, and for the examination and characterization of products. The storage of materials under vacuum in sealed glass ampoules is routine. A myriad of techniques have been devised to allow for the characterization of air-sensitive materials.[31]

The air sensitive nature of these materials is only one of the synthetic problems facing the chemist. The remaining problems result primarily from the relatively high temperatures required to overcome kinetic barriers during reaction. Like all materials, the zirconium iodides are subject to the primary law of high temperature chemistry: "At high temperatures everything reacts with everything else".[32] At the temperatures typically used in the zirconium iodide system, this law is manifested in the deleterious reaction of ZrI_4 with fused silica. The high temperatures also result in high pressures of gaseous ZrI_4. To overcome these side reactions and high pressures, techniques have been developed for the use of tantalum as a reaction container. It is this development, more than any other, that is responsible for the synthesis and characterization of a multitude of reduced early transition metal and rare earth metal halides in the past two decades. A review of the use of tantalum reaction containers has appeared recently.[33]

Typically, the steps taken to synthesize reduced zirconium iodides proceeded as follows: A tantalum tube 5 cm in length was cut from a piece of 9.5 mm o.d. stock using a plumber's tube cutter. The tubing was then placed in tantalum cleaning solution (55% conc. H_2SO_4, 25% conc. HNO_3, and 20% conc. HF, by volume) for 30 seconds to a few minutes until the tubing was judged to be sufficiently cleaned. The tube was then rinsed with tap water a few times, followed by rinsing with distilled water and finally with acetone before being placed in an oven at 100°C to dry. After drying, one end of the tube was crimped in a vise and was then welded closed in a specially designed helium arc welder.[34] The tube

was then loaded with reactants in an nitrogen-filled dry box. It is important not to attempt 'recleaning' the once-crimped-and-welded tube with tantalum cleaning solution as it is extremely difficult to remove resulting nonvolatile materials from the crimped portion of the tube, even after repeated rinsing. Acetone rinses in such acidic conditions may also leave a polymeric residue in the reaction tube. These impurities were largely ignored in the past, but the role of very small quantities of these impurities in the course of a reaction is remarkable and forms the basis from which this dissertation began.

After the reactants were weighed in the dry box on an electronic balance (±1 mg) and placed in the tantalum tube, the open end of the tube was crimped closed with a pair of Vice-Grip pliers. The tube was then placed in a large rubber-stoppered test tube and was transported to the welder. Brass heat sinks were clamped around the reaction tubes to hold them in place and to prevent the loss of more volatile reactants during welding. The tubes were placed in the welder, evacuated to 10 μ, then backfilled with He. The total time the crimped but unwelded reaction tube was exposed to air was <15 sec. After welding, the reaction tube was placed in a fused silica jacket to protect the tantalum from air oxidation at reaction temperatures. The jacket and tube were rinsed with tantalum cleaning solution, then distilled water and finally acetone before being evacuated. The evacuated jacket was then 'flamed out' under dynamic vacuum with a fairly hot gas/oxygen flame to remove traces of water absorbed on the surface of the fused silica and was then sealed.

The reaction tube was then placed in a furnace for between 2 and 6 weeks reaction time.

A variety of furnaces were used. The simplest of these were 'tube' furnaces which were purchased as separate heating elements, wired together, and insulated. More refined furnaces included both Marshall and three-zone Lindberg furnaces. The temperature of reactions was monitored by attaching chromel-alumel thermocouples on the outside of the fused silica jackets. The technique was convenient, but any measured gradient was undoubtedly an exaggeration of the actual gradient within the tantalum tube. The temperature of the reaction was regulated by a temperature controller. Both on-off and proportional controllers were used.

Reactions were generally 'air quenched' upon completion by simply removing them from the furnace onto the lab bench. When the reaction had cooled to room temperature (10-15 min) the fused silica jacket was opened and the tantalum reaction tube was removed in air. All reaction containers were opened in a dry box[27] equipped with a nearly horizontal window. A binocular microscope mounted above the window allowed for careful optical examination of reaction products. When appropriate, single crystals for X-ray diffraction were picked up on a glass wand that had been dipped in either Vaseline or silicon grease. The crystals were then mounted in 0.3 mm o.d. glass capillaries. Samples of the products were ground (often directly on the tape) and mounted between layers of Scotch brand tape for Guinier diffraction, as previously described.[35] Most reaction products were stored under vacuum in sealed glass ampoules.

Characterization

Powder X-ray diffraction

Guinier diffraction was used during this research to determine the identity, estimate relative yields, and to obtain precise lattice parameters of products. Patterns were photographically collected using an Enraf-Nonius (Delft) Guinier camera equipped with a silicon monochromator to give clean Cu $K\alpha_1$ radiation. Samples were mounted between layers of Scotch tape in a nitrogen-filled dry box as previously described.[35] National Bureau of Standards silicon (SRM 640) was included in samples as a diffraction reference. Initially, an oscillating sample holder with three rectangular slits for independent samples was used. Later, an accessory that rotated a circular sample holder was found to give sharper patterns and was more often used. Patterns were read using an Enraf-Nonius Guinier film reader. The reading from the film was converted to 2θ values by applying a quadratic equation obtained from the least-squares fit of the five silicon lines to known diffraction angles using the program GUIN.[36] The patterns were indexed and lattice parameters were obtained from the least-squares program LATT[37] with a constraint to the indicated crystal system. By using NBS diffraction standard Al_2O_3, the lattice parameters obtained in this way were checked for their accuracy and found to be within 2σ of the parameters reported by NBS.[38] Typical lattice parameters of phases synthesized during this work and those of related materials are compiled in Table I.

Calculated powder patterns of known or postulated structures were obtained from the program POWD.[39] Selected patterns are given in

Table 1. Cell parameters and volumes of Zr-I-X cluster compounds[a]

Compound	a	b	c	V
$Zr_6I_{14}C$	15.690(3)	14.218(3)	12.808(3)	2857(1)
$K_{0.58}Zr_6I_{14}C$	15.727(2)	14.278(3)	12.798(2)	2874(1)
$KZr_6I_{14}C$	15.757(2)	14.314(2)	12.807(2)	2889(1)
$RbZr_6I_{14}C$	15.768(2)	14.296(2)	12.849(2)	2896(1)
$CsZr_6I_{14}C$	15.803(2)	14.305(3)	12.934(1)	2924(1)
$Zr_6I_{12}C$	14.508(1)		10.007(1)	1822(1)
'$CsZr_6I_{14}$'[b]	15.83-94	14.29-33	12.94-99	2930-58
$Zr_6I_{14}K$[c]	15.933(3)	14.377(2)	12.952(2)	2967(1)
$Zr_6I_{14}K_{0.46}$	15.892(4)	14.288(4)	12.899(3)	2929(2)
$KZr_6I_{14}B$	15.849(2)	14.277(2)	12.876(1)	2913(1)
$CsZr_6I_{14}B$	15.939(2)	14.263(2)	12.974(1)	2950(1)
$Zr_6I_{12}B$	14.534(1)		9.986 (1)	1825(1)
$Cs_{0.3}Zr_6I_{14}Si$	15.997(1)	14.283(1)	12.996(1)	2969(1)
$Cs_{0.7}Zr_6I_{14}Al$	15.907(1)	14.284(1)	12.973(1)	2948(1)

[a]Axial lengths are reported as Å and cell volumes as $Å^3$. $MZr_6I_{14}X$ phases crystallized in the orthorhombic space group Cmca and $Zr_6I_{12}X$ phases in the space group $R\bar{3}$, reported here in the hexagonal setting. All values were obtained from Guinier powder diffraction, unless otherwise noted.

[b]These lattice parameters represent a range of values found in previous investigations by D. H. Guthrie, ref. 2.

[c]Lattice parameters obtained from Ames Laboratory diffractometer data.

Appendix A. Calculated powder patterns were automatically plotted on the scale of the Guinier camera by the program PPPLOT.[40] The powder patterns of many well-characterized materials were obtained from standard diffraction files.[41]

Single crystal X-ray diffraction

The importance of single crystal X-ray diffraction to the complete understanding of these materials cannot be overemphasized. Powder diffraction of the $MZr_6I_{14}X$ phases formed in the course of this research revealed a 3.5% variation from the largest to the smallest cell volume observed. While this was highly significant in a statistical sense, it could easily be dismissed as a nonstoichiometry of the alkali metal atom. Only by single crystal diffraction are the effects of interstitial atoms fully appreciated, for example, in the observation of a 8.5% variation of metal-metal distances in the same materials noted above. Single crystal diffraction also provided accurate geometries and changes therein that were invaluable for a theoretical treatment of the bonding in these clusters by extended Hückel methods.

Three automated four circle diffractometers were used in this research. The Ames Laboratory diffractometer[42,43] was equipped with a graphite monochromator to give Mo Kα radiation (λ = 0.70954 A) and was interfaced with PDP-15 computer. The DATEX diffractometer[40] was also equipped with a graphite monochromator to give Mo Kα (λ = 0.71069 A). It was driven by a VAX 11/730 minicomputer interfaced to the diffractometer by a PDP-11 microcomputer. Both of these diffractometers used an

extremely convenient interactive package of software ALICE developed in Ames Lab by Dr. R. A. Jacobson and described elsewhere.[44] The third diffractometer, a commercial SYNTEX $P2_1$, was equipped with a Mo tube and used Zr filters to eliminate Mo K_β.

Crystals that had previously been mounted in capillaries in the dry box were examined under a Zeiss binocular microscope to sort from the remainder those whose singularity seemed most likely. The capillaries containing these crystals were secured with Apiezon W Wax in brass pins that could be clamped in goniometer heads. Initially, preliminary oscillation photos using Weissenberg cameras were taken of these crystals to ensure their singularity. As the work proceeded, it became clear that visual sorting was adequate as about 90-95% of the gems mounted in the dry box were found to be single, and the preliminary oscillation photos were discontinued. The crystals were then mounted and optically centered on one of the diffractometers. The single crystals were automatically indexed by locating and tuning on 8 to 15 reflections obtained from either oscillation or rotation photos. On the AL and DATEX diffractometers this was accomplished with the software ALICE.[44] When working with the SYNTEX diffractometer, the SYNTEX software for locating and tuning reflections was used, but it was found to be faster and more reliable to input the angles at which reflections were found into the program BLIND[45] to determine the cell than to use the SYNTEX autoindexing program. The Miller indices obtained from BLIND could then be assigned to the correct reflections in SYNTEX reflection array to obtain the appropriate orientation matrix before proceeding with standard selection.

After the correct cell was found, three standards were selected and tuned to obtain a better orientation matrix. The collection of data was then initiated. Reflection intensities were obtained with ω-scans on the monochromator-equipped AL and DATEX diffractometers and with $2\theta/\omega$-scans on the SYNTEX. When data collection was complete, a reflection at about 90° in χ and with moderately strong intensity was chosen, and intensities were collected at 36 10° intervals in ψ for use in an empirical absorption correction program ABSN.[46] On the AL and DATEX diffractometers these intervals were begun at 0° in ϕ and ended at 350°. On the SYNTEX, it was most convenient to do a ψ-scan where ψ was not necessarily evenly divisible by 10. Since ABSN was written to expect ψ values evenly divisible by 10, intensities from the SYNTEX ψ-scans were converted to ψ values and intensities appropriate for ABSN by linear interpolation using the program PHINUM.[47] Inspection of the standards monitored every 75 reflections showed no evidence for decay of any of the data crystals in the beam. After absorption correction, the data were corrected for Lorentz-polarization effects and then reduced using the program REDDAT.[48] To be considered observed, observed reflection intensities (I_{obs}) and structure factor amplitudes ($|F_{obs}|$) were both required to be three times their respective estimated standard deviations. The observed data were then averaged in their appropriate space group using the program FDATA.[49] All calculations were carried out on a VAX 11-780 computer.

Since these phases are isotypic with materials whose structures were previously determined, it was unnecessary to solve any phase problems.

Structure factor calculations and least-squares refinements were carried out using the block-diagonal, full-matrix program ALLS,[50] and Fourier series calculations were done with the program FOUR.[51] Anisotropic thermal parameters of the form $\exp[-1/4(B_{11}h^2a^{*2} + B_{22}k^2b^{*2} + B_{33}\ell^2c^* + 2B_{12}hka^*b^* + 2B_{13}h\ell a^*c^* + 2B_{23}k\ell b^*c^*)]$ were used. The neutral atom scattering factors included corrections for the real and imaginary parts of anomalous dispersion for the heavier elements (Na or greater).[52] All drawings of the structures were produced using the program ORTEP,[53] with thermal ellipsoids drawn at the 75% probability level unless otherwise indicated. In all cases, refinement of the structures was begun by using the zirconium and iodine positions from a known structure. For $Zr_6I_{12}C$, the structure reported for 'Zr_6I_{12}' was used and for $MZr_6I_{14}X$ clusters, the published positions in '$CsZr_6I_{14}$' were used.[6] The scale factor and positions of the heavy atoms were first refined, then the isotropic thermal parameters of these atoms were allowed to vary. Finally, the anisotropic thermal parameters were allowed to vary. It was believed at this point, because of the large increase in synthetic yield of reactions containing purposefully added interstitial 'impurities', that an atom was occupying the center of the cluster. The electron density maps generated, however, often showed no electron density at this position and attempts to refine an atom here led to an increase in the residuals or very large thermal parameters.

The observation at this point that $F_{calc} > F_{obs}$, for all large F's, and that negative peaks appeared at atom positions in electron density difference maps indicated the need for a secondary extinction

correction. Whether this was a result of the 'perfectness' of the crystals or a problem of coincidence (saturation) at the X-ray detector is uncertain. The secondary extinction correction was done using a previously described method.[54] In most cases, the correction led to a decrease in R and R_w of a few percent, the large F_{calc}'s and F_{obs}'s agreed more closely, and the negative peaks in difference maps disappeared. But the most important effect of the correction was the appearance of a small peak in the center of the zirconium octahedron. It was initially thought that this peak might be the effect of one or two mismeasured reflections, but a careful analysis (RHOCON[55]) of the contribution that individual structure factors make to the electron density at the inversion point at the center of all the clusters revealed that the large reflections contribute very strongly to the total density at this point. This is not the case for general points in the real cell, where the large reflections do not significantly contribute to the electron density disproportionately. Because the secondary extinction correction has the effect of increasing the magnitude of these large reflections to agree more closely with those calculated, it is reasonable to expect that an increase in these F_{obs}'s will cause an increase in the electron density at the center of the cluster. Because the secondary extinction correction seems appropriate given the improved residuals, it was assumed that the model with the interstitial in the center was equally appropriate. It is interesting to note that without the extinction correction, the structures of $CsZr_6I_{14}B$ and $CsZr_6I_{14}C$ both appear to be '$CsZr_6I_{14}$' but with inexplicable differences in the Zr-Zr distances. A full

understanding of these structures depends on the presence of small interstitial atoms which are observed only after a secondary extinction correction.

This, of course, serves to illustrate the main weakness of single crystal X-ray diffraction, the inability to observe light atoms accurately where the scattering is dominated by very heavy atoms. For this reason, the appearance of interstitial atoms is not based solely on the presence of a peak in the center of the cluster, but also on the positions the heavy atoms in the cell, the distances therebetween, on formation of phases in large yield only in the presence of added interstitials, and the use of complementary measurements such as magnetic susceptibility, PES, and solid state NMR.

The occupancy and thermal parameters of the alkali metal atoms and the heavier interstitial atoms were varied where possible. If the occupancy remained within 3σ of unity, it was returned to unity and not varied further. In structures with lighter interstitials, it was found that the occupancy and the isotropic B could not be varied simultaneously. In these cases, the occupancy was held at unity and the isotropic B refined to slightly negative numbers (though not significantly different from zero), indicating an unreasonable occupancy greater than one. A statistical reweighting[56] of the data in 10 to 15 overlapping groups corrected these 'negative' B's and in all cases B's of the interstitial atom were positive. Although unit occupancy is not necessary in a crystallographic sense, there has been no observation of gross interstitial nonstoichiometry in the syntheses of these materials with

the exception of the unusual clusters $Zr_6I_{14}K_x$. That is to say, if a reaction mixture was deficient in graphite, for example, the yield of interstitial-containing product was correspondingly small instead of a large yield of presumably carbon deficient product and lattice parameters remained constant.

Accurate distances and estimated standard deviations from refined single crystal structures were calculated using a standard program. Because of their higher accuracy, available lattice parameters obtained from Guinier powder diffraction of the sample from which the single crystal was taken were used in lieu of lattice parameters obtained from diffractometer data.

Table II lists details for the single crystal X-ray diffraction studies completed.

X-ray photoelectron spectroscopy

During this research, XPS spectra were collected by J. Anderegg using an AEI 2008 spectrometer equipped with Al Kα radiation. To ensure their integrity, samples sealed under vacuum in glass ampoules were introduced into a dry box (<1 ppm H_2O, O_2) attached directly to the spectrometer. After being ground in an agate mortar, the samples were mounted on double-sided adhesive tape to reduce the broadening effects of differential charging by electrically separating the sample from ground. The mounting also made the tape's carbon 1s peak available as a convenient reference for calibrating the energy of sample peaks. Data were obtained by signal averaging using a Nicolet 1180 computer system.

Table 2. Crystallographic data for single crystal investigations

	$Zr_6I_{14}C$	$K_{0.58}Zr_6I_{14}C$	$CsZr_6I_{14}C$	$Zr_6I_{12}C$
Space group	Cmca	Cmca	Cmca	$R\bar{3}$
Z	4	4	4	3
Crystal dimensions (mm)	0.20 0.20 0.16	0.24 0.18 0.14	0.30 0.16 0.20	- - -
$2\upsilon_{max}$ (°)	55	55	55	65
Reflections				
measured	3776	3761	3644	4160
observed[a]	1785	1927	1969	2558
independent	931	1025	1068	883
R_{ave} (%)	2.9	2.6	2.3	3.2
R (%)	3.6	3.6	3.3	3.2
R_w (%)	4.5	4.2	3.9	4.2
2nd extinction coeff. (10^{-4})	1.2(2)	4.5(4)	2.7(3)	2.0(1)
Absorption coeff. (1/cm)	173	173	182	178
Range of trans.	0.81-1.00	0.55-1.00	0.81-1.00	0.77-1.00
# of parameters	90	101	101	46
# of variables	52	54	56	30

[a]Reflections with $F_{obs} \geq 3\sigma_F$ and $I_{obs} > 3\sigma_I$ were considered observed, unless indicated.

[b]Reflections with $F_{obs} \geq 2\sigma_F$ and $I_{obs} > 2\sigma_I$ were considered observed.

$Zr_6I_{14}K$	$Zr_6I_{14}K_{0.46}$	$CsZr_6I_{14}B$	$Cs_{0.3}Zr_6I_{14}Si$	$Cs_{0.7}Zr_6I_{14}Al$
Cmca	Cmca	Cmca	Cmca	Cmca
4	4	4	4	4
0.26	0.20	-	0.15	0.22
0.16	0.20	-	0.12	0.18
0.14	0.08	-	0.08	0.12
55	55	55	55	50
3841	3291	4026	3847	1499
2547	2547	1977	2026	596[b]
1228	1228	1057	1043	596
4.6	4.8	3.1	5.2	-
4.5	5.8	4.0	5.7	3.6
6.3	8.1	4.0	6.5	4.5
-	-	0.7(1)	-	0.29(8)
168	170	180	171	177
0.52-0.99	0.25-0.99	0.79-1.00	0.39-0.99	0.60-1.00
90	90	101	101	101
54	53	55	57	57

Magnetic susceptibility

Magnetic susceptibilities were measured from 95 to 298 K using the Faraday method. The sample was contained in a screw-top Teflon bucket suspended from a Cahn Rh electronic balance by a tungsten wire. The bucket and wire were calibrated at the temperature above to correct for their magnetic effects. A more complete description of the balance can be found elsewhere.[57]

Electron spin resonance measurements

ESR measurements were made on a Bruker ER 200D-SRC spectrometer with an Oxford ESR-900 flow-through cryostat, a DTC-2 digital temperature controller and a Hewlett-Packard 5342A microwave frequency counter.

Electron microprobe analysis

Microprobe analyses were conducted on some samples by F. Laabs using an Applied Research Laboratories Model EMX electron microprobe, formerly available in Ames Laboratory. Samples were transferred by attaching a plastic glove bag flushed by dry nitrogen to the entry port of the spectrometer.

^{13}C nuclear magnetic resonance

^{13}C nuclear magnetic resonance spectra of two carbon-centered clusters were kindly obtained by C. Fry and B. Gerstein to provide information complementary to the X-ray results. The spectra were taken at 55.35 MHz on a spectrometer built at Ames Laboratory.[56] Typically, 32500 accumulations were taken of the normal free-induction decay (FID), with

appropriate phase cycling done to minimize DC offset. Eight μsecond 90° pulses at a repetition time of 0.2 second were used. Spin counting was used to confirm that the signals observed were originating from the samples.

Extended Hückel calculations

Extended Hückel calculations were conducted using programs that have been previously described.[59,60] The atomic orbital energies not included in these programs were obtained elsewhere[61] or were derived from spectroscopic data.[62] Double zeta expansions were used to describe the radial distribution functions of zirconium 4d orbitals,[63] and normal single zeta functions were used elsewhere.[64] Geometries of clusters and atomic orbital parameters are given in Appendix B.

RESULTS

Description of the Structures

As noted earlier, zirconium iodide clusters have been found in two structure types, $Zr_6I_{12}X$ and $MZr_6I_{14}X$. Both contain $Zr_6I_{12}X$ clusters, where the zirconium atoms form a slightly distorted octahedron the 12 edges of which are bridged by iodine atoms. The center of the octahedron is occupied by an 'interstitial' atom. A convenient, and oft quoted, way of conceptualizing these clusters is based on a cube, as shown in Figure 1. In the 'ideal' case, the interstitial atom X occupies the body center of the cube, the six zirconium atoms are centered on the faces of the cube, and the 12 iodines are located at the center of the 12 edges of the cube. In most known metal halides containing the M_6X_{12} clusters, the metal atoms occupy positions slightly off the faces towards the center of the cube because of the opposing effects of metal-metal bonding and anion-anion repulsion. This so-called 'matrix effect'[65] is more pronounced for the iodide clusters of a given metal than for the other halides since the metal-metal bonding potential remains essentially constant while the minimum distance the halides can approach each other increases. This matrix effect is important because of the geometric constraints it places on the cluster, as will be discussed later in conjunction with cluster bonding.

In addition to the 12 edge-bridging iodines associated with each cluster, each zirconium is also bonded to an additional iodine atom that occupies the terminal position on each apex of the octahedron, so that

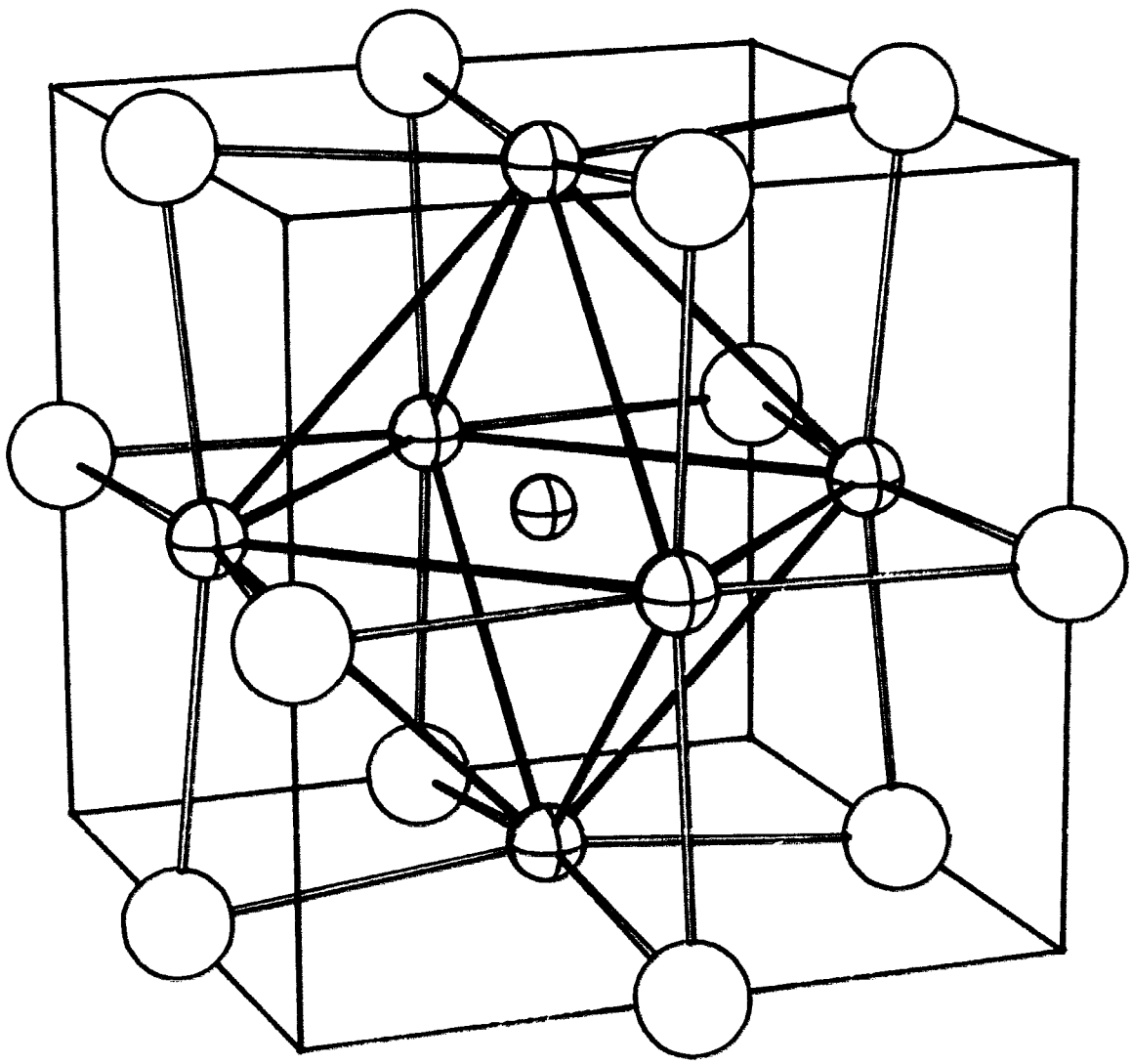

Figure 1. Idealized $M_6X_{12}Y$ cluster. Open circles = halide (X); cross hatched circles = metal (M) and interstitial (Y)

the interstitial atom, the zirconium atom, and this terminal iodine are ideally colinear. To differentiate these two types of iodine functionalities, a convention[66] has been devised. The edge-bridging iodines are denoted 'inner' iodines as I^i and those occupying the terminal positions are labeled 'äusser' (outer) iodines as I^a. Thus a cluster unit could be symbolized $Zr_6I^i_{12}I^a_6X$.

In this work, the stoichiometries of the two structure types synthesized are a result of the manner that these clusters are interconnected through the sharing of iodines at terminal positions to achieve three-dimensional networks of clusters. A full description of these interconnectivities and the structures of phases with these Zr/I compositions has appeared previously.[6]

In $Zr_6I_{12}X$, the octahedra are stacked with a three-fold axis parallel to the $\vec{c}$ direction of the hexagonal setting of the unit cell as shown in Figure 2. The six I^i atoms that bridge the edges around the waist of the antiprismatic cluster are also terminal iodines bonded to zirconium atoms of adjacent clusters. Likewise, the six I^a of this cluster bridge edges around the waist of adjacent clusters. Since these iodines demonstrate both functionalities they are denoted as I^{i-a} for the former and I^{a-i} for the latter. The intercluster bridging of one cluster to six adjacent clusters is illustrated in Figure 3. A useful formulation for this interconnectivity is $Zr_6I^i_6I^{i-a}_{6/2}I^{a-i}_{6/2}X$. The cluster possesses D_{3d} point symmetry resulting from a three-fold axis that passes through an inversion point at the center of the cluster (X).

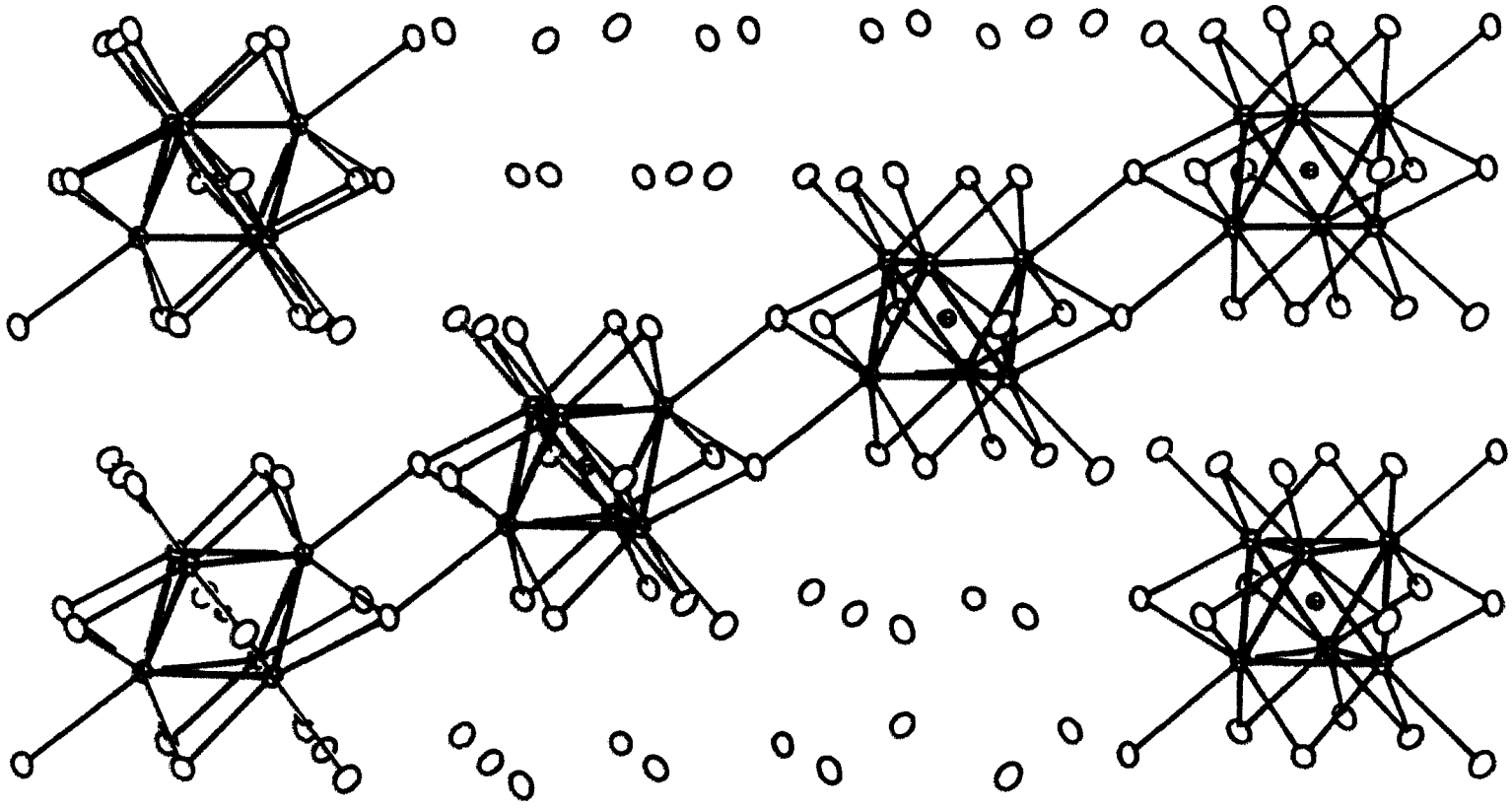

Figure 2. A $[1\bar{1}0]$ projection of the structure of $Zr_6I_{12}X$. $\vec{c}$ perpendicular to the iodine (open circles) layers

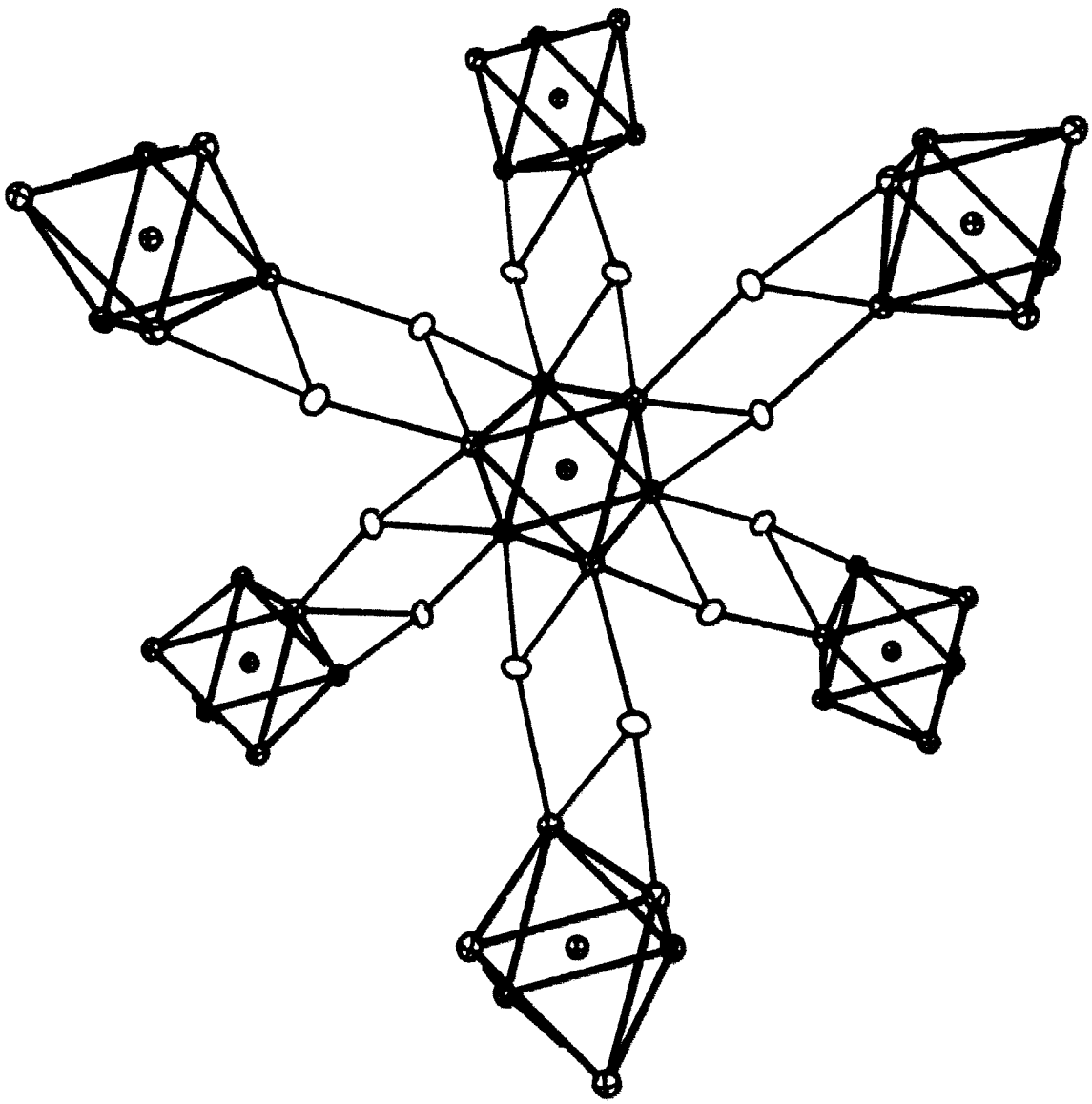

Figure 3. Intercluster bridging in $Zr_6I_{12}X$. Only the I^{i-a} and I^{a-i} of the central cluster are shown (open circles). The $\vec{c}$ axis is perpendicular to the page

The interconnectivity accompanying the stoichiometry of the $MZr_6I_{14}X$ phases is more complex, and the symmetry of the cluster is accordingly reduced. In this cluster, 10 of the 12 octahedral edges are bridged by inner iodines that have no connection to adjacent clusters. As shown in Figure 4, the other two edges of the octahedron are bridged by inner iodines that are also terminal iodines bonded to zirconium atoms in adjacent clusters. The other four terminal iodines only bridge to similar positions on adjacent clusters. The formulation of phases with this interconnectivity is thus $MZr_6I^i_{10}I^{i-a}_{2/2}I^{a-i}_{2/2}I^{a-a}_{4/2}X$. The clusters in $MZr_6I_{14}X$ phases possess C_{2h} point symmetry resulting from a two-fold axis passing through a center of inversion on the interstitial atom at the center of the cluster. The zirconium octahedra in the 6-14 phases show a marked 'compression' along a pseudo four-fold axis, with the two zirconium atoms bound to the terminal I^{a-i} atoms defining that axis. The isostructural nature of these $MZr_6I_{14}X$ phases with Nb_6Cl_{14} and Ta_6I_{14} (excluding the alkali metal and interstitial atoms) has previously been noted.[6]

Descriptions of both of these structures as well as other related examples in terms of close-packed layers of nonmetal (iodine) atoms have appeared previously.[6] The structure of $Zr_6I_{12}X$ consists of ccp layers of iodine with zirconium atoms occupying half the octahedral holes between these in triangular groups of three. These Zr_3 units pair up about a 'vacant' iodine position in the intervening iodine layer to form trigonal antiprismatic Zr_6 clusters as seen in Figure 2. The 'vacant' iodine

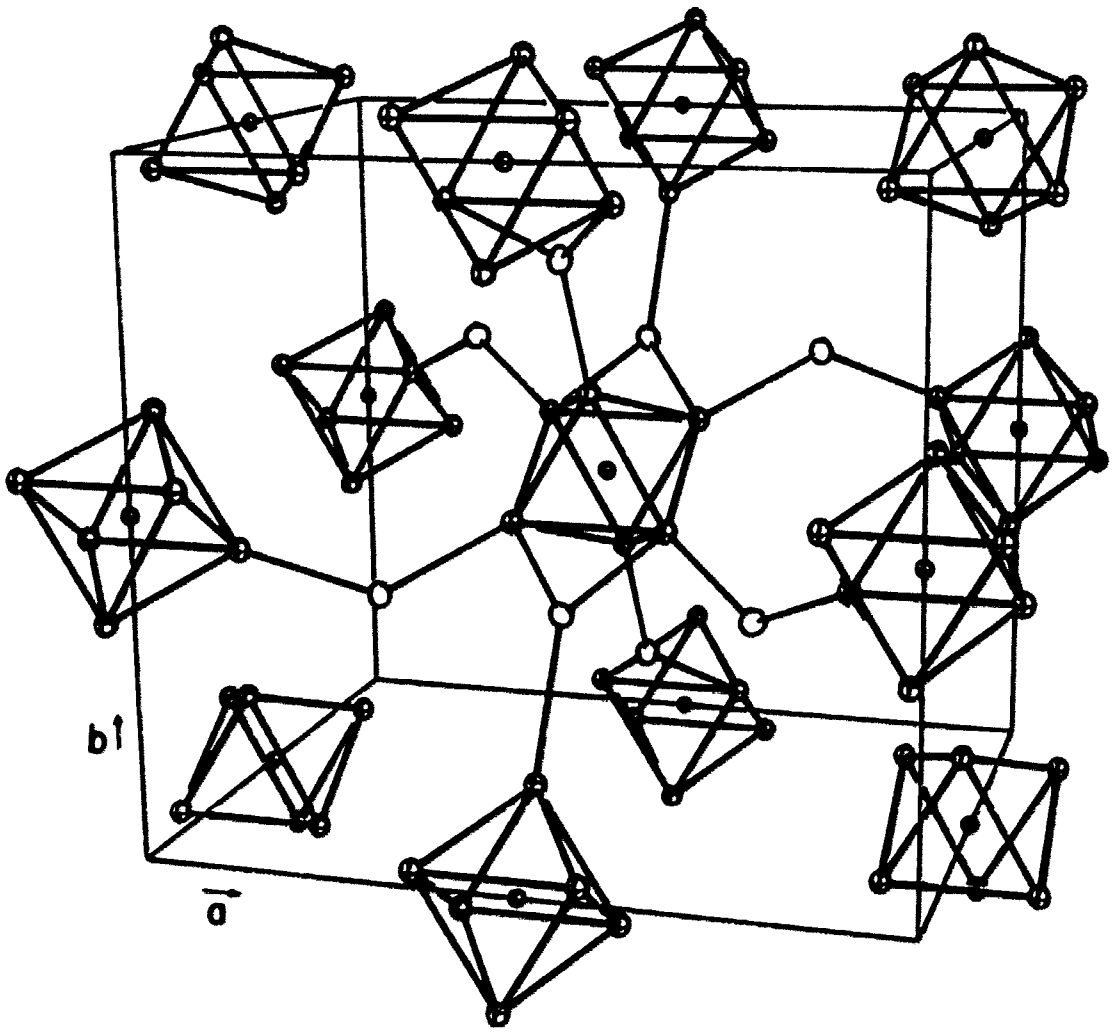

Figure 4. Interconnectivity of $Zr_6I_{14}X$. Only the I^{a-a}, I^{a-i}, and I^{i-a} of the central cluster are shown (open circles)

position about which this cluster is formed is occupied by the interstitial atom X.

In $MZr_6I_{14}X$ phases, the layering sequence perpendicular to the c axis is ABAC [or $(hc)_2$ ...] and again clustering occurs around 'missing' iodine sites in the c (or A) layers that are again occupied by interstitial atoms. These same layers also exhibit a second halide vacancy, apparently generated by requirements of the iodine bridging. These vacancies can be occupied by alkali metal atoms (Cs, Rb, K, but evidently not Na or Li with iodide) to form $MZr_6I_{14}X$ phases (seen in Figure 5), but they have also been found unoccupied giving $Zr_6I_{14}X$.

Figure 6 shows the isolated clusters of the $Zr_6I_{12}X$ and $MZr_6I_{14}X$ structures. The atoms are labeled as they are in parameter listings.

Carbon-Containing Clusters

Synthesis

A series of clusters that contain carbon were among the first of the interstitial clusters to be synthesized and were the phases that have been best characterized.

The first and most reduced of these clusters was found in low (10%) yield in binary ZrI_4-Zr reactions run between 800 and 900°C in earlier studies of this system.[2,6] The highly crystalline nature of this material allowed the easy isolation of single crystals. The single crystal X-ray diffraction study was done and the material was reported as Zr_6I_{12}. The present investigation establishes that this phase is in fact $Zr_6I_{12}C$. If a stoichiometric amount of graphite were included in reactions at

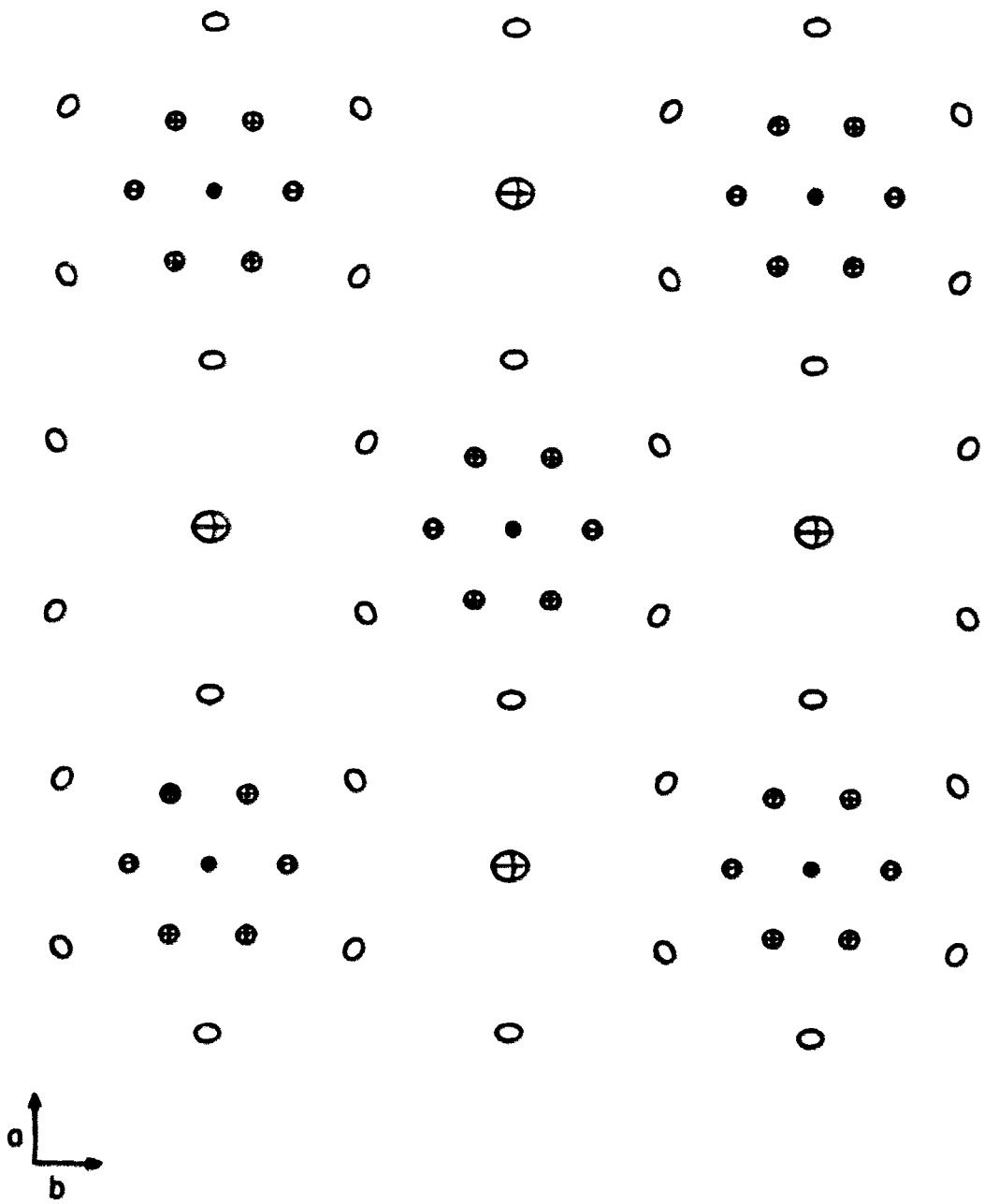

Figure 5. The close-packed MIX layer in $MZr_6I_{14}X$ projected on Z = 1/2. Iodines are shown as open ellipsoids, M^I atom in the 'Cs' sites are the largest crossed ellipsoids. The smallest ellipsoids represent the interstitial X. Zirconium atoms above and below the Z = 1/2 section are shown forming octahedral clusters around the interstitial atom

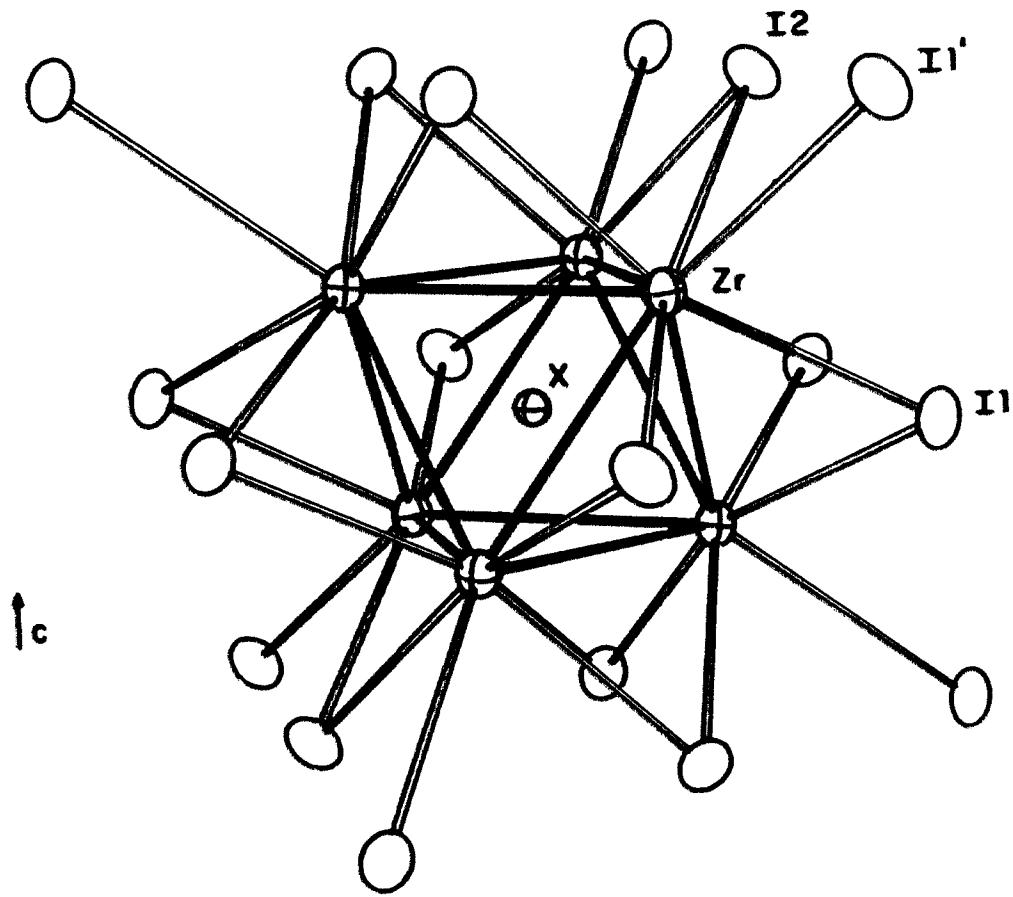
I2
I1'
Zr
I1
c

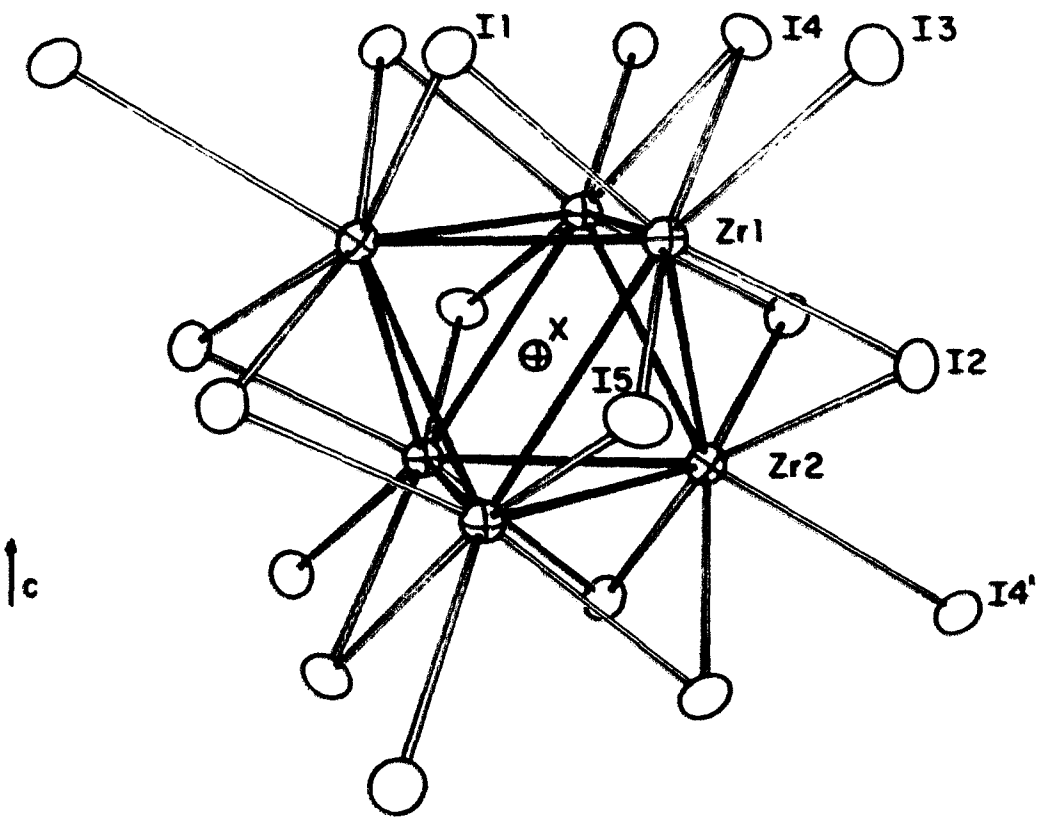

Figure 6. (Top) $Zr_6I_{12}X$. A center of inversion lying at X and a 3-fold axis along $\vec{c}$ give the cluster D_{3d} point symmetry. I1 = I^{1-a}, I2 = I^{1}, I_1' = I^{a-1}

(Bottom) $Zr_6I_{14}X$. A 2-fold axis passing through atoms I5 and X and a mirror plane containing atoms I4, X, and Zr2 give the cluster C_{2h} point symmetry. (A center of inversion lies at X, I1, I2, I5 ≡ I^{1}, I3 = I^{a-a}; I4 = I^{1-a}; I4' = I^{a-i})

850°C of ZrI_4 with excess zirconium metal in either the form of strips or powder, essentially quantitative yields of $Zr_6I_{12}C$ were obtained in two weeks. The product formed shiny black gems that grew on the surface of the zirconium strips and on the walls of the Ta reaction tube. $Zr_6I_{12}C$ was also formed by reacting layered α,β-ZrI_2 with stoichiometric amounts of graphite at 850°C for two weeks.

The material that was formed in earlier studies [2,7,8] was reported as being unreactive in air, and the material that formed in some reactions conducted in this investigation behaved similarly. In other cases, however, the product reacted fairly rapidly with water, decomposing to give a greenish-black suspension. No evolution of gas was visually observed, but the odor of acetylene was detected above the liquid. No difference in the powder patterns of these materials was observed beforehand, and perhaps the stability seen in some batches of this material is attributable more to kinetic factors related to the 'perfectness' of the crystals grown in one reaction compared with another than to thermodynamic considerations.

The phases $MZr_6I_{14}C$ (M = Cs, Rb, or K) are only slightly less reduced than $Zr_6I_{12}C$. $CsZr_6I_{14}C$ and $RbZr_6I_{14}C$ were most easily prepared by reacting stoichiometric amounts of CsI or RbI, ZrI_4, and graphite with excess Zr strips at 850°C for two weeks. The products form in greater than 95% yield as beautiful, shiny, black, many-faceted gems up to 0.4 mm in diameter. The gems are not visibly different from $Zr_6I_{12}C$, but give a distinctly different X-ray powder diffraction pattern. The materials were also prepared in reactions containing stoichiometric amounts of Zr

powder, but obtaining complete reactions required a thorough grinding of the products formed after one week, followed by re-equilibration for an additional week at 850°C. A reaction that was loaded to stoichiometrically form $Cs_{0.5}Zr_6I_{14}C$ and run for two weeks at 850°C resulted in a large yield of material whose lattice parameters were slightly smaller than those found for $CsZr_6I_{14}C$.

When reactions stoichiometrically loaded to form $KZr_6I_{14}C$ were run for two weeks at 850°C, the resulting product was a 90% yield of shiny, black gems. The single crystal X-ray diffraction study that ensued resulted in an X-ray composition of $K_{0.58}Zr_6I_{14}C$. Presumably fully stoichiometric product with a slightly larger cell volume was obtained when a two-fold excess of KI was included in the reaction.

Reactions to form '$NaZr_6I_{14}C$' or '$LiZr_6I_{14}C$' resulted instead in $Zr_6I_{12}C$ and unreacted alkali metal iodide.

The least reduced of the carbon-containing clusters is $Zr_6I_{14}C$. This phase was prepared from a stoichiometric reaction of ZrI_4, Zr powder, and graphite. After one week at 850°C, the reaction was opened and large amounts of ZrI_3, ZrI_4 and $Zr_6I_{12}C$ were found. The reaction products were ground and re-equilibrated for an additional week at 850°C. When the reaction was reopened some ZrI_3 remained, but the major product was $Zr_6I_{14}C$ and no $Zr_6I_{12}C$ was observed in the powder pattern. $Zr_6I_{14}C$ has also been observed together with ZrC as the lone iodine-containing phase in reactions loaded to the stoichiometry Zr:I:C::1:1:1 and run for one week at temperatures between 650 and 750°C.

Characterization

Single crystal X-ray diffraction studies have been conducted on four of these carbon containing phases: $Zr_6I_{12}C$, $CsZr_6I_{14}C$, $K_{0.58}Zr_6I_{14}C$, and $Zr_6I_{14}C$. The details of these studies are compiled in Table 2. Final atomic positions and thermal parameters and esd's are given in Table 3 and bond distances and their esd's are listed in Table 4. Average bond distances and esd's are compiled in Table 5.

The first of these structures completed was that of $Zr_6I_{12}C$. The 'perfectness' of these crystals noted above is almost certainly responsible for the secondary extinction problems that both the earlier and the present single crystal diffraction studies experienced. The failure to adequately correct this problem in the first study[7,8] was probably the reason that no peak was observed in the center of the cluster. In fact, in the present study, no peak was observed until the secondary extinction correction was applied. The relationship between electron density in Fourier maps and secondary extinction for these clusters was noted earlier. Application of the correction reduced the residuals by a few percentage points and the final R and R_w of the present study were 3.2 and 4.2%, compared to the fairly high values of 10.9 and 12.1% in the earlier work.[8]

All bond distances and angles for $Zr_6I_{12}C$ are within 3σ of those reported earlier as 'Zr_6I_{12}'. The lattice parameters reported for 'Zr_6I_{12}' are slightly smaller than those found for $Zr_6I_{12}C$, but they were determined by two different methods. The earlier constants were found by tuning on 12 peaks using the AL diffractometer whose effective wavelength

Table 3. Atomic positions and thermal parameters for carbon-centered Zr-I clusters

	x	y	z	B_{11}	B_{22}	B_{33}	B_{12}	B_{13}	B_{33}
$Zr_6I_{14}C$									
I1	0.12943(6)	0.09099(6)	0.24965(9)	1.21(4)	1.16(4)	1.16(3)	6.17(3)	0.47(4)	0.26(3)
I2	0.12541(5)	0.25704(7)	0.00898(8)	1.22(4)	0.92(4)	1.28(4)	0.34(3)	-0.23(3)	-0.18(3)
I3	1/4	0.34773(9)	1/4	1.05(6)	1.11(6)	1.34(5)	0	-0.40(5)	0
I4	0	0.1530(1)	0.7665(1)	1.00(6)	1.47(6)	1.16(5)	0	0	-0.45(5)
I5	0.24622(9)	0	0	0.65(5)	1.45(5)	1.14(5)	0	0	0.19(4)
Zr1	0.39308(8)	0.0639(1)	0.8901(1)	0.66(5)	0.93(5)	0.69(4)	0.01(5)	-0.07(4)	-0.04(5)
Zr2	0	0.3657(1)	0.9028(2)	0.75(7)	0.88(8)	0.75(7)	0	0	-0.03(7)
C	1/2	1/2	1/2	0.8(5)					
$K_{0.58}Zr_6I_{14}C$									
I1	0.12498(4)	0.09064(5)	0.24860(7)	1.16(3)	1.02(4)	1.21(33)	0.15(2)	0.44(2)	0.29(2)
I2	0.12568(4)	0.25754(5)	0.0089(6)	1.14(3)	0.88(3)	1.29(3)	0.32(2)	-0.22(2)	-0.19(2)
I3	1/4	0.34852(8)	1/4	1.06(4)	1.08(5)	1.34(4)	0	-0.46(3)	0
I4	0	0.15407(7)	0.76624(9)	0.91(4)	1.26(5)	1.18(4)	0	0	-0.39(3)
I5	0.24644(6)	0	0	0.62(3)	1.46(4)	1.18(4)	0	0	0.30(4)
K[a]	0	0	0	6.9(7)					
Zr1	0.39406(6)	0.06342(8)	0.89107(9)	0.69(3)	0.89(4)	0.74(4)	0.00(3)	0.04(3)	0.05(4)
Zr2	0	0.3671(1)	0.9030(1)	0.75(5)	0.74(6)	0.81(6)	0	0	-0.07(5)
C	1/2	1/2	1/2	0.5(3)					

$CsZr_6I_{14}C$									
I1	0.12536(4)	0.08999(4)	0.25040(5)	1.05(3)	1.15(3)	1.04(2))	0.12(2)	0.34(2)	0.22(2)
I2	0.12574(4)	0.25739(4)	0.00594(5)	1.16(3)	0.99(2)	1.25(3)	0.30(2)	-0.25(2)	-0.12(2)
I3	1/4	0.34908(6)	1/4	1.14(4)	1.21(4)	1.34(4)	0	-0.37(3)	0
I4	0	0.15832(6)	0.76052(7)	0.95(4)	1.24(4)	1.04(4)	0	0	-0.36(3)
I5	0.24756(6)	0	0	0.72(4)	1.71(4)	1.09(4)	0	0	0.23(3)
Cs	0	0	0	2.27(7)	3.61(7)	1.95(6)	0	0	0.54(6)
Zr1	0.39486(6)	0.06363(7)	0.89269(7)	0.73(3)	0.91(3)	0.81(3)	0.01(3)	-0.01(3)	-0.01(3)
Zr2	0	0.36805(9)	0.9031(1)	0.78(5)	0.88(5)	0.87(5)	0	0	-0.07(4)
C	1/2	1/2	1/2	0.1(3)					
$Zr_6I_{12}C$									
I1	0.035525(4)	0.10257(4)	0.33250(6)	0.83(2)	1.12(2)	1.53(2)	0.24(2)	-0.13(2)	0.29(2)
I2	0.12642(4)	0.17766(4)	0.32488(6)	1.16(2)	1.33(2)	1.28(2)	0.73(2)	-0.30(2)	-0.45(2)
Zr	0.14301(6)	0.04066(6)	0.13012(8)	0.70(3)	0.80(3)	0.94(3)	0.37(2)	-0.03(2)	0.00(2)
C	0	0	0	0.5(3)					

[a]Occupancy = 0.58(3).

Table 4. Bond distances in Zr-I clusters (Å)

		$Zr_6I_{14}C$	$K_{0.58}Zr_6I_{14}C$	$CsZr_6I_{14}C$		$Zr_6I_{12}C$
Zr-Zr intralayer[a]						
Zr1-Zr1	(x2)	3.355(3)	3.332(2)	3.324(2)	(x6)	3.200(1)
Zr1-Zr2	(x4)	3.284(2)	3.264(2)	3.257(2)		
Zr-Zr interlayer[b]						
Zr1-Zr1	(x2)	3.345(3)	3.325(2)	3.321(2)	(x6)	3.190(1)
Zr1-Zr2	(x4)	3.292(2)	3.272(2)	3.270(2)		
Zr1-Zr1	(x2)	4.738(3)	4.707(2)	4.699(2)	(x3)	4.518(1)
Zr2-Zr2	(x1)	4.560(4)	4.536(3)	4.530(2)		
$Zr\text{-}I^{i}$						
Zr1-I5	(x2)	2.847(2)	2.855(1)	2.860(1)	(x6)	2.873(1)[c]
Zr1-I1	(x2)	2.860(2)	2.872(1)	2.884(1)	(x6)	2.861(1)
Zr1-I2	(x2)	2.868(2)	2.881(1)	2.895(1)		
Zr2-I1	(x2)	2.840(2)	2.852(1)	2.862(1)		
Zr2-I2	(x2)	2.848(2)	2.856(1)	2.867(1)		
$Zr\text{-}I^{i\text{-}a}$						
Zr1-I4	(x2)	2.908(2)	2.916(1)	2.920(1)	(x6)	2.940(1)[d]
					(x6)	2.912(1)
$Zr\text{-}I^{a\text{-}i}$						
Zr2-I4	(x2)	3.491(3)	3.509(2)	3.522(2)	(x6)	3.403(1)[e]
$Zr\text{-}I^{a\text{-}a}$						
Zr1-I3	(x4)	3.138(2)	3.158(1)	3.195(1)		
Zr-interstitial						
Zr1-int.	(x2)	2.369(2)	2.354(1)	2.349(1)	(x6)	2.259(1)
Zr2-int.	(x2)	2.280(1)	2.268(1)	2.265(1)		
M-I						
M-I1	(x4)		3.957(1)	4.010(1)		
M-I2	(x4)		4.176(1)	4.185(1)		
M-I4	(x2)		3.713(1)	3.837(1)		
M-I5	(x2)		3.876(1)	3.914(1)		

[a]Intralayer refers to Zr-Zr distances roughly perpendicular to the $\vec{c}$ axis of the cell, Figure 6.

[b]Interlayer refers to Zr-Zr distances roughly parallel to the $\vec{c}$ axis of the cell.

[c]$Zr\text{-}I^{i}$ distances in $Zr_6I_{12}C$ are Zr1-I2 bonds.

[d]$Zr\text{-}I^{i\text{-}a}$ distances in $Zr_6I_{12}C$ are Zr1-I1 bonds.

[e]$Zr\text{-}I^{a\text{-}i}$ distances in $Zr_6I_{12}C$ are Zr1-I1 bonds.

Table 5. Average bond distances (A) in carbon-centered Zr-I clusters

	$Zr_6I_{14}C$	$K_{0.58}Zr_6I_{14}C$	$CsZr_6I_{14}C$	$Zr_6I_{12}C$
$d_{ave}(Zr\text{-}Zr)$	3.309(3)	3.288(2)	3.283(2)	3.195(1)
$d_{ave}(Zr\text{-}I^{i})$	2.862(2)	2.872(2)	2.881(1)	2.897(1)
$d(Zr\text{-}I^{a\text{-}i})$	3.491(3)	3.509(2)	3.522(2)	3.403(1)
$d(Zr\text{-}I^{a\text{-}a})$	3.138(2)	3.158(1)	3.195(1)	-
$d_{ave}(Zr\text{-}C)$	2.339(2)	2.325(1)	2.321(1)	2.259(1)
r_C[a]	1.48	1.46	1.46	1.40

[a]Crystal radius of the carbon. See text for explanation.

is dependent on the setting of graphite monochomator and where no calibrant is readily available. The lattice parameters of $Zr_6I_{12}C$, as noted earlier, were determined on the basis of Guinier powder diffraction using NBS silicon as a standard and are therefore more accurate. Similar differences have ben observed in other related systems.[67]

The structure of $CsZr_6I_{14}C$ refined uneventfully to the residuals listed in Table 2. The occupancy and anisotropic thermal parameters of the cesium were varied simultaneously. The occupancy did not vary significantly from unity and so it was returned there and in the final refinement was not varied. It is very apparent from the bond distances

found in $CsZr_6I_{14}C$, that it is not the material previously reported as $CsZr_6I_{14}$,[8] unlike the case of $Zr_6I_{12}C$ and 'Zr_6I_{12}'. This point will be discussed in some detail later in this work.

Initially, the structure found to be $K_{0.58}Zr_6I_{14}C$ was thought to be $Zr_6I_{14}C$. It was believed that a potassium atom would be too small to occupy the 'cesium' position. At first, only one octant (HKL) was collected on the SYNTEX diffractometer. When the refinement was thought to be complete, a difference electron density map revealed a peak of Z = 4-5 on the 'cesium' position at the origin of the cell. To eliminate doubts that this peak was the erroneous effect of one or two mismeasured reflection intensities, a second octant ($HK\bar{L}$) of data was collected. Unfortunately, some adjustments had been made on the SYNTEX diffractometer in the intervening time. The result was a difference in intensities between equivalent reflections. To correct this problem, the total counts and background counts of a group of 25 reflections of moderate intensity from the first data set were compared with the equivalent reflections from the second octant to obtain a scalar by which the raw data of the weaker octant were multiplied. The two octants were then corrected for absorption, reduced, and averaged, resulting in an R_{ave} of 2.6% with no reflections discarded. When the zirconium, iodine and carbon positions were refined with this averaged data set, the peak at the origin of the cell remained. A potassium atom was then included at this position, and refinement of both isotropic thermal paramater and occupancy of the potassium led to improved residuals and an X-ray composition of $K_{0.58(2)}Zr_6I_{14}C$.

After it was found that the structure of what was thought to be '$Zr_6I_{14}C$' was actually the potassium-deficient material above, a single crystal of a 6-14 phase from a reaction where no alkali metal was present was mounted for a diffraction study. Data were collected, reduced, and averaged. The refinement of the structure proceeded smoothly to the residuals in Table 2. A final difference electron density map showed no peaks at the alkali metal site.

The paramagnetic behavior of $CsZr_6I_{14}C$ has been confirmed by magnetic susceptibility measurements. As shown in Figure 7, the material demonstrates Curie-Weiss behavior between 100 and 298 K, with $\mu = 1.48\ \mu_B$ and $\theta = -6$ K that is appropriate for one unpaired electron per formula. Odd electron $Ta_6X_{12}^{3+}$ clusters have been shown to display similar behavior.[66] $CsZr_6I_{14}C$, however, shows no esr signal even at 4 K between 0 and 13 KG fields. Presumably this is due to very rapid electron spin-lattice relaxation, but a low temperature magnetic transition has not been ruled out. Similar behavior was observed for the cluster compound Nb_6I_{11}, that is also paramagnetic but shows no low temperature esr signal.[69-71]

The NMR Fourier transform spectrum of the free-induction decay of 400 mg of $CsZr_6I_{14}{}^{13}C$ together with a least-squares fit of the data are shown in Figure 8. The shift scale has TMS at 0.0 ppm, and positive shifts are downfield. As expected, there is only one tensor in the spectrum. Within error, the tensor is axially symmetric with $\sigma_\parallel$ at 15 ppm and $\sigma_\perp$ at 54 ppm.

The NMR Fourier transform of the FID of 100 mg of $Zr_6I_{12}C$ showed an extremely broad signal. Because of this breadth and the small sample

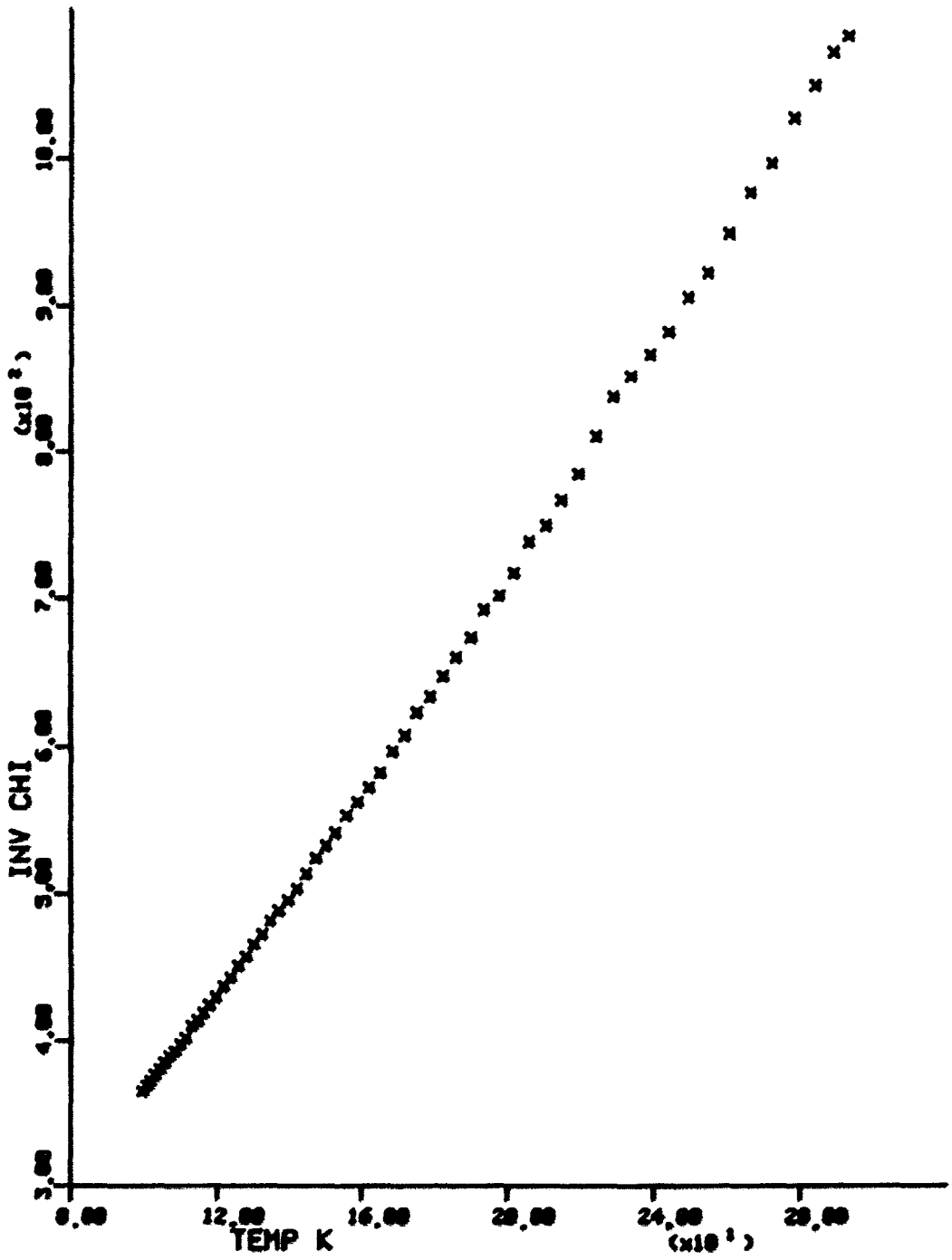

Figure 7. Magnetic susceptibility of $CsZr_6I_{14}C$, corrected for temperature-independent terms

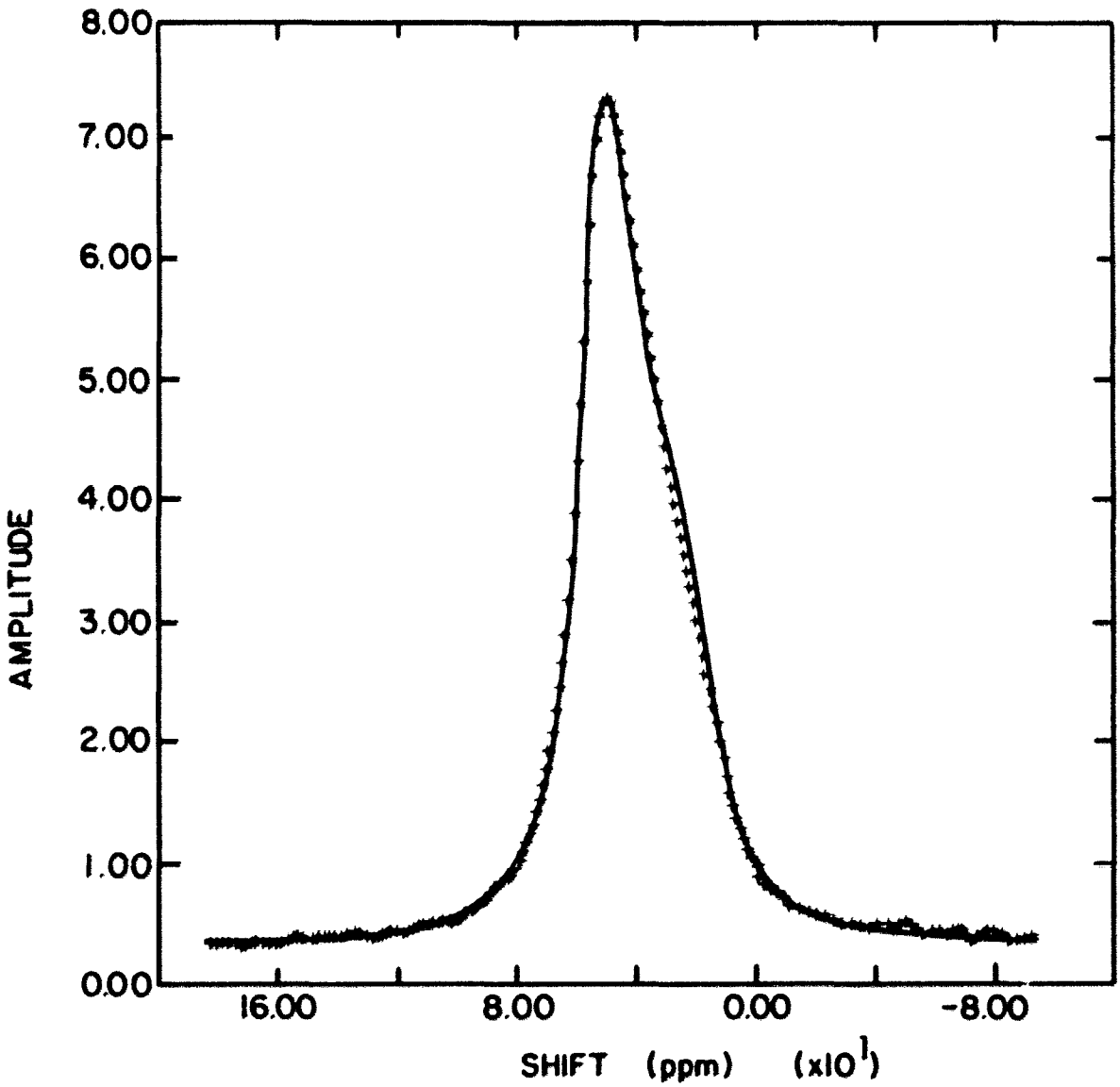

Figure 8. Solid state ^{13}C NMR spectrum of $CsZr_6I_{14}C$. The chemical shift of TMS is at 0.00 ppm and shifts to positive values are downfield. $\sigma_\perp$ = 54, $\sigma_\parallel$ = 15 (ppm). Crosses = experimental spectrum. Smoothed line = fit to an axially symmetric tensor

size, it was necessary to subtract background noise and an accurate tensor was not obtained. It seems clear, however, that the tensor lies between at least 28 to 480 ppm. (480 ppm is the highest ^{13}C shift value ever reported.)[72]

Interpretation of the spectra, especially the chemical shifts, is difficult. It seems clear that the carbon atoms in the centers of the zirconium clusters are responsible for the signals observed, but the chemical shifts and the tensor shapes are very different considering the similarity predicted by the current understanding of bonding in these clusters. Further elucidation of the NMR spectra awaits future study.

Alkali Metal-Centered Clusters

Synthesis

The synthesis and characterization of alkali metal-centered clusters is the most surprising aspect of this research. This work has been reported previously as a communication.[73]

The compound $Zr_6I_{14}K$ was prepared in reactions of stoichiometric amounts of KI, ZrI_4, and excess Zr metal strips in a temperature gradient between 840 and 860°C for six weeks. A 10-20% yield of black, rectangular gems were found growing on the metal strips. The remaining products were α,β-ZrI_2, ZrI_3, and unreacted KI in the cooler end of the reaction tube. Single crystals were mounted and one was indexed on the Ames Laboratory diffractometer. Surprisingly, the lattice parameters of this single crystal were larger than those reported for $CsZr_6I_{14}$! Subsequent reactions showed that materials with slightly smaller lattice parameters

could also be formed in 10-20% yields. The isolation of single crystals was again possible.

Similar reactions have been run with RbI, NaI, and LiI with less success. The reactions with RbI resulted in 10-20% yields of gems with smaller lattice parameters than those found for the potassium-centered phases, suggesting that rubidium occupies the more normal 'cesium' position as in $CsZr_6I_{14}C$. The remaining products were a mixture of ZrI_3, α,β-ZrI_2, and $Rb_3Zr_2I_9$. NaI and LiI reactions have resulted in small yields of materials that are similar in both habit and lattice constants to the gem-shaped products of the KI reactions. It has proven difficult to isolate these phases and their identification is based on the observation and indexing of lines in powder patterns corresponding to 6-14 type phases with cell volumes between 2920(2) and 2937(6) A^3. Remaining products were identified by powder pattern as ZrI_3, α,β-ZrI_2, a few well-formed crystals of $Zr_6I_{12}C$ (carbon from undetermined source), and unreacted alkali metal iodide.

Characterization

The single crystal structures of two potassium-containing clusters were determined. The first of these was the material with the larger cell parameters. After the refinement of the iodine and zirconium positions and isotropic thermal parameters (R = 14%), a peak of Z = 18 was observed in the center of the cluster in an electron density map and although it was considered highly unusual, a potassium atom was included in the model at this position. The refinement proceeded smoothly with

all atoms refined anisotropically to the residuals listed in Table 2. The occupancy of the potassium was allowed to vary and refined to a value of 1.05 (3) so it was returned to unity and not varied further. The cesium position in the cell within the iodine polyhedron was unoccupied.

The second crystal structure studied was of a gem from a phase with a slightly smaller cell volume. Again, the iodine and zirconium positions were refined and a peak was observed in the center of the zirconium cluster. This peak was somewhat smaller than that in the previous structure. A potassium was included at this position and its occupancy and isotropic thermal parameter were varied while the remaining atoms were refined anisotropically. The occupancy of the potassium refined to a value of 0.46 (2) with the residuals listed in Table 2. While this peak might be interpreted as a combination of potassium and carbon atoms randomly distributed in the zirconium octahedra, the average Zr-Zr distance predicted for such a cluster by a linear combination of the distances found in $Zr_6I_{14}K$ and $Zr_6I_{14}C$ is 0.1 Å shorter than the average Zr-Zr distance observed in $Zr_6I_{14}K_{0.46}$. Linear extrapolation of the change in average Zr-Zr bond distance with potassium content results in an expected Zr-Zr bond distance of 3.42 Å for the hypothetical 'Zr_6I_{14}'.

The final refined atomic positions and thermal parameters of these two structures are given in Table 6 and bond distances found in these structures together with those for $Zr_6I_{14}C$ are given in Table 7. A compilation of average bond distances is given in Table 8.

Because of the unusual nature of a potassium atom within a cluster, some additional measurements have been made. An electron microprobe

Table 6. Positional and thermal parameters for $Zr_6I_{14}K_{1.0}$ and $Zr_6I_{14}K_{0.46}$

Atom	x	y	z	B_{11}
$Zr_6I_{14}K_{1.0}$				
I1	0.12513(6)	0.08981(6)	0.24784(7)	1.79(5)
I2	0.12567(5)	0.25609(6)	0.00725(7)	1.74(4)
I3	1/4	0.34728(9)	1/4	1.60(6)
I4	0	0.15615(9)	0.7660(1)	1.50(6)
I5	0.24601(8)	0	0	1.26(5)
Zr1	0.39034(9)	0.06613(9)	0.8883(1)	1.50(6)
Zr2	0	0.3612(1)	0.8980(1)	1.12(8)
K[a]	1/2	1/2	1/2	0.9(2)
$Zr_6I_{14}K_{0.46}$				
I1	0.12518(6)	0.08942(9)	0.24741(9)	1.28(5)
I2	0.12579(6)	0.25582(8)	0.00729(9)	1.31(5)
I3	1/4	0.3459(1)	1/4	1.11(6)
I4	0	0.1562(1)	0.7765(1)	0.99(6)
I5	0.24686(9)	0	0	0.84(6)
Zr1	0.3905(1)	0.0662(1)	0.8881(1)	1.24(7)
Zr2	0	0.3610(2)	0.8977(2)	0.74(8)
K[b]	1/2	1/2	1/2	0.1(3)

[a]Occupancy refined to 1.05(3).
[b]Occupancy refined to 0.46(2).

B_{22}	B_{33}	B_{12}	B_{13}	B_{23}
1.53(4)	1.38(4)	0.20(3)	0.48(3)	0.32(3)
1.43(4)	1.45(4)	0.37(3)	-0.31(3)	-0.22(3)
1.61(5)	1.40(5)	0	-0.45(4)	0
1.82(6)	1.29(5)	0	0	-0.48(4)
2.04(6)	1.37(5)	0	0	0.34(4)
1.29(5)	1.04(5)	-0.18(4)	0.13(4)	-0.10(4)
1.59(7)	1.17(7)	0	0	0.20(6)
1.2(2)	0.4(2)	0	0	0.1(2)
1.68(6)	1.62(5)	0.14(3)	0.45(3)	0.32(4)
1.69(6)	1.61(5)	0.36(3)	-0.31(3)	-0.19(4)
1.80(8)	1.61(7)	0	-0.47(5)	0
1.92(8)	1.45(7)	0	0	-0.45(5)
2.13(8)	1.56(6)	0	0	0.26(6)
1.51(8)	1.38(7)	-0.20(5)	0.28(5)	-0.10(6)
2.21(11)	1.38(9)	0	0	0.41(9)

Table 7. Bond distances in Zr-I-K clusters (A)

		$Zr_6I_{14}C$	$Zr_6I_{14}K$	$Zr_6I_{14}K_{0.46}$
Zr-Zr Intralayer				
Zr1-Zr1	(x2)	3.355(3)	3.494(3)	3.478(3)
Zr1-Zr2	(x4)	3.284(2)	3.427(2)	3.408(3)
Zr-Zr Interlayer				
Zr1-Zr1	(x2)	3.345(3)	3.462(3)	3.447(3)
Zr1-Zr2	(x4)	3.292(2)	3.436(3)	3.424(3)
Zr1-Zr1	(x2)	4.738(3)	4.920(3)	4.897(3)
Zr2-Zr2	(x1)	4.560(4)	4.785(4)	4.765(5)
$Zr\text{-}I^{i}$				
Zr1-I5	(x2)	2.847(2)	2.880(2)	2.858(2)
Zr1-I1	(x2)	2.860(2)	2.896(2)	2.878(2)
Zr1-I2	(x2)	2.868(2)	2.903(2)	2.888(2)
Zr2-I1	(x2)	2.840(2)	2.874(1)	2.864(2)
Zr2-I2	(x2)	2.848(2)	2.881(2)	2.871(2)
$Zr\text{-}I^{i\text{-}a}$				
Zr1-I4	(x2)	2.908(2)	2.953(4)	2.941(2)
$Zr\text{-}I^{a\text{-}i}$				
Zr2-I4	(x2)	3.491(3)	3.408(2)	3.377(2)
$Zr\text{-}I^{a\text{-}a}$				
Zr1-I3	(x4)	3.138(2)	3.124(2)	3.118(2)
Zr-interstitial				
Zr1-int.	(x2)	2.369(2)	2.460(1)	2.448(2)
Zr2-int.	(x2)	2.280(1)	2.393(2)	2.382(2)

Table 8. Bond distances in Zr-I-K clusters (A)

	$Zr_6I_{14}C$	$Zr_6I_{14}K$	$Zr_6I_{14}K_{0.46}$
$d_{ave}(Zr-Zr)$	3.309(3)	3.448(3)	3.432(3)
$d_{ave}(Zr-I^{i})$	2.862(2)	2.898(2)	2.883(2)
$d(Zr-I^{a-i})$	3.491(3)	3.408(2)	3.377(2)
$d(Zr-I^{a-a})$	3.138(2)	3.124(2)	3.118(2)
$d_{ave}(Zr-int)$	2.339(2)	2.437(2)	2.426(2)
r_{int}^{a}	1.48	1.58	1.57

[a]Crystal radius of interstitial as described in the text.

analysis of single crystals of the X-ray sample $Zr_6I_{14}K_{1.0}$ showed only zirconium, iodine and potassium, excluding the possibility of a heavy nonmetal occupying the potassium position. The microprobe results of six individual crystals gave an average composition of $K_{1.4}Zr_6I_{14.4}$ very consistent with the X-ray formulation, especially since unreacted KI in the system is likely to be on the surface of the crystals.

Magnetic susceptibilities of a phase with the smaller cell parameters measured on a Faraday balance yielded a Curie-Weiss behavior from

298 to 100 K, with μ_{eff} = 0.82 (1) μ_B, θ = -2 K and χ_{mol} = 2.71 x 10^{-4} emu/mole at 298 K as shown in Figure 9. A term χ_0 that includes contributions from both temperature-independent paramagnetism and core diamagnetism was obtained by fitting the susceptibility data to the Curie law of the form $\chi = C/T + \chi_0$. This temperature independent term was subtracted from each data point prior fitting the data to Curie-Weiss behavior. The molar susceptibility obtained is consistent with the presence of an average of approximately 0.5 unpaired electron per cluster.

XPS measurements of a sample of a potassium-deficient phase $Zr_6I_{14}K_x$ (x = 0.5), KI, and K_2ZrI_6 have also been conducted. The low XPS cross-section of the potassium required some 500 scans to be averaged so that the potassium $2p_{3/2}$ peak in $Zr_6I_{14}K_x$ could be observed. The data of KI and K_2ZrI_6 were more easily obtained because of the higher potassium content. The BE's were obtained by applying the following formula

$$BE = 1486.6 - KE - \phi$$

where 1486.6 is the energy of the Al Kα radiation used, KE is the observed kinetic energy of the electrons in question, and ϕ is a work function obtained by assigning the carbon 1s peak of the adhesive tape (used for mounting) a measured value of 285 eV. Table 9 contains a compilation of the potassium, zirconium, and iodine core level binding energies (BE) obtained.

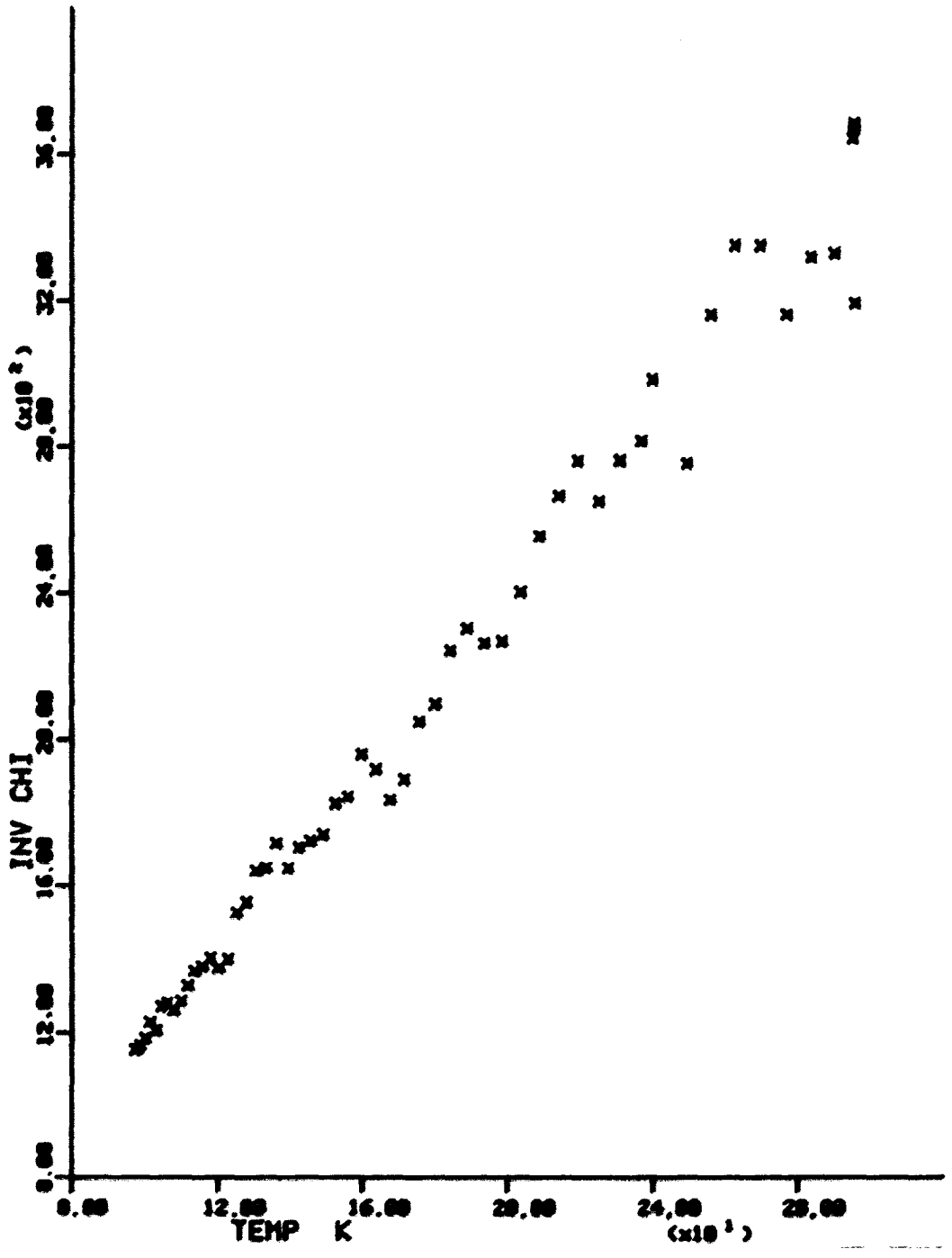

Figure 9. Magnetic susceptibility of $Zr_6I_{14}K_x$, corrected for temperature-independent terms

Table 9. XPS data for zirconium, potassium, and iodine core levels

	Binding Energy (eV)			
	Zr $3d_{5/2}$	K $2p_{3/2}$	I $3d_{5/2}$	Δ^a
KI	-	293.5	619.6	326.1
K_2ZrI_6	183.5	294.0	620.6	326.6
$Zr_6I_{14}K_x$	180.6	294.4	620.6	326.2

[a]Difference in binding energy of I $3d_{5/2}$ and K $2p_{3/2}$ core levels.

Boron-Containing Clusters

Synthesis

Three boron-containing clusters have been synthesized to date and the single crystal X-ray structure of one of these has been investigated.

The first of the clusters $CsZr_6I_{14}B$ was initially synthesized using high purity boron chunks in a stoichiometric reaction of ZrI_4, CsI, and Zr powder at 850°C for one week. A 10-20% yield of black gems were found growing on the surface of the boron in the reaction. Gems were mounted in capillaries for single crystal diffraction. Further reactions of amorphous boron, ZrI_4, CsI, and Zr metal powder resulted in a >90% yield of black gems. The powder patterns of this material showed it to be a

6-14 type phase with larger lattice parameters than $CsZr_6I_{14}C$. The lattice parameters obtained from the diffractometer on gems of the earlier low yield reaction matched those of the Guinier pattern within 3σ.

A reaction to form '$Zr_6I_{14}B$' with the same chunks of high purity boron, ZrI_4, and Zr powder had a similar result as the earlier reaction that formed $CsZr_6I_{14}B$. A small yield of black gems were found on the surface of the boron. These gems were too small to mount for single crystal X-ray diffraction, but a Guinier powder pattern demonstrated them to be a Zr_6I_{12}-type phase with a slightly larger cell volume than $Zr_6I_{12}C$. Reactions with amorphous boron, ZrI_4, and Zr powder were loaded to form $Zr_6I_{12}B$ and run for 2 weeks at 850°C. They resulted in a large yield of $Zr_6I_{12}B$, with the same lattice parameters as the material formed using high purity boron. The presumed paramagnetic nature of these materials has not been verified.

Attempts to synthesize '$NaZr_6I_{12}B$', that would be isoelectronic with $Zr_6I_{12}C$ and isostructural with $Sc_7Cl_{12}N$,[71] resulted in a large yield of black gems whose lattice parameters, as determined by Guinier powder diffraction, were within 2σ of $Zr_6I_{12}B$. The strong lines of NaI were faintly observed in the powder pattern. It has been concluded from this result that '$NaZr_6I_{12}B$' does not exist. A similar reaction loaded with stoichiometric amount of KI to form '$KZr_6I_{12}B$' resulted in a 95% yield of black gems. A powder pattern of the bulk showed it consisted of a mixture of approximately 20% $Zr_6I_{12}B$ and 80% of a 6-14 type material with a cell volume smaller than that of $CsZr_6I_{14}B$. Interestingly, the

difference in the cell volumes of $CsZr_6I_{14}C$ and $KZr_6I_{14}C$, 35 A^3, is the same as the difference between the cell volumes of the materials above. Based on this observation, the black gems have been tentatively identified as $KZr_6I_{14}B$, but additional information is needed to confirm this assumption.

Characterization

The refinement of the single crystal structure of $CsZr_6I_{14}B$ proceeded smoothly to the residuals listed in Table 2. The occupancy and anisothermal parameters of the cesium was allowed to vary simultaneously. The resulting occupancy of cesium did not vary significantly from unity and it was returned to one and not varied further. The occupancy of the boron was held at unity as well and only the isotropic thermal parameter was allowed to vary. As in the case of many of the carbon-centered clusters, the isotropic thermal parameter was near zero or slightly negative until the data were reweighted, after which it refined to its given value. The final refined atomic positions and thermal parameters are given in Table 10. The bond distances in $CsZr_6I_{14}B$ are compiled in Table 11, together with those for $CsZr_6I_{14}C$ and two compounds yet to be discussed, $Cs_{0.3}Zr_6I_{14}Si$ and $Cs_{0.7}Zr_6I_{14}Al$. Average bond distances are given in Table 12.

Table 10. Atomic positions and thermal parameters for $CsZr_6I_{14}B$

	x	y	z	B_{11}
I1	0.035525(4)	0.10257(4)	0.33250(6)	0.83(2)
I2	0.12642(4)	0.17766(4)	0.32488(6)	1.16(2)
I3	1/4	0.34703(8)	1/4	1.43(4)
I4	0	0.16036(8)	0.76037(9)	1.33(4)
I5	0.24802(7)	0	0	1.03(4)
Cs	0	0	0	2.65(8)
Zr1	0.39291(7)	0.06556(8)	0.89102(9)	1.16(4)
Zr2	0	0.3637(1)	0.9002(1)	1.20(6)
B	1/2	1/2	1/2	0.3(3)

B_{22}	B_{33}	B_{12}	B_{13}	B_{33}
1.12(2)	1.53(2)	0.24(2)	-0.13(2)	0.29(2)
1.33(2)	1.28(2)	0.73(2)	-0.30(2)	-0.45(2)
1.69(5)	1.69(4)	0	-0.37(4)	0
1.78(5)	1.36(4)	0	0	0.36(4)
2.03(5)	1.57(4)	0	0	0.34(4)
3.70(9)	.247(8)	0	0	0.34(8)
1.37(4)	1.12(3)	0.04(4)	-0.06(4)	0.02(4)
1.56(7)	1.21(6)	0	0	-0.03(6)

Table 11. Bond distances in interstitial-centered Zr-I clusters

		$Zr_6I_{14}C$	$CsZr_6I_{14}B$	$Cs_{0.3}Zr_6I_{14}Si$	$Cs_{0.7}Zr_6I_{14}Al$
Zr-Zr Intralayer					
Zr1-Zr1	(x2)	3.355(3)	3.414(2)	3.632(4)	3.462(5)
Zr1-Zr2	(x4)	3.284(2)	3.349(2)	3.562(3)	3.408(4)
Zr-Zr Interlayer					
Zr1-Zr1	(x2)	3.345(3)	3.390(2)	3.574(4)	3.444(5)
Zr1-Zr2	(x4)	3.292(2)	3.357(2)	3.574(3)	3.391(4)
Zr1-Zr1	(x2)	4.738(3)	4.811(2)	5.096(4)	4.833(5)
Zr2-Zr2	(x1)	4.560(4)	4.671(3)	4.996(6)	4.730(8)
$Zr\text{-}I^{i}$					
Zr1-I5	(x2)	2.847(2)	2.865(1)	2.861(3)	2.866(4)
Zr1-I1	(x2)	2.860(2)	2.886(1)	2.887(2)	2.880(3)
Zr1-I2	(x2)	2.868(2)	2.895(1)	2.898(3)	2.891(3)
Zr2-I1	(x2)	2.840(2)	2.840(2)	2.875(2)	2.862(4)
Zr2-I2	(x2)	2.848(2)	2.876(1)	2.881(2)	2.872(3)
$Zr\text{-}I^{i\text{-}a}$					
Zr1-I4	(x2)	2.908(2)	2.933(1)	2.957(3)	2.932(3)
$Zr\text{-}I^{a\text{-}i}$					
Zr2-I4	(x2)	3.491(3)	3.421(1)	3.256(4)	3.405(5)
$Zr\text{-}I^{a\text{-}a}$					
Zr1-I3	(x4)	3.138(2)	3.177(1)	3.068(2)	3.137(3)
Zr-interstitial					
Zr1-int.	(x2)	2.369(2)	2.406(1)	2.548(2)	2.442(3)
Zr2-int.	(x2)	2.280(1)	2.335(2)	2.498(3)	2.356(4)
M-I					
M-I1	(x4)		4.011(1)	3.998(1)	4.007(2)
M-I2	(x4)		4.163(1)	4.149(1)	4.168(2)
M-I4	(x2)		3.860(1)	3.808(2)	3.826(3)
M-I5	(x2)		3.953(1)	3.948(2)	3.932(3)

Table 12. Bond distances in Zr-I-X clusters (Å)

	$Zr_6I_{14}C$	$CsZr_6I_{14}B$	$Cs_{0.3}Zr_6I_{14}Si$	$Cs_{0.7}Zr_6I_{14}Al$
d(Zr-Zr)	3.309(3)	3.366(3)	3.580(3)	3.417(4)
$d(Zr-I^{i})$	2.862(2)	2.889(1)	2.893(2)	2.884(3)
$Zr-I^{a-i}$	3.491(3)	3.421(1)	3.256(4)	3.405(5)
$Zr-I^{a-a}$	3.138(2)	3.177(1)	3.068(2)	3.137(3)
d(Zr-X)	2.339(2)	2.382(1)	2.531(2)	2.416(3)
r_X[a]	1.48	1.52	1.67	1.56

[a]Crystal radius of the interstitial. See text for explanation.

Silicon- and Aluminum-Containing Clusters

Synthesis

The success of including second period nonmetals in the centers of zirconium clusters led to synthetic attempts to form clusters that included third period nonmetals.

The first such compound synthesized was found in a reaction loaded with CsI, ZrI_4, Si, and excess Zr strips to form '$CsZr_6I_{14}Si$'. The reaction was run for only three days at 850°C. When the reaction was opened, a 30% yield of black gems was found growing on the metal strips together

with α,β-ZrI_2, $Cs_3Zr_2I_9$, and ZrI_3. The Guinier pattern of the gems demonstrated them to be a 6-14 type material with markedly increased lattice parameters (see Table I). Single crystals of this material were mounted for X-ray diffraction. The composition determined from the diffraction study that followed was $Cs_{0.30(1)}Zr_6I_{14}Si$. Subsequent reactions that were loaded with stoichiometric amounts of ZrI_4 and silicon and a two-fold excess of CsI and Zr powder and that were run at 850°C for two weeks resulted in the formation of a 30-40% yield of black gems that gave an identical powder pattern. The remainder of the products were a combination of ZrI_3 and $Cs_3Zr_2I_9$. The lattice parameters of the 6-14 phases from the two preparations matched within 3σ.

Reactions were run in attempts to synthesize '$Zr_6I_{12}Si$' and '$Zr_6I_{14}Si$'. These reactions were run with stoichiometric amounts of ZrI_4, Si, and Zr powder (or excess Zr for '$Zr_6I_{12}Si$') at 850°C for two weeks. The products of these reactions were a combination of ZrI_3, α,β-ZrI_2, and unreacted metal. Faint lines were once observed that could be indexed on a large 6-12 cell, but the standard deviations were very high and the correctness of the indexing of these lines is in doubt.

The discovery that silicon could successfully be incorporated in the octahedral zirconium clusters led to attempts to prepare the analogous aluminum compounds. Reactions were loaded with stoichiometric amounts of CsI, ZrI_4, AlI_3, and Zr powder and were run at 850°C for two weeks. A 50% yield of black gems and shiny black powder was found together with a mixture of ZrI_3, ZrI_4, and $Cs_3Zr_2I_9$. The powder pattern of the black gems and powder showed them to be the same 6-14 type phase with somewhat

smaller lattice parameters than the silicon-containing material above. This difference in cell volumes was somewhat surprising considering the larger cell volume in $CsZr_6I_{14}B$ compared with that of $CsZr_6I_{14}C$. Therefore, a single crystal diffraction study was initiated to determine the exact nature of the structure of this material.

Reactions that were loaded to form '$Zr_6I_{12}Al$' with stoichiometric amounts of ZrI_4 and AlI_3 and a two-fold excess of Zr powder and run for two weeks at 850°C resulted in a fibrous material giving a powder pattern that had not previously been observed. A similar result and product, though a second new pattern, was obtained when a reaction to form '$CsZr_6I_{14}Al$' was loaded with stoichiometric amounts of ZrI_4 and AlI_3 but two-fold excesses of Zr powder and CsI. ZrI_3 was also found as a product in both of the above reactions.

Characterization

The single crystal structures of both the 6-14 phases containing silicon and aluminum were studied.

The structural refinement of the silicon-containing cluster was begun using the cesium, zirconium, and iodine positions of $CsZr_6I_{14}C$ and a silicon atom was included at full occupancy with an isotropic B of 1.0 at the center of the zirconium octahedron. After the atomic positions were refined, the isotropic thermal parameters of the iodines and cesium were allowed to vary. The thermal parameter of cesium immediately moved to the large value of 14.5(4) and showed no sign of refining. The cesium atom was removed from the model and the zirconium and iodine atoms were

refined anisotropically to residuals of 8.2 and 10.1%. At this point, an electron density map showed a peak of about one-third of a cesium in the 'cesium' position. The cesium atom was reintroduced at this position and both the multiplier and isotropic B were allowed to vary. This model refined to the X-ray composition given above. The isotropic B of silicon was then allowed to vary and refined to a value of 0.4 (2). A final reweighting resulted in somewhat lower esd's but did not result in other significant changes in the model. The final refined atomic positions and thermal parameters are given in Table 13 and bond distances have been compiled in Table 11 and 12.

Because the structure of the 6-14 phase was well established, only a single octant of data to a $2\theta_{max}$ of 50° was collected for the structure of the aluminum-containing material. Since a small crystal had been mounted for data collection, a higher-than-normal ratio of reflections were unobserved. To help correct this problem, the cutoff for observed reflections was reduced to $2\sigma_I$ and $2\sigma_F$. After data reduction, the cesium, zirconium, and iodine positions from $Cs_{0.3}Zr_6I_{14}Si$ were used as a model from which to begin refinement. An aluminum atom was included in the center of the zirconium octahedron. The refinement proceeded smoothly to the residuals listed in Table 2. The model at this point included anisotropic thermal parameters for zirconium, iodine and cesium, and the multiplicity of cesium. The X-ray stoichiometry obtained was $Cs_{0.66(1)}Zr_6I_{14}Al$. Some questions of the thermal parameter of aluminum and its exact occupancy remain as they were highly coupled. If the B was held constant at 0.6 or 1.0, the occupancy obtained was 0.88 (3) or

Table 13. Atomic positions and thermal parameters for $Cs_{0.30(1)}Zr_6I_{14}Si$ and $Cs_{0.68(1)}Zr_6I_{14}Al$

	x	y	z	B_{11}
$Cs_{0.30(1)}Zr_6I_{14}Si$				
I1	0.12550(8)	0.08897(8)	0.2475(1)	1.66(6)
I2	0.12583(7)	0.2539(1)	0.0069(1)	1.70(5)
I3	1/4	0.3437(1)	1/4	1.40(7)
I4	0	0.1589(1)	0.7647(2)	1.32(8)
I5	0.2468(1)	0	0	1.22(7)
Cs[a]	0	0	0	3.3(5)
Zr1	0.3865(1)	0.0691(2)	0.8853(2)	1.31(8)
Zr2	0	0.3545(2)	0.8932(2)	1.1(1)
Si	1/2	1/2	1/2	0.4(2)
$Cs_{0.68(1)}Zr_6I_{14}Al$				
I1	0.1251(1)	0.08939(8)	0.2494(1)	1.59(10
I2	0.12566(9)	0.2560(1)	0.0064(1)	1.58(8)
I3	1/4	0.3469(2)	1/4	1.4(1)
I4	0	0.1587(2)	0.7624(2)	1.4(1))
I5	0.2472(2)	0	0	1.2(1)
Cs[b]	0	0	0	3.1(3)
Zr1	0.3912(2)	0.0662(2)	0.8892(2)	1.52(11)
Zr2	0	0.3624(3)	0.8987(3)	1.3(2)
Al[c]	1/2	1/2	1/2	1

[a]Occupancy refined to 0.30(1).
[b]Occupancy refined to 0.68(1).
[c]The B was held arbitrarily at unity and the occupancy refined to 0.92(3). See text for further discussion.

B_{22}	B_{33}	B_{12}	B_{13}	B_{33}
1.67(6)	1.53(5)	0.18(4)	-0.45(5)	0.34(5)
1.45(5)	1.74(5)	0.32(5)	-0.28(5)	-0.10(4)
1.65(8)	1.73(7)	0	-0.48(6)	0
1.90(9)	1.84(7)	0	0	-0.56(7)
2.20(8)	1.49(6)	0	0	0.27(7)
2.3(5)	2.1(4)	0	0	0.3(4)
1.50(8)	1.19(8)	0.01(8)	-0.05(7)	0.21(8)
1.6(1)	1.3(1)	0	0	0.1(1)
1.33(7)	0.86(6)	0.15(6)	0.44(6)	0.31(5)
1.13(6)	0.99(6)	0.48(7)	-0.28(6)	-0.18(4)
1.2(1)	1.1(1)	0	-0.29(8)	0
1.6(1))	1.06(9)	0	0	-0.39(8)
1.7(1)	0.98(9)	0	0	0.26(8)
4.0(4)	2.0(3)	0	0	0.4(2)
1.21(8)	0.81(8)	-0.2(1)	0.19(9)	-0.14(8)
1.7(2)	0.6(1)	0	0	0.4(1)

0.93 (3). If the occupancy was held at 1.0, the B refined to 2.2 (2). The average B of the zirconiums was about 1.5 and the range of B's from other interstitials where the occupancy was held at unity is 0.2 to 1.4. An attempt to refine this position as fully occupied carbon led to a B of 0.069, even after reweighting, and this has been interpreted as unreasonable, especially when the bond distances obtained from this structure were considered. Some of the problem of successful refinement experienced was attributed to the lack of sufficient high angle data that contributes much to the accurate determination of this 'light' atom. A better resolution of this problem would probably be possible with further data collection or a larger crystal that is available.

The final refined atomic positions and thermal parameters of these structures are given in Table 13. A complete listing of bond distances are compiled in Table 11. A summary of average bond distances is included in Table 12.

Other Attempted Syntheses

During the course of this investigation, other attempts at synthesizing clusters containing other interstitials failed. These failures, however, provide some useful information concerning the electronic and steric restrictions limiting the syntheses of these clusters.

Several reactions have been attempted at temperatures between 600 and 850°C to form nitrogen-centered clusters from ZrI_4, Zr metal, ZrNI, and occasionally CsI. These reactions invariably resulted in the formation of mixtures of ZrN_x, ZrI_3, α,β-ZrI_2, and $Cs_3Zr_2I_9$ (CsI present).

This is contrary to the experience in both the scandium[74] and zirconium[75] chloride systems, where nitrogen-centered clusters are known.

Attempts to form oxygen-centered clusters from ZrI_4, Zr metal, and either ZrO_2 or $ZrO_{0.4}$, with and without CsI, resulted in the formation of very low (5%) yields of isolated black gems. When CsI was included, the gems were found to be a '$CsZr_6I_{14}$' phase, with fairly large lattice parameters (V = 2950 $Å^3$), typical of the materials previously produced by Guthrie.[6] Gems found in reactions run without CsI, were invariably found to be $Zr_6I_{12}C$. AES analysis of the ZrO_2 (used to synthesize the $ZrO_{0.4}$) showed a fairly substantial contamination by silicon. Although the source of this impurity has not been verified, possibilities include the unfiltered ammonium hydroxide (used to precipitate zirconium hydroxide) or a silica gel column over which solutions of the hydrated $ZrOCl_2$ had been passed in order to remove hafnium impurities.[76]

Some effort has been made to synthesize '$BaZr_6I_{14}C$' by including stoichiometric amounts of BaI_2 in reactions of ZrI_4, zirconium and graphite. These reactions have invariably formed $Zr_6I_{12}C$ and unreacted BaI_2 as the products. At least two factors may contribute to the instability of '$BaZr_6I_{14}C$'. The first of these is the relatively large enthalpy of formation of BaI_2 (-143.9 kcal/mole), compared with CsI (-82.8 kcal/mole) or KI (-78.4 kcal/mole). The second factor is the small size of the barium atom, the 12-coordinate radius[77] of which is 0.03 Å less than that of potassium. As will be discussed later, the size of the cavity in the $MZr_6I_{14}C$ phases is too large for either potassium or barium. The formation of $KZr_6I_{14}C$ is apparently allowed by the more energetically

forgiving nature of the lower charged potassium compared with the barium. The inclusion of other alkaline or rare earth atoms in the 'cesium' site have not been attempted as the radii of these atoms are smaller than that of barium. An attempt to synthesize '$Zr_6I_{14}Ca$' was likewise unsuccessful, presumably because of the high enthalpy of formation of CaI_2 and the higher coulombic repulsion of zirconium and the divalent cation compared with the monovalent potassium.

Prior to the discovery that interstitial atoms could be included at the centers of the zirconium octahedra, many attempts were made to synthesize unoccupied clusters. With the exception of the partially-occupied cluster in $Zr_6I_{14}K_x$, no empty clusters have been observed. Truly binary reactions led to the slow formation of either ZrI_3, or α,β-ZrI_2 and the addition of CsI apparently gives only $Cs_3Zr_2I_9$ as the sole reduced ternary phase in the CsI-ZrI_4-Zr system. The formation of '$CsZr_6I_{14}$' reported early was probably interstitially stabilized, as will be discussed later.

The kinetic problems plaguing synthesis in the binary and ternary systems that have been reported previously were also observed in similar reactions in this study. The formation of ZrI_3 is usually only complete in the presence of an excess of zirconium metal (strips or powder). For the complete reduction of ZrI_4 to the layered diiodides, however, the presence of excess zirconium strips was not sufficient. As noted earlier, the reduced product must be removed from the metal strips and re-equilibrated at 750°C with fresh metal to achieve quantitative yield. Attempts to overcome blockage of the zirconium strips at higher

temperatures leads inevitably to the formation of sizeable quantities of ZrI_3, but it is unclear whether this is the result of decomposition of lower iodides or a worsening of the blockage problem. The kinetic difficulties in the binary systems are in dramatic contrast to the ease of forming large yields of carbon-centered cluster-containing phases upon the addition of quite small amounts of graphite. This effect of added graphite will be discussed later in this work.

DISCUSSION

Comparison of the Structures

The number of phases that have been investigated by single crystal X-ray diffraction allows the rather thorough examination of the effects on bond distances of the degree of reduction, gross structural changes, and the atom contained in the center of the cluster. In the course of this discussion, attention will initially be focused on the series of carbon-containing clusters that have been studied: $Zr_6I_{14}C$, $K_{0.58}Zr_6I_{14}C$, $CsZr_6I_{14}C$, and $Zr_6I_{12}C$ and the effects of reduction and structural changes will be examined. After development of a model of bonding for the series of carbon-containing clusters, the model will be applied to gain an understanding of the bonding in clusters containing other post-transition nonmetals and metalloids. Since the potassium-containing clusters may be expected to exhibit somewhat different bonding, an extended Hückel treatment has also been applied to these clusters.

There are no unusual iodine-iodine distances in any of these structures. The nearest-neighbor distances range from about 3.9 to near 4.1 Å, typical of van der Waals contacts. In the 6-14 phases that contain cesium, the average Cs-I distances to 12 neighbors are between 4.008 and 4.027 Å, in good agreement with the sum of crystal radii[77] for these atoms (3.94 Å for 8-coordinate cesium and 4.08 Å for the 12-coordinate sum). The same alkali metal-iodine distances in the phase $K_{0.58}Zr_6I_{14}C$ are somewhat long for typical K-I distances, averaging 3.976 Å compared

with the sum of 12-coordinate radii[74] at 3.80 Å. This, however, is reflected in the rather large thermal parameter (6.9 $Å^2$) associated with the potassium in this structure. Presumably, the size of this 'cesium' site is at least one reason that attempts to synthesize '$NaZr_6I_{14}C$' have been unsuccessful.

The lengths of the $Zr-I^i$ bond distances in all of these cluster-containing compounds are also what might be expected from the sum of six-coordinate crystal radii (2.92 Å),[74] ranging from an average of 2.862 (1) Å in $Zr_6I_{14}C$ to 2.898 (1) Å in $Zr_6I_{14}K$. The crystal radii above were derived from rather polar compounds, and some covalent shortening in these zirconium iodide clusters would be expected and is apparently observed. As seen in Table 5, a trend of increasing $Zr-I^i$ distances with increasing degree of reduction is observed for the series of carbon-containing clusters and this trend will be discussed later.

The bond distances that show the greatest contrast in these compounds are those most directly involved with the metal octahedra: Zr-Zr bonds, Zr-interstitial bonds, and the $Zr-I^a$ bonds. In the carbon-containing 6-14 clusters, there is a small decrease in the length of the Zr-Zr and Zr-C bonds and a small increase in the $Zr-I^a$ bond lengths as the clusters are reduced by one electron from $Zr_6I_{14}C$ to $CsZr_6I_{14}C$. On the transition to $Zr_6I_{12}C$, representing a further one-electron reduction, there is a marked decrease in the Zr-Zr and Zr-C bond lengths. The $Zr-I^a$ bonds are more difficult to compare as the difference in structure type dictates changes in the $Zr-I^a$ bonding that is found. It is important to note that the four $Zr-I^{a-a}$ bonds that are found in the 6-14

clusters are replaced by four $Zr\text{-}I^{a\text{-}i}$ bonds of significantly greater length in the 6-12 clusters. The effect of this difference will be discussed in conjunction with the theoretical model developed.

The Zr-Zr, Zr-interstitial, and $Zr\text{-}I^{a}$ bond lengths in the clusters containing atoms other than carbon vary widely. These changes in distances, as well as the relatively constant $Zr\text{-}I^{i}$ distances, can be understood to a first approximation from simple geometry by assuming the iodine positions remain essentially fixed by matrix repulsions, while the octahedron of zirconium atoms varies to accommodate the interstitial atom included in the cluster center. The application of this model means that the changes in Zr-interstitial distances and $Zr\text{-}I^{a}$ distances in two different clusters should be equal in magnitude and opposite in sign, i.e., d(interstitial-I^{a}) should be constant. (This distance only varies by ~0.08 Å.) The ratio of the differences in Zr-Zr distances to Zr-interstitial distances in an octahedron should ideally be $\sqrt{2}$. The $Zr\text{-}I^{i}$ distances should change by the product of the Zr-interstitial difference and one-half the average sine of the $I^{i}\text{-}Zr\text{-}I^{i}$ angles formed by I^{i}'s that are trans across the square plane of inner iodines bonded to the zirconium atom (Figure 6). Since these angles are between 155 and 170°, the $Zr\text{-}I^{i}$ distances change only slightly.

Applying this model to the two extremes of $Zr_6I_{14}C$ and $Cs_{0.3}Zr_6I_{14}Si$, one finds an average difference in Zr-Zr distances of 0.271 Å. Division of this number by root two gives an expected difference in the Zr-interstitial distances of 0.192 Å, comparing quite favorably with the 0.192 Å difference observed. The difference in $Zr\text{-}I^{a\text{-}i}$

distances is -0.235 Å, very nearly what is expected and the Zr-I^{i} distances vary by only 0.031 Å.

The only bond distances that do not follow this argument are the Zr-I^{a-a} distances that are only shorter by 0.07 Å in $Cs_{0.3}Zr_6I_{14}Si$ than in $Zr_6I_{14}C$. This is not well-understood. The intercluster bridging of these terminal iodines may be affected by the inclusion of or changes in alkali metal atoms. The addition or increasing size of alkali metal atoms results in a considerable lengthening in the $\vec{a}$ and $\vec{c}$ axes of the cell, as seen in Table I. Since these are the directions along which the Zr-I^{a-a} bonds bridge clusters in the cell, it may be expected that the Zr-I^{a-a} bonds are rather heavily influenced by changes in these axes. If one limits the geometric comparisons above to only cesium-containing phases, the geometric arguments more accurately predict the changes in Zr-I^{a} bond lengths.

From another viewpoint, the smaller changes in these Zr-I^{a-a} bonds may be related to the fact that they are already fairly short Zr-I distances. They range from 3.068 (2) to 3.195 (1) Å in the clusters that have been structurally characterized and these are not very different from the Zr-I distance predicted by the sum of crystal radii (2.92 Å).[14] These distances are significantly shorter than those of the Zr-I^{a-i} bonds that range from 3.256 (4) to 3.522 (2) Å. A possible rationalization for the smaller changes of Zr-I^{a-a} bond distances compared with Zr-I^{a-i} is that the former are for the most part perfectly satisfactory Zr-I distances and expansion of the zirconium octahedron is simply matched by an expansion of these iodine positions. The latter

bonds, being significantly longer than typical Zr-I distances, have more leeway to 'soak' up the expansion of the zirconium cluster in the form of more reasonable Zr-I^{a-i} distances.

Other comparisons between the distances of clusters occupied by different interstitials fare equally well. Of course, the effects of the additional alkali metal atom (and the structural change for $Zr_6I_{12}C$) perturb the geometry of the iodines somewhat and this simple argument does not hold rigorously. This model does serve very well to explain why the cell volumes of the 6-14 phases vary by only 3-4% (even when the effect on cell volume of the additional alkali metal atom is ignored) while the Zr-Zr distances change by nearly 8.5%, emphasizing the need for X-ray structural studies.

Cluster Bonding

While the argument illustrated above allows a simple rationalization of distance changes, it remains unsatisfying so far as an understanding of the rather remarkable range of the interstitial atoms successfully incorporated into these clusters. To gain a clearer understanding of the bonding in these systems, extended Hückel calculations on isolated clusters were conducted.

Unoccupied clusters

To understand the bonding of interstitial atoms in the center of the zirconium octahedra, it is first helpful to understand the bonding in the unoccupied octahedral cluster. Several theoretical studies of isolated $M_6X_{12}^{n+}$ (M = Nb or Ta; X = Cl or Br; n = 2, 3, or 4) clusters have

previously been reported.[12,13] As noted earlier, these group V metal halide clusters are isostructural with the $Zr_6I^i_{12}$ portion of clusters found during this investigation. In two of the better known studies, a group theoretical treatment of the molecular orbitals led to two different results.[12,13] Both used identical coordinate systems. The local coordinate system of each individual metal atom in the octahedron was chosen so that the z axis was defined by a vector from the metal to the center of the cluster. The x and y axes were orthogonal to the z axis and were directed towards the four bridging (inner) halides coordinated to each metal. With this choice of coordinates, the $d_{x^2-y^2}$ orbital of each metal was plausibly assumed to be used for metal-halide bonding, leaving the d_{z^2}, d_{xy}, d_{xz} and d_{yz} orbitals of each metal for metal-metal interactions. So that the molecular orbitals constructed from these four d orbitals can be easily distinguished, these will henceforth be denoted as (z^2), (xy), or (xz,yz). (The d_{xz} and d_{yz} orbitals form a degenerate pair in O_h symmetry.) Although the calculations done in the present investigation used a different coordinate system because of limitations of the program, to avoid confusion the molecular orbitals arising from symmetry-equivalent atomic orbitals will be identified as if the earlier coordinate system was used.

In the earlier calculations, two major assumptions were made to simplify the problem. First, the terminal halides were not included in the model because their effect on the bonding of the cluster was assumed to be unimportant. Secondly, the inner halogen pπ interactions with the various metal d orbitals were assumed to be equal. To the extent that

these assumptions are incorrect, the bonding schemes that arise from these models are also in error.

To determine the effect that the addition of terminal iodides has on the molecular orbitals, extended Hückel calculations[61] were carried out on both $Zr_6I_{12}^{2+}$ and $Zr_6I_{18}^{4-}$ clusters isoelectronic with 'Zr_6I_{14}'. Since the zirconium iodide clusters in the materials synthesized in this work do not exist as isolated Zr_6I_{12} units, some approximation of the bridging between clusters was deemed important. To accomplish this, a basic $Zr_6I_{18}X^{n-}$ (X = interstitial atom, if present; n = 4 or 6) cluster was chosen to represent the clusters occurring in the $Zr_6I_{14}X$ and $Zr_6I_{12}X$ phases, respectively. The additional six iodides were included to simulate the bridging iodines of other clusters. The assumption was made, and later found to be justified, that the valence levels of the terminal iodides would be lower in energy than the cluster orbitals derived from the zirconium 4d orbitals and that they would be preferentially filled. To simplify the results, idealized octahedral clusters were used. The atomic coordinates and orbital parameters used for these calculations are given in Appendix B.

The single electron energies resulting from these calculations are shown in Figure 10. The molecular orbital diagram of the $Zr_6I_{12}^{2+}$ cluster is shown on the left side of the figure. Although it would be desirable to isolate orbitals involved in Zr-I bonding from those that are simply iodine lone pairs, the high degree of mixing between orbitals, especially those involving iodine p contributions, makes this extremely difficult. When it is possible and of interest, the major contribution

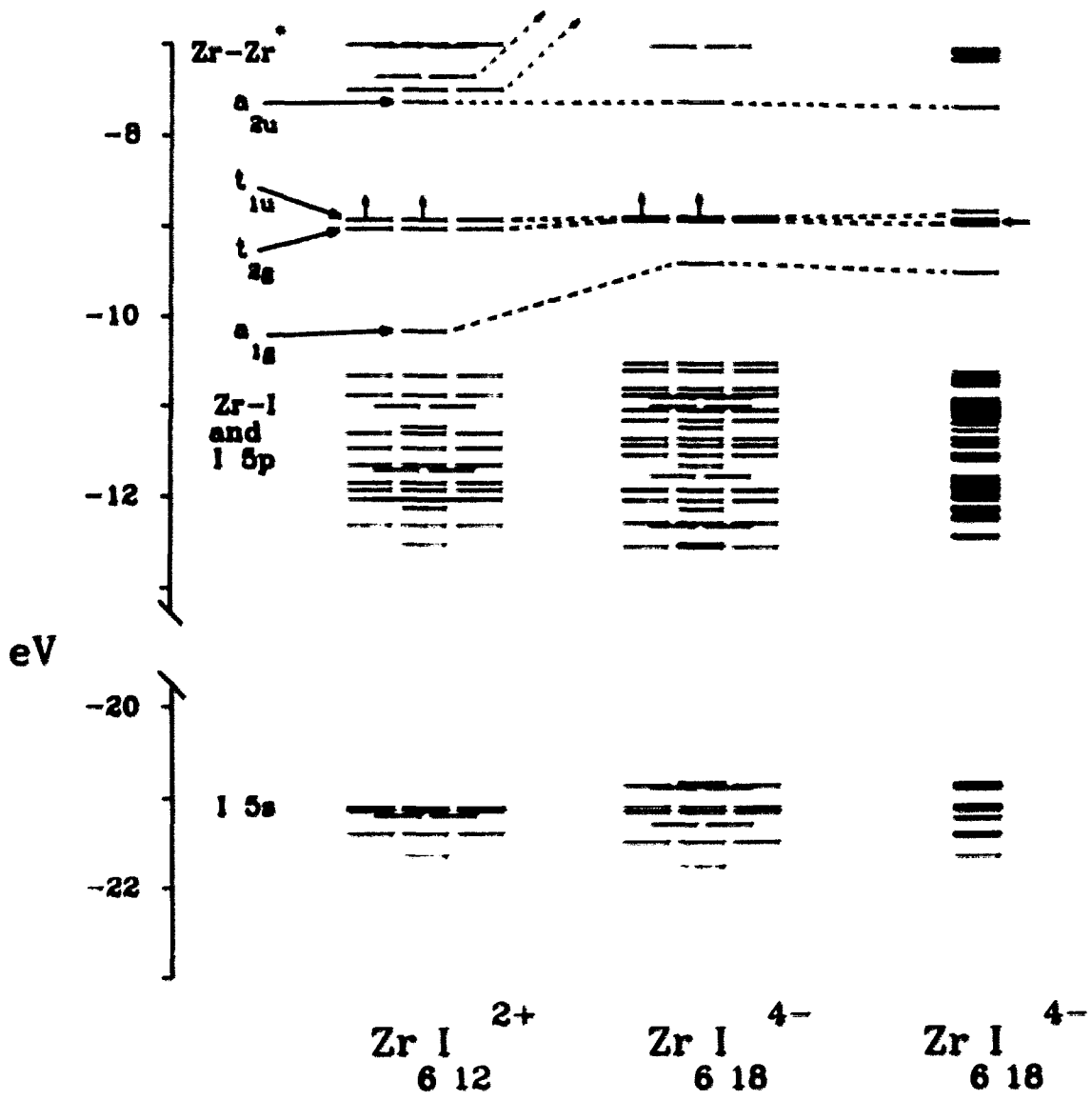

Figure 10. Molecular orbital diagrams from extended HUckel calculations with important Zr-Zr bonding orbitals labeled by symmetry. Idealized $Zr_6I_{12}^{+2}$ with O_h symmetry (left); idealized $Zr_6I_{18}^{4-}$ with O_h symmetry (includes 6 terminal iodides) (center); distorted $Zr_6I_{18}^{4-}$ with D_{2h} symmetry (right). HOMO is the t_{1u} set of O_h cluster with two electrons. HOMO of D_{2h} cluster is indicated with an arrow

to molecular orbitals is given, but it should be remembered that there are other minor, possibly significant, contributions to these orbitals. There is a block of 12 molecular orbitals between -21 and -20 eV that are comprised of combinations of the 12 iodine 5s orbitals, with little or no zirconium contribution. The next higher energy block of 37 molecular orbitals, occurring between -13 and -10.5 eV, are composed primarily of iodine 5p lone pairs and Zr-I bonding combinations, but one orbital of $a_{1g}(z^2)$ symmetry is almost exclusively involved in Zr-Zr bonding. The next seven orbitals are also primarily involved in Zr-Zr bonding. Together with the low-lying a_{1g} orbital, there are eight Zr-Zr bonding molecular orbitals that would be filled in a hypothetical 16 electron cluster like $Nb_6I_{12}^{2+}$. In order of increasing energy, these Zr-Zr orbitals correspond to the irreducible representations (O_h symmetry): $a_{1g}(z^2)$, $t_{2g}(xz,yz)$, $t_{1u}(xz,yz)$, and $a_{2u}(xy)$, and these are labeled in Figure 10. These orbitals agree closely with those reported by Cotton and Haas,[12] although the order of the orbitals is different and stated to be in error by Mingos.[14] An assignment of the aqueous electronic spectra of the niobium and tantalum 6-12 clusters above led Robbins and Thomson to derive a somewhat different bonding scheme.[13] The bonding orbitals assigned in their study are $a_{1g}(z^2)$, $t_{1u}(xz,yz)$, $t_{1u}(z^2)$, and $a_{2u}(xy)$, in increasing energy. The axially directed $e_g(z^2)$ and $t_{1u}(z^2)$ are observed in the molecular orbital diagram of $Zr_6I_{12}^{2+}$, but at a slightly higher energy (-7.5 eV) than the eight bonding orbitals given, as seen in Figure 10. Without considering the effect of the terminal ligands, Robbins and Thomson argued that crystal field interactions

would stabilize the $t_{1u}(z^2)$ orbitals. While the reordering of the $t_{2g}(xz,yz)$ and $t_{1u}(z^2)$ orbitals may seem at least reasonable in the $M_6X_{12}^{n+}$ clusters, the effect of interactions with the six terminal halides makes this highly improbable.

As seen in the center of Figure 10, the inclusion of the six terminal iodides strongly affects the three Zr-Zr orbitals originating from the d_{z^2} orbitals: $a_{1g}(z^2)$, $e_g(z^2)$, and $t_{1u}(z^2)$. The six iodine orbitals that are constructed from the p_z orbitals of the terminal iodines also transform as a_{1g}, e_g, and t_{1u}. They interact quite strongly with the (z^2) Zr-Zr set to form Zr-I^a bonding orbitals below the primarily Zr-Zr bonding orbitals, and Zr-I^a antibonding/Zr-Zr bonding combinations at higher energy. While the $a_{1g}(z^2)$ Zr-I^a antibonding/Zr-Zr bonding combination does move to higher energy, it remains as the lowest Zr-Zr bonding orbital at -9.96 eV. Because of similarly strong σ interactions, the other two Zr-I^a antibonding orbitals (that would also be Zr-Zr bonding) are found off scale at energies several eV above what they were in the cluster without the terminal iodines, and it is doubtful that they could be involved in metal-metal bonding. Similar results have been previously reported for the antibonding interactions in the e_g and t_{1u} molecular orbitals of the metal (z^2) set with the p_z orbitals of terminal ligands in octahedral $Mo_6Br_8^{4+}$ clusters.[76] There are also slight increases in energies of the Zr-Zr $t_{2g}(xy,zy)$ and, to a lesser extent, in the $t_{1u}(xy,yz)$ orbital upon the inclusion of the six terminal iodines because of some π antibonding interactions of these Zr-Zr bonding orbitals with the terminal iodine p_x,p_y set. Similar

destabilizing effects on the Mo-Mo $t_{2g}(xz,yz)$ and $t_{1u}(xz,yz)$ orbitals are seen in the molybdenum cluster study cited above.[78] The metal-metal bonding scheme resulting from the inclusion of the six terminal iodines is much more peripheral in nature than that proposed by Robbins and Thomson,[13] as the $t_{2g}(xz,yz)$ orbitals are more or less centered on the faces of the octahedron in contrast to the axially directed $t_{1u}(z^2)$ orbitals.

While the symmetry of the unoccupied clusters used for the calculations here are ideally octahedral, the symmetry found for the cluster in $Zr_6I_{14}C$ is actually C_{2h}. To simplify the calculation somewhat, the observed geometry was altered slightly to give the higher D_{2h} symmetry. The distortion of the cluster from O_h to the appropriate D_{2h} symmetry results in a molecular orbital diagram for $Zr_6I_{18}^{4-}$ (D_{2h}) that is shown on the right side of Figure 10. The distortion has little effect, except that the degeneracy of many orbitals, imposed by O_h symmetry, is removed. However, orbitals that belong to these previously degenerate sets differ in energy only slightly, in no case by more than 0.1 eV. This distortion to lower symmetry will be discussed later. The Zr-Zr bonding orbitals transform in D_{2h} symmetry as a_{1g}, b_{1g}, b_{2g}, b_{3g}, b_{1u}, b_{2u}, b_{3u}, and b_{1u}, but to simplify discussion of these orbitals they will continue to be referred to in their O_h-equivalent description unless otherwise noted.

To check the effect of lower zirconium 4d orbital energies on the results of the extended Hückel calculations, the zirconium 4d orbital energies were changed from -8.30 to -9.30 eV for a $Zr_6I_{18}^{4-}$ (D_{2h})

cluster. Although the charges on the atoms changed because of greater zirconium participation in bonding, the order of the resulting molecular orbitals did not vary.

Nonmetal-centered clusters

The compound chosen as a model for the initial extended Hückel calculations of nonmetal-centered clusters was $Zr_6I_{14}C$. The cluster used to represent an isolated unit in this compound, as described above, was $Zr_6I_{18}C^{4-}$. The coordinates of atoms in the clusters and the parameters used to describe the energy and radial extension of atomic orbitals are given in Appendix 8.

The results of the calculations are shown in Figure 11. The molecular orbital diagram of the distorted (D_{2h}) but unoccupied $Zr_6I_{18}^{4-}$ cluster is shown on the left. The inclusion of a carbon atom in the center of the Zr octahedron results in a considerable interaction of the carbon 2s (a_{1g}) and 2p (t_{1u}) orbitals with Zr-Zr bonding orbitals of like symmetry, giving rise to four rather strongly bonding orbitals at lower energy and four antibonding orbitals at higher energy. Not surprisingly, the three a_{1g} orbitals that result from the interaction of the carbon 2s and the two Zr-I^a a_{1g} (z^2) orbitals undergo considerable rehybridization. The low-lying (-22.8 eV) a_{1g} is comprised mostly of carbon 2s with some zirconium d_{z^2} contribution, but little or no terminal iodine p_z component. The a_{1g} orbital that arises from the terminal iodine p_z orbitals no longer interacts significantly with the zirconium $a_{1g}(z^2)$ orbital and is essentially a nonbonding set at

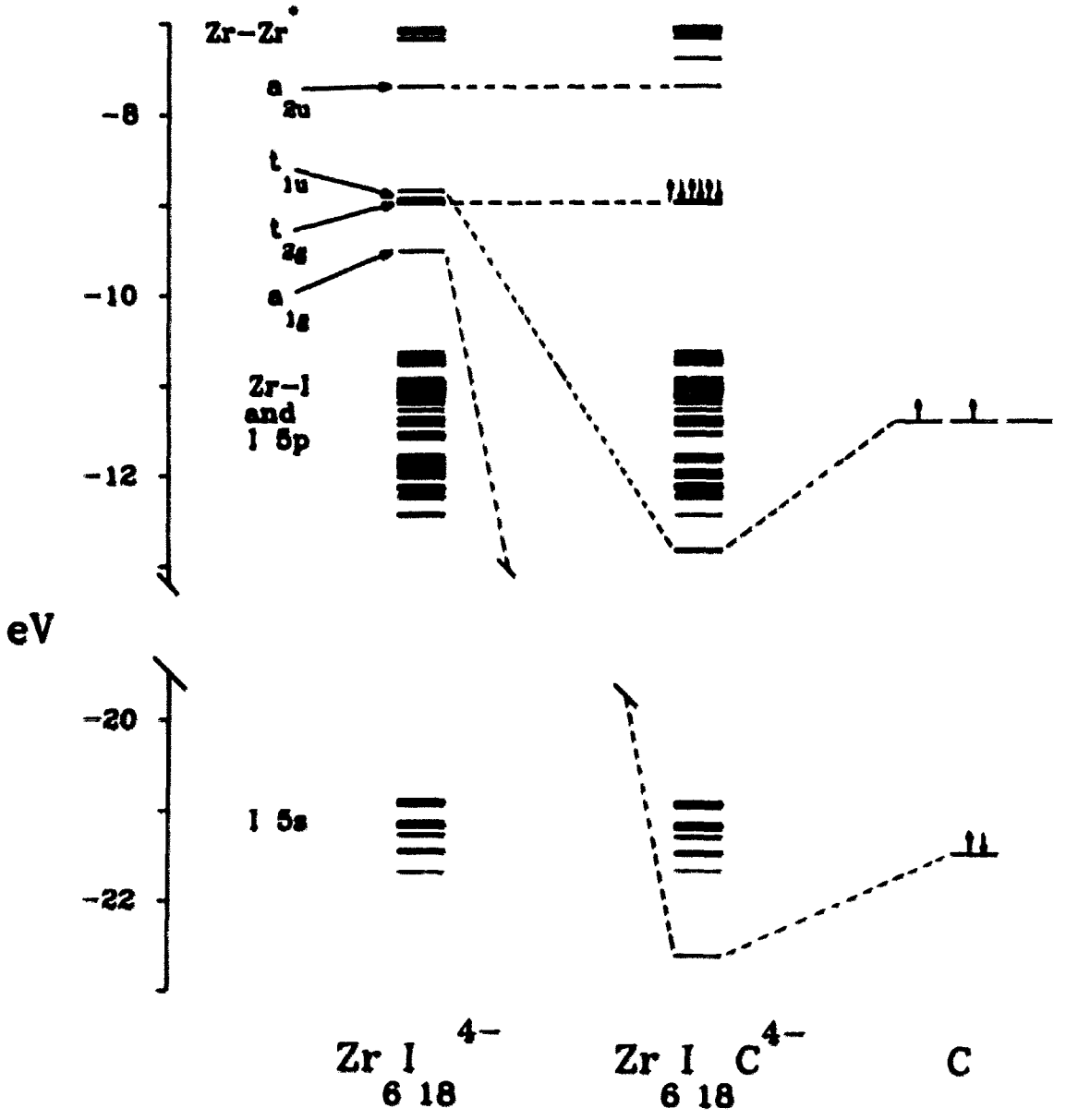

Figure 11. Molecular orbital diagrams from extended HUckel calculations. $Zr_6I_{18}^{4-}$ with D_{2h} symmetry (left); atomic C (right); $Zr_6I_{18}C^{4-}$ with D_{2h} symmetry (center). Orbital labels refer to reducible representations in O_h symmetry. The carbon 2s and 2p orbitals interact with the Zr-Zr a_{1g} and t_{1u} orbitals, respectively, resulting in four Zr-C bonding orbitals. The HOMO of $Zr_6I_{18}C^{4-}$ is the fully occupied t_{2g} set

-11.5 eV. The other a_{1g} combination of the three original orbitals is Zr-C antibonding and occurs at very high energy. The Zr-C interactions between the zirconium $t_{1u}(xz,yz)$ set and the carbon p orbitals is largely π in character (though not entirely because of mixing that occurs) and again has little or no contribution from the terminal iodine orbitals. The result is, as shall be noted later, that changes in the Zr-I^a distances have little or no <u>direct</u> effect on Zr-C bonding.

The effect of the inclusion of the carbon atom is that the carbon 'donates' its valence electrons to the bonding cluster MO's, affecting the energies but not the number of bonding orbitals. While this 'donation' is useful in electron counting schemes, this should <u>not</u> be inferred as a charge transfer. Rather the bonding is quite covalent, with somewhat more carbon 2s and 2p contribution to the four new orbitals formed, so that the charge on the carbon derived from the extended Hückel calculations is about -1.8. Though this charge is probably an exaggeration, it most certainly is correct in sign. The stabilizing effect of the interstitial carbon here then is the strong interaction of the s and p orbitals with a subset of the Zr-Zr cluster orbitals.

With the plausible assumption that the iodine valence band is filled, there are 14 electrons in $Zr_6I_{14}C$, 15 in $CsZr_6I_{14}C$, and 16 in $Zr_6I_{12}C$ available from the carbon, zirconium, and alkali metal for cluster bonding. These cluster electrons fill the 7th (through t_{2g} in Figure 11) and 8th (a_{2u}) bonding cluster orbitals generated by the Zr-Zr and Zr-C interactions. The effect of the reduction is a decrease in the average Zr-Zr bond distances from 3.309(3) Å in $Zr_6I_{14}C$ to 3.283(2) Å

in $CsZr_6I_{14}C$, and a slight increase in the Zr-I^a distances in the same clusters. As noted earlier, there is a rather large decrease in the Zr-Zr bond distances to 3.195(2) Å upon the further reduction in $Zr_6I_{12}C$. The total number of electrons involved in the bonding of these carbide clusters are exactly the same as are involved in metal-metal bonding of the group V metal clusters $M_6X_{12}^{n+}$, where n = 4, 3, and 2. Trends in bond distances previously observed in isolated $Nb_6Cl_{18}^{n-}$ cluster anions[9] are similar to those found in the carbon-containing zirconium clusters above. However, the changes in distances from the most oxidized to the most reduced niobium clusters are continuous, and the discontinuity in metal-metal distances between the 15- and 16-electron clusters (seen on comparing $CsZr_6I_{14}C$ with $Zr_6I_{12}C$) is not observed. Presumably the a_{2u} molecular orbitals that are being filled with the 15th and 16th electrons are correspondingly similar and the dramatic changes of Zr-Zr distances in the zirconium carbide clusters above are related to the change in structure.

It is interesting to note that for $Zr_6I_{12}C$ all Zr-Zr bonding orbitals derived for an ideal octahedron are filled and that indeed the cluster is very close to O_h symmetry. This, however, appears not to be solely the result of the number of electrons involved. The 16-electron clusters in Ta_6I_{14}[10] and Nb_6Cl_{14}[9] show the same tetragonal 'compression' that is found in the 6-14 carbide clusters reported here that contain one or two fewer electrons, while the clusters in $Nb_6Cl_{18}^{2-}$,[79] Ta_6Cl_{15},[11] Ta_6I_{15},[60] and $K_4Nb_6Cl_{18}$[61] (containing 14, 15, 15, and 16 cluster electrons, respectively and either symmetric or no bridging terminal halides)

all demonstrate close to octahedral symmetry. Within the 14- to 16-electron range, the number of electrons involved in metal-metal bonding has little effect on the distortions observed for some clusters.

To determine the effect on metal-metal bonding of the rather anisotropic sharing of the I^a's in the 6-14 phases compared to that in the 6-12, 6-15 or 4-6-18 type phases (where all terminal halides are X^{a-i}, X^{a-a} or X^a, respectively), extended Hückel calculations were done for both unoccupied and carbon-centered clusters similar in geometry to the $Zr_6I_{18}^{4-}$ (O_h) cluster discussed above. The Zr, C, and I^i positions were left unchanged in the new clusters, but the four I^{a-a} were replaced with I^{a-i} at longer Zr-I^a type distances to represent the bridging in Zr_6I_{12}-type structures, or the two I^{a-i} were replaced with I^{a-a} at shorter distances as in the M_6X_{15}- and $M_6X_{18}^{n-}$-type structures. Analysis of the atomic orbital contributions to molecular orbitals in the two calculations shows rather conclusively that these shorter Zr-I^a distances in the latter correspond to a greater Zr contribution to the Zr-I^a bonding and a corresponding decrease in contribution to the Zr-Zr bonding, leading to the observed distortion. Conversely, longer Zr-I^a distances represented a smaller zirconium contribution to orbitals involving Zr-I^a bonding and correspondingly larger zirconium contributions to Zr-Zr bonding orbitals, as seen in the smaller $Zr_6I_{12}C$ cluster. In calculations of this sort for unoccupied clusters, the change in Zr-Zr bonding was found almost exclusively in the Zr-Zr $a_{1g}(z^2)$ orbital. The inclusion of carbon in the clusters changes this scheme rather dramatically. The Zr-C $a_{1g}(z^2)$ orbital (because

there is no I^a contribution to this orbital) is unaffected by differences in Zr-I^a bonding, and the changes in Zr-Zr bonding are more diffuse but still evidenced by the differences in reduced overlap populations of Zr-Zr interactions. In $Zr_6I_{12}C$, where the Zr-I^{a-i} bonds are all the same length and significantly longer than the Zr-I^{a-a} bonds in 6-14 clusters, not only is a more symmetric cluster observed, but also one that has stronger Zr-Zr and Zr-C bonding judging from the shorter distances there. While not explicitly predicted by the calculations, a synergistic increase in Zr-C interactions must result from the increase in Zr-Zr bond strength and the decrease of Zr-Zr distances. One may expect, then, that 14 to 16 electron clusters that have only one type of terminal ligand will have metal cores that are nearly octahedral. Clusters that have more asymmetric terminal ligands will show distortions because of differences in metal-terminal ligand and metal-metal bonding. Such a distortion has previously been reported in the 6-8 cluster $Mo_6Br_{12}\cdot 2H_2O$.[76]

The observation that cluster geometry is strongly affected by Zr-interstitial bonding led to consideration of other interstitials that would allow between 14 and 16 bonding electrons and possess crystal radii that would allow for both good Zr-interstitial and Zr-I^i bonding. The maximum crystal radii was approximated by using a typical 6-14 cluster, expanding the zirconium positions outward to the center of the square plane of coordinated inner iodines and then calculating the resulting distance from the zirconium atom to the center of the cluster. By subtracting crystal radius of zirconium from this distance, an

approximate maximum interstitial crystal radius of 2.0 Å was obtained. Another way of visualizing this process uses the layered description of these clusters. Since the cluster forms around a 'vacant' iodine position in a close-packed layer, one obtains the same result if the zirconium atoms are returned to their ideal octahedral sites between the layers and an additional iodine atom is included in the center of the cluster!

Three clusters with 'nonmetal' interstitials have been structurally characterized, $CsZr_6I_{14}B$, $Cs_{0.5}Zr_6I_{14}Si$, and $Cs_{0.7}Zr_6I_{14}Al$. These clusters support the interstitially dominated model described above. The increased Zr-Zr bond distances for these clusters can be understood for the most part by the simple geometric requirements of the larger interstitial that are imposed on the cluster, as noted earlier.

Interesting observations can be made for these clusters concerning the crystal radii obtained for the interstitial atoms. By subtracting the six-coordinate Zr^{4+} radius (0.86 Å[77]) from the Zr-C distances in the carbon-containing clusters, one obtains an effective crystal radius for the interstitial carbon. The carbon radius obtained in this way for the clusters synthesized here are found in Table 5. The radius for the interstitial carbon in the 6-14 clusters match very well the radius obtained as an average from a number of rock-salt transition metal carbides[62] (1.46 Å). Only in $Zr_6I_{12}C$ is there much of a discrepancy between the observed crystal radius for the interstitial carbon (1.40 Å) and that found in the rock-salt carbides, and as discussed above, this is probably because of the reduction in the Zr-I^a bonding and the increase in Zr-Zr

and Zr-C bonding related to the crystal structure. (This would not occur in a NaCl-like arrangement.)

In the boron-containing cluster, the average Zr-B distance is 2.382 (1) Å, compared with a similar value of 2.339 (2) Å for the isoelectronic $Zr_6I_{14}C$. The crystal radius of the boron in $CsZr_6I_{14}B$, as determined in the carbon-centered clusters, is 1.52 Å. Difficulty in comparing this radius with that in other borides is encountered because of B-B bonding that is present in these phases. The changes in Zr-I^a distances between $Zr_6I_{14}C$ and $CsZr_6I_{14}B$, however, do not conform to the previously described simple geometric arguments as well. The Zr-I^{a-i} distances in the $CsZr_6I_{14}B$ cluster are 0.07 Å less than those in the isoelectronic $Zr_6I_{14}C$, a difference that is large compared to the change in interstitial sizes. On the other hand, the Zr-I^{a-a} distances in the boride cluster are 0.039 (1) Å longer than those in $Zr_6I_{14}C$, contrary to the shortening expected by the geometric model. This may be because of the influence of the cesium atom that is bonded to the I^{a-i} at a distance of 3.860 (1) Å, and the lengthening of the $\vec{a}$ and $\vec{c}$ axes because of the added cesium. These differences may also be caused by some undetermined electronic aspect of the Zr-B interactions compared to Zr-C bonding.

The effect on the geometry of the cluster by the inclusion of a Si atom is very impressive indeed and fits quite well with the geometric arguments outlined earlier. The average Zr-Si distance of 2.531 (2) Å results in a crystal radius for the interstitial silicon of 1.67 Å. The crystal radius of isolated silicon in the compound Ca_2Si (anti-$PbCl_2$)[83]

is 1.89 Å. The reason for the 0.22 Å difference in crystal radii from these two compounds is not fully understood, but may be the result of increased covalency of the bonding in the cluster, compared with that in Ca_2Si. The Zr-Zr bond distances now average 3.580 (3) Å, and must be considered as fairly weak interactions. The $Zr-I^{a-i}$ distances are also markedly shorter here, and if one considers the layered nature of these structures, the zirconium atoms would now be much closer to the 'ideal' octahedral coordination.

The expansion of the zirconium octahedron in $Cs_{0.7}Zr_6I_{14}Al$ is somewhat smaller than had been expected on the basis of the silicon-containing structure above, and the difference found between the carbon- and boron-containing clusters discussed earlier. In this aluminum-centered cluster, the average Zr-Al distance is only 2.416 (3) Å, fully 0.11 Å less than the Zr-Si distance in the structure above. While this distance is slightly larger than that of the boron-centered cluster, the difference is almost negligible compared with the difference that occurs between the carbon- and silicon-centered clusters.

To gain an understanding of the bonding in clusters containing interstitials other than carbon, extended Hückel calculations of the boron-, silicon-, and aluminum-centered clusters were conducted with the same treatment of terminal iodines. Appendix B gives the coordinates of the atoms in these clusters and the orbital energies and exponents used.

The bonding scheme that results from these calculations is very similar to that found for the carbon-containing clusters. The valence s and p orbitals of the nonmetal interact with the $a_{1g}(z^2)$ and $t_{1u}(xz,yz)$

bonding orbitals to give four Zr-interstitial bonding orbitals at energies below the remaining Zr-Zr bonding orbitals. However, some differences among the nonmetal-centered clusters are observed. The molecular orbitals that are primarily involved in Zr-Zr and Zr-interstitial bonding are shown in Figure 12. It is quite clear from the figure that as the nonmetal becomes increasingly electropositive, the energies of the molecular orbitals that have nonmetal contributions increase. This rise in energy is primarily caused by the higher energies of the valence orbitals of the nonmetals involved. The valence orbital energies of many post-transition elements are given in Table 14. As these valence energies increase, the nonmetal contributions to the four Zr-interstitial bonding orbitals decreases and the zirconium contribution to these orbitals increases. The results of these changes are quantified in Table 15.

It is quite clear from an inspection of Table 14 that the valence s orbitals of carbon, boron, and silicon are at an energy considerably below the zirconium a_{1g} orbital (-10 eV) in the empty cluster with which they interact. Because of this difference in energy, the resulting Zr-interstitial a_{1g} orbital is primarily interstitial in character. Quantitatively, the degree of interstitial character of this molecular orbital can be assessed by the charge matrix element corresponding to the interstitial s orbital contribution to the a_{1g} Zr-interstitial molecular orbital. The charge matrix elements for $Zr_6I_{14}C$, $CsZr_6I_{14}B$, and $Cs_{0.3}Zr_6I_{14}Si$ show that the a_{1g} molecular orbitals are between 70 and 76% interstitial s in character. A similar treatment of the valence p orbitals of boron, carbon, and silicon shows that they are at energies

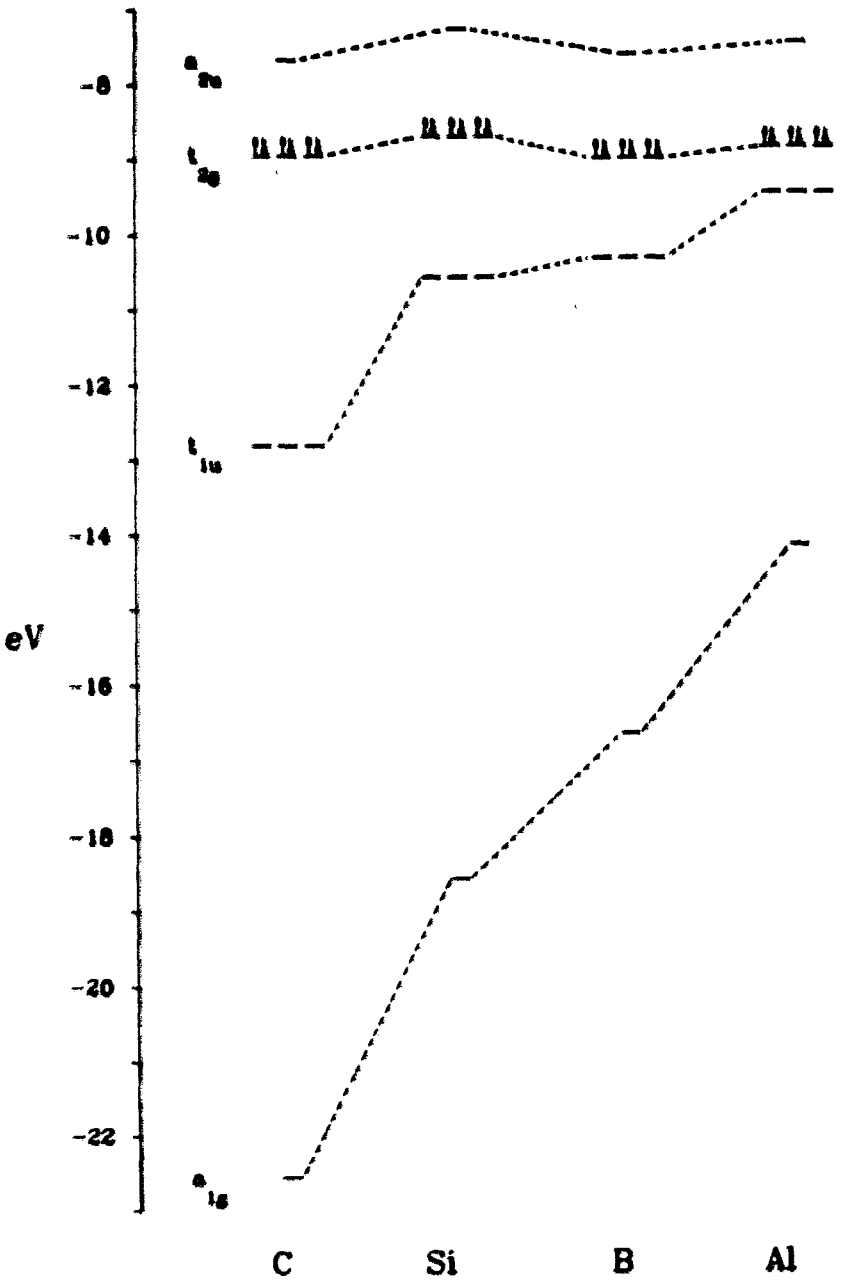

Figure 12. Molecular orbital diagram of Zr-Zr and Zr-interstitial bonding orbitals of fourteen electron $Zr_6I_{18}X^{n-}$ clusters with the interstitials noted. The orbital labels refer to irreducible representations in O_h symmetry. In each cluster the HOMO is the fully occupied t_{2g} set

Table 14. Valence orbital ionization energies (eV)[a]

	B	C	N	O
2s	-15.2	-21.4	-26.0	-32.3
2p	- 8.5	-11.4	-13.4	-14.8
	Al	**Si**	**P**	**S**
3s	-12.3	-17.3	-18.6	-20.0
3p	- 6.5	- 9.2	-14.0	-13.3
	Ga	**Ge**	**As**	**Se**
4s	-14.58	-18.6	-16.2	-20.5
4p	- 6.8	- 9.4	-12.2	-14.4
	In	**Sn**	**Sb**	**Te**
5s	-12.6	-16.2	-18.8	-20.78
5p	- 6.2	- 8.3	-11.7	-14.8

[a]Ref. 61.

Table 15. Selected details from extended Hückel calculations of 14-electron clusters

	Charge on interstitial	Average Zr-Zr distance	Occupation of interstitial p orbital in Zr-interstitial t_{1u}	Occupation of interstitial s orbital in Zr-interstitial a_{1g}	Zr-Zr reduced overlap population[a]
$Zr_6I_{14}C$	-1.8	3.309	1.24	1.52	0.128
$CsZr_6I_{14}B$	-1.2	3.366	0.85	1.39	0.144
$Cs_{1.3}Zr_6I_{14}Si$	-0.6	3.580	0.81	1.46	0.107
$Cs_{0.7}Zr_6I_{14}Al$	+0.1	3.417	0.53	1.14	0.163
$Zr_6I_{14}K$[b]	+0.3	3.448	0.06	0.11	0.174

[a]The average sum of the overlap of atomic orbitals on pairs of adjacent zirconium atoms for all occupied molecular orbitals.

[b]11 cluster electrons.

roughly equal to that of t_{1u} set (-9 eV) with which they interact. Analysis of the charge matrices from the extended Hückel calculations of clusters containing these atoms show that the resulting Zr-interstitial t_{1u} set is 41, 42, and 61% interstitial p in character for $Cs_{0.3}Zr_6I_{14}Si$, $CsZr_6I_{14}B$, and $Zr_6I_{14}C$, respectively. The high degree of interstitial character in the four Zr-interstitial bonding orbitals results in calculated charges on carbon, boron, and silicon of -1.8, -1.2, and -0.6, respectively. Admittedly, these charges are probably somewhat exaggerated.

For the cluster $Cs_{0.7}Zr_6I_{14}Al$, the contribution of interstitial orbitals to the bonding is considerably less. For aluminum, the 3s and 3p orbitals lie at -12.3 and -6.5 eV, respectively. Because the 3s orbital is at about the same energy as the Zr-Zr a_{1g} orbital (in contrast to the interstitials discussed above), the resulting a_{1g} Zr-Al orbital is only 57% aluminum in character. Similarly, the energy difference between the aluminum 3p orbitals and the Zr-Zr t_{1u} set results in an aluminum 3p contribution of only 27% to the bonding molecular orbitals. As a result, the charge on the aluminum atom, as obtained from these calculations, is slightly positive, +0.1. Apparently, the lower mixing of aluminum orbitals into the bonding set is responsible for the contraction of its orbitals, compared with the negatively charged interstitial atoms in other clusters, and accounts for the shorter-than-expected Zr-Al bonds found for this cluster. To the degree that this is true, the crystal radius that is found for aluminum in this cluster may be more appropriate for an Al^{1+} than a negatively charged aluminide!

The quantification provided by the extended Hückel calculations of the nonmetal-containing clusters also demonstrates some interesting features concerning the degree to which Zr-interstitial bonding dominates the geometry of these clusters. In Table 15, the average Zr-Zr reduced overlap population per Zr-Zr bond is given for each of the 14-electron clusters containing a nonmetal. The reduced overlap population is a measure of the bonding interaction between two atoms and was obtained by assuming that the highest occupied molecular orbital was the Zr-Zr $t_{2g}(xz,yz)$, i.e., 14-cluster electrons.

The Zr-Zr reduced overlap populations are primarily affected by three factors. The reduced overlap population decreases with increasing Zr-Zr distances in the clusters, increasing degree of nonmetal contribution to the a_{1g} and t_{1u} Zr-interstitial bonding orbitals and increased interactions of the remaining Zr-Zr bonding orbitals with terminal iodides, as previously discussed. As seen in Table 15, the cluster with the least remaining Zr-Zr bonding is $Cs_{0.3}Zr_6I_{14}Si$. This is not unreasonable considering the very long Zr-Zr distances, the fairly short Zr-I^a distances and the degree of interaction between the silicon and the zirconiums. The relatively low Zr-Zr overlap population of the $Zr_6I_{14}C$ cluster may also be expected because of the high carbon character of the Zr-C bonding orbitals. While the Zr-Zr bond lengths are greater in $CsZr_6I_{14}B$ than in the isoelectronic carbon-centered cluster, the lower boron contribution to the Zr-B orbitals results in an average Zr-Zr reduced overlap population that is slightly greater than in $Zr_6I_{14}C$. Of the nonmetal-centered clusters studied, the one with the greatest amount

of remaining Zr-Zr bonding is $Cs_{0.7}Zr_6I_{14}Al$, having an average Zr-Zr reduced overlap population of 0.163.

To give some perspective of the degree to which Zr-Zr bonding is lost (in favor of Zr-interstitial bonding), the average Zr-Zr reduced overlap population of a hypothetical, unoccupied, 14-electron zirconium cluster (with Zr-Zr bond distances equal to those in $Zr_6I_{14}C$) is 0.311. Although this is a somewhat arbitrary standard, it is clear that, compared with unoccupied clusters, the Zr-Zr bonding is of secondary importance in clusters containing interstitial atoms with s and p valence orbitals at energies conducive to strong Zr-interstitial interactions. Even in the 16-electron cluster of $Zr_6I_{12}C$, the Zr-Zr reduced overlap population is only 0.166, again indicating the extent to which Zr-Zr bonding is lost. On the other hand, the cluster is not held together only by Zr-interstitial bonding either.

The model of bonding that emerges from these calculations is rather different than what has been presented earlier, especially the impression gained from the ORTEP drawings shown in the previous figures. Instead of these clusters being stabilized by very strong Zr-Zr bonds, the dominant bonding role seems to be that of Zr-interstitial and Zr-I interactions that are augmented by rather weak Zr-Zr bonding. Figure 13 shows the same view of atomic positions that was shown earlier in Figure 6, but the bonds have been drawn differently to more closely conform to this interstitially dominated model.

An inspection of Table 14 demonstrates that most of the post-transition elements have s and p orbital energies that are in the range

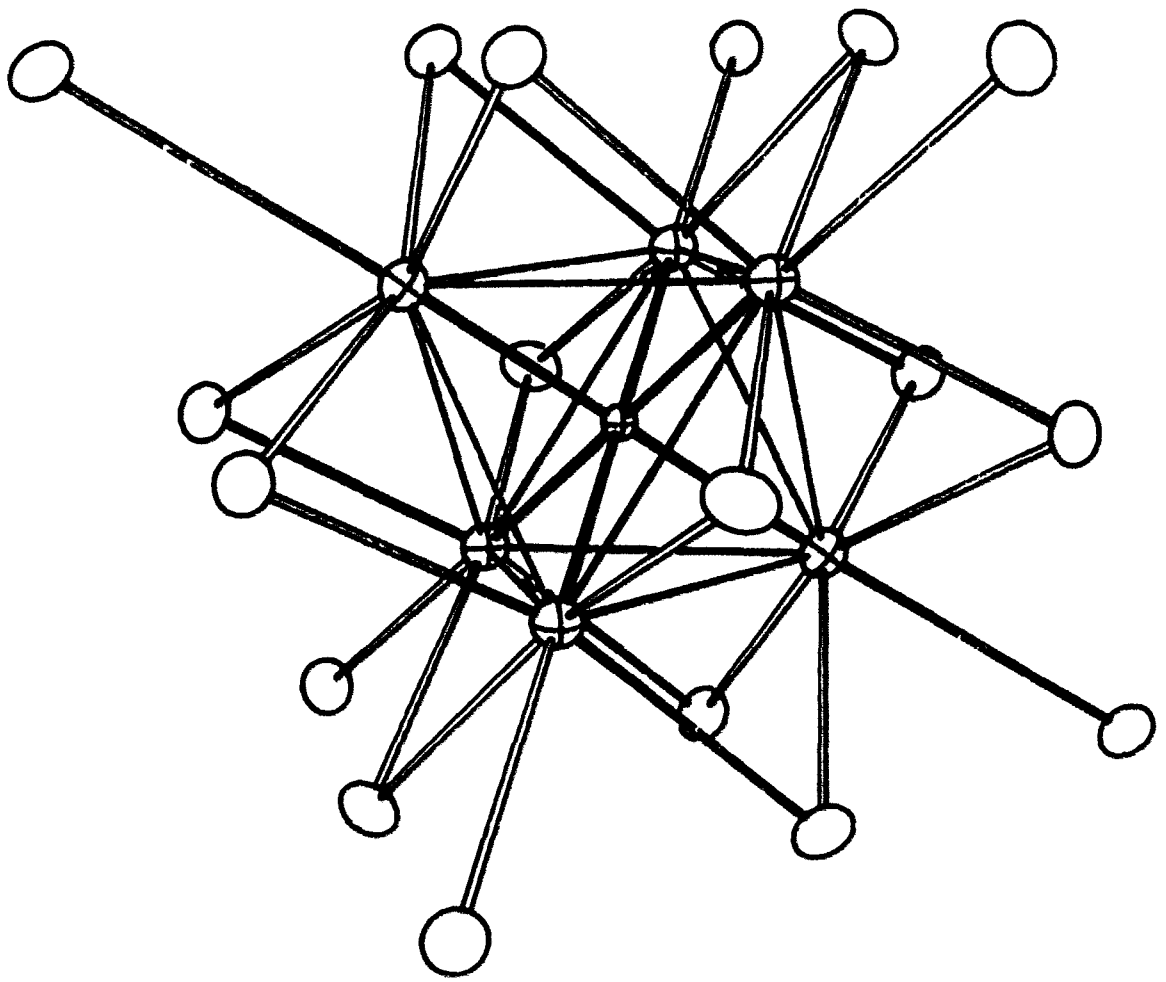

Figure 13. An ORTEP drawing of a $Zr_6I_{18}X$ cluster more accurately reflecting the strong Zr-interstitial bonding than clusters shown in Figure 6. Iodine (open ellipsoids); zirconium (larger crossed ellipsoids); interstitial (smaller crossed ellipsoids)

suitable for good cluster-interstitial bonding, but many as yet remain untried. Included in those that have been attempted are oxygen and nitrogen, as outlined in the RESULTS chapter. While the energies of the 2s and 2p orbitals would be appropriate for strong Zr-interstitial interactions, the radii of these atoms is so small that the Zr-I interactions are apparently reduced to the point that the compounds are not stable. It is interesting to note that nitrogen-centered clusters are known for the zirconium chloride and scandium chloride systems[25,74,75] (as are clusters that contain carbon and boron) where the matrix effect caused by the chloride is much smaller. Attempts to include the larger silicon and aluminum atoms in the centers of zirconium chloride clusters have been thus far unsuccessful,[75] again presumably due to dominant Zr-interstitial requirements that combine unfavorably with the Zr-Cl bonding. There is one reported nitrogen-centered cluster in the rare earth metal halide systems Gd_2Cl_3N.[64] But here the nitrogen is located in a smaller tetrahedral cluster of gadolinium. Similar size arguments can be invoked to account for the occurrence of dimeric carbon units instead of isolated carbon atoms in the much larger octahedral clusters that have been reported in the rare earth metal halides.[23,24]

Thus far, no M_6X_{12}-type cluster has been synthesized in the group V halides or for these interstitial-containing zirconium clusters that contain interstitial atoms where more than 16-cluster electrons are found in the MO's derived from M-M or M-interstitial interactions. While this 16-electron upper limit may provide a guide for clusters that are likely to be synthesized, it is noted that the gap between the calculated HOMO

and LUMO in the 16-electron carbon-centered clusters studied here is small, about 0.5 eV.

Alkali metal-centered clusters

The bond distances in the alkali metal clusters $Zr_6I_{14}K$ and $Zr_6I_{14}K_{0.46}$ for which crystal structures have been refined also fit quite well into the simple geometric model noted earlier. The Zr-Zr bonds are markedly longer in both clusters than the isostructural carbide cluster. The interstitial crystal radius that is obtained for the potassium atom in the fully occupied crystal (1.58 Å) is very close to the crystal radius for a six-coordinate K^+ at 1.56 Å.[77] As might be expected from the simple geometric model above, the Zr-I^i distances of these potassium-centered clusters are very close to those for the carbon-centered clusters. The Zr-I^{a-i} distances of the potassium-centered clusters are somewhat shorter than the same bonds in the carbide clusters, again following simple geometric arguments. Zr-I^{a-a} bond distances, however, are only marginally shorter than those in $Zr_6I_{14}C$, possibly because of factors discussed earlier.

There are some slight differences between the fully and partially occupied clusters potassium-centered that are noteworthy. First is the somewhat longer Zr-Zr distances in the fully occupied cluster. In conjunction with this difference, there is an observable elongation of the zirconium thermal ellipsoids along all the K-Zr axes of the partially occupied cluster that is not seen in $Zr_6I_{14}K$. These differences may be thought of in terms of a relaxation of the Zr positions around unoccupied

clusters in $Zr_6I_{14}K_{0.46}$. The Zr-I^a bond distances also show an unexpected change. The fully occupied cluster has significantly longer Zr-I^{a-i} and Zr-I^{a-a} distances than the partially occupied cluster, exactly opposite of what is expected from simple geometric arguments.

To describe the bonding in these clusters containing alkali metal atoms, the model derived above for nonmetal-centered clusters cannot be applied directly because the s and p orbitals for the alkali metal atoms are at considerably higher energy than for any of the nonmetals discussed earlier. Thus, the formation of low-lying Zr-K bonding molecular orbitals does not occur.

To investigate the bonding in these materials, an additional extended Hückel calculation was initiated. In addition to the original program described,[60] a second program was used that allowed for reiterative calculations in which the valence orbital energies of all atoms varied as a function of the calculated charge until self-consistency was attained.[59] Results from the programs were very similar, except that the noniterative program showed slightly more interactions of the Zr-Zr orbitals with the atomic orbitals of potassium, presumably because of the better description of the radial distribution of zirconium d orbitals that was included. Three clusters were included in this study: $Zr_6I_{18}^{5-}$ with the coordinates of $Zr_6I_{14}C$, $Zr_6I_{18}^{5-}$ with the coordinates of the larger $Zr_6I_{14}K$, and $Zr_6I_{18}K^{4-}$. The geometries and atomic orbital energies and exponents are given in Appendix B. While the choice of the cluster with Zr-Zr distances appropriate for a carbon-centered cluster is

somewhat arbitrary, the observation that Zr-Zr distances decrease with decreasing potassium content indicates that at least the geometry changes are in the correct direction. The charges on the clusters were present because of the extra iodides that were included to simulate the bridging between clusters that is present in the solid, as was previously described for the nonmetal-containing clusters.

The molecular orbitals that are obtained from the unexpanded $Zr_6I_{18}^{5-}$ cluster are exactly the same as those obtained from the previously described calculations on the $Zr_6I_{18}^{4-}$ cluster. These molecular orbitals are shown on the left side of Figure 14. The results of the calculations on the expanded, but unoccupied, cluster are shown in the center of the figure. As expected from the longer Zr-Zr distances, the eight Zr-Zr bonding orbitals move to higher energy upon the expansion. Even though only eleven electrons occupy the six lowest of these orbitals, this expansion appears to be a highly unfavorable distortion. A second and subtler effect, however, offsets this loss of Zr-Zr bonding. The block of 54 orbitals that lie directly below the Zr-Zr orbitals includes approximately 30 molecular orbitals that are primarily involved in Zr-I^a and Zr-I^i bonding. As a result of the expansion of the zirconium atoms, these molecular orbitals drop in energy by up to 0.1 eV each, and this relatively small decrease in energy of this large block of orbitals nearly offsets the more dramatic increase of the fewer number of occupied Zr-Zr bonding orbitals. The total energy of the unexpanded cluster is -2090.7 eV, compared with -2090.0 eV for the expanded but unoccupied cluster. It should be noted that the decrease in energy of

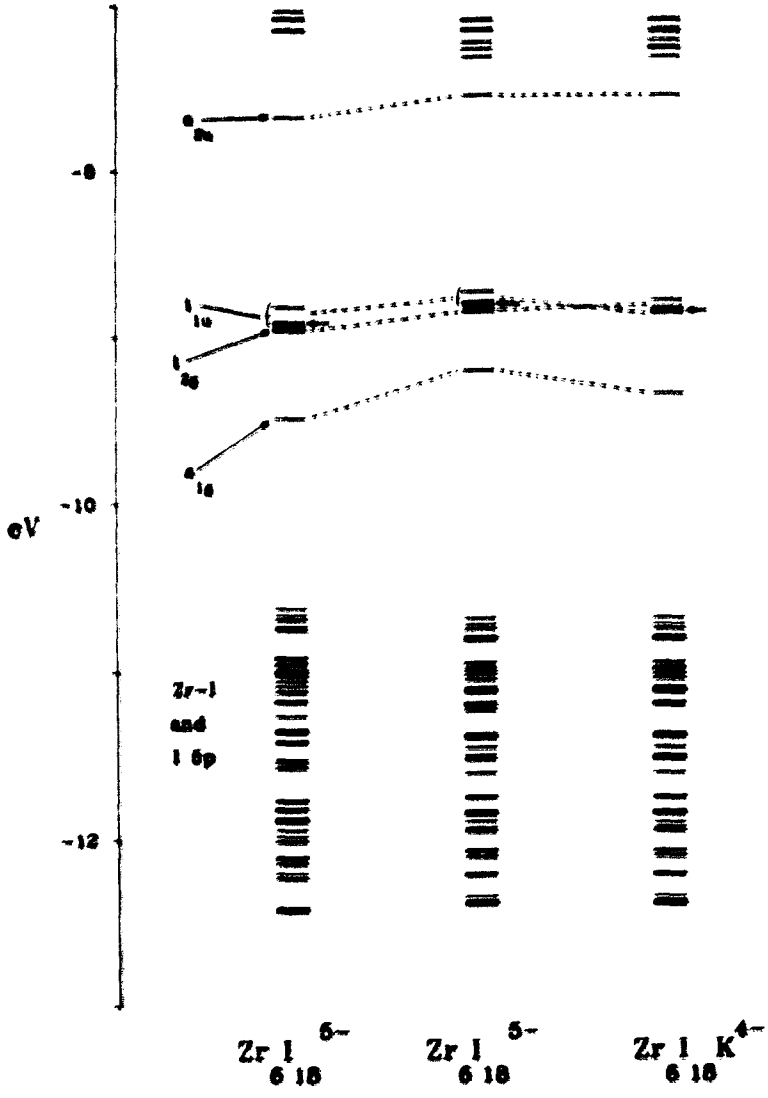

Figure 14. Molecular orbital diagram from extended Hückel calculations. $Zr_6I_{18}^{5-}$ with coordinates from $Zr_6I_{14}C$, d(Zr-Zr = 3.30 Å (left); $Zr_6I_{18}^{5-}$ with coordinates from $Zr_6I_{14}K$, d(Zr-Zr) = 3.45 Å (center); $Zr_6I_{18}^{4-}$ with coordinates from $Zr_6I_{14}K$ (right). The orbital labels refer to irreducible representations in O_h symmetry. All clusters have eleven electrons involved in Zr-Zr bonding. The HOMO of each cluster is indicated with a small arrow. The loss of Zr-Zr bonding upon expansion of the cluster is nearly offset by the subtle decrease in energy of many Zr-I orbitals

the Zr-I bonding orbitals is not solely the decrease in $Zr\text{-}I^a$ bond distances. In fact, the $Zr\text{-}I^i$ inner distances are slightly longer in $Zr_6I_{14}K$ than they are in $CsZr_6I_{14}C$. Instead, a portion of the decrease is apparently the effect of better $Zr\text{-}I^i$ overlap that is facilitated by the expansion of the zirconium atoms toward the square planes of inner iodines that surround them. In other words, the cluster receives a fair amount of stabilization through the relaxation of the 'matrix effect' described earlier. When the potassium atom is included in the center of the cluster, the potassium 4s orbital interacts with the a_{1g} Zr-Zr bonding molecular orbital and with a lower lying iodine a_{1g} orbital, and the potassium 4p orbitals interact very slightly with the appropriate t_{1u} Zr-Zr molecular orbitals. These interactions slightly decrease the overall energy of the cluster and make the potassium-centered cluster stable with respect to the unexpanded, unoccupied cluster (-2091.0 vs -2090.7 eV).

The unexpected changes in $Zr\text{-}I^a$ distances with reduced potassium content can be understood from the molecular orbital diagram, as well. As derived from the calculation, the highest occupied orbital for $Zr_6I_{14}K$ originates from the Zr-Zr $t_{2g}(xz,yz)$ set. This orbital is significantly antibonding with respect to the $Zr\text{-}I^a$ bonds. Thus, the partial removal of an electron from this orbital in the phase $Zr_6I_{14}K_{0.46}$ leads to a shortening of $Zr\text{-}I^a$ bonds compared with those in the fully occupied cluster, even though the lengthening of these bonds as the zirconium atoms relax towards the center of unoccupied cluster would be expected from simple geometric arguments.

An inspection of the average Zr-Zr reduced overlap populations of the three clusters studied shows that the expanded cluster has only about 64% of the Zr-Zr bonding of the unexpanded cluster. However, because of the small potassium contributions to the Zr-Zr bonding orbitals, 87% of the remaining Zr-Zr bonding is retained when the potassium is included. The potassium-centered cluster, and to some degree the aluminum-centered cluster discussed earlier, give the impression of a more loosely bound interstitial atom with the dominant bonding in the cluster contributed by Zr-I and Zr-Zr interactions.

The charge on the potassium was estimated at +0.4 by application of the reiterative extended Hückel.[59] The same calculations give charges of about +0.1 for the zirconium atoms, -0.1 for the inner iodine atoms, and charge of approximately -0.7 for the terminal iodides (the terminal iodides were given an average charge of -0.666 by the assumptions made to account for intercluster bridging). The atomic charges, that may be overestimated because of the nature of extended Hückel calculations, emphasize the covalent nature of these clusters. This covalent nature de-emphasizes the unfavorable coulombic effects between the potassium and zirconium atoms that would be expected to destabilize an ionic cluster of this type. Recent calculations of the Madelung part of the lattice energy, using the charges similar to those found in the extended Hückel calculations, show only a 10 kcal/mol difference favoring the more 'normal' structure with the potassium occupying the 'cesium' site compared with the observed potassium-centered cluster.[85] Of course, the coulombic interactions that give rise to this difference in lattice

energy have been ignored in the extended Hückel calculation. It has been noted, however, that the presence of a positive point charge in the center of the cluster, while having unfavorable coulombic interactions with the positively charged zirconiums, would also serve to lower the energies of the occupied Zr-Zr and Zr-K orbitals.[66]

Although the charge obtained for the potassium atom in this cluster is probably not of high numerical accuracy, it is lower than one might expect to find in an ionic salt of potassium. A significant shift of the core binding energy of potassium in such an electron-rich environment was first considered possible. An inspection of the XPS data collected for $Zr_6I_{14}K_{0.46}$ in Table 9 shows an opposite shift of 0.4 eV in the potassium-centered cluster vs K_2ZrI_6 (relative to the internal iodine standard). Presumably, this is because of the unusual coulombic effect that a somewhat positive zirconium cluster would have on ionization of the enclosed potassium compared with potassium surrounded by iodide ions in K_2ZrI_6.

The stabilizing effect of relaxation of the zirconium into more ideal octahedral sites is, of course, not limited to clusters that contain alkali metal atoms at their centers. The clusters that contain the larger nonmetals also gain stability in this fashion, but the gains from this relaxation effect are much smaller than the stability that arises from the interaction of the nonmetal s and p orbitals with Zr-Zr bonding molecular orbitals. The offsetting effects of loss of Zr-Zr bonding and of the stability gained by 'matrix relaxation' must result in relatively shallow potential for total cluster energy vs Zr-Zr distance. This

shallow potential may, in part, be the reason such a variety of interstitial atoms are found in the zirconium iodide clusters. If, however, clusters with smaller matrix effects are considered (i.e., M_6X_8 clusters or M_6X_{12} clusters with smaller bridging nonmetals), the potential described above may be much more restrictive.

Relationship of Carbon-Containing Clusters to SCC

The relationship between fission product ZrI_4 and the stress-corrosion-cracking (SCC) of Zircaloy cladding[1] in fission reactors led to the recent investigations of the nature of reduced zirconium iodides, as mentioned earlier. The role of interstitially stabilized clusters, especially those containing carbon, in this process may also be important. For example, one of the techniques for reducing SCC involves coating the interior walls of the Zircaloy cladding with graphite.[67] The graphite was believed to act as a physical lubricant in reducing stress between the fuel pellets and the cladding that occurs with the pressurization of the system as well as heating and cooling of the fuel elements. The discovery, during the course of this investigation, that zirconium clusters could be stabilized by carbon led to some lower temperature reactions that more closely correspond to reactor conditions.

As described earlier, graphite was included in reactions as the source of carbon. Reactions were typically run at 850°C, and there was much evidence for the vapor phase transport of the product. Since this temperature is far below the temperature where gaseous carbon is present in any detectible concentrations, the method by which carbon was being

transported was sought. The instability of gaseous carbon iodides at these temperatures eliminates them as possible candidates in this process. Evidence presented by Schäfer concerning transport mechanisms in other inorganic systems suggested the possibility that hydrogen may play an important role.[88] Hydrogen is virtually impossible to completely eliminate from reactions of this sort. It is present as water on the surface of the quartz jackets, arises from hydrolysis of reactants, and is present in small concentrations in graphite and powdered zirconium. It is possible that the hydrogen produced from these sources reacts with the graphite to give gaseous hydrocarbons at reaction temperatures used. These gaseous hydrocarbons, combined with gaseous ZrI_3 and ZrI_4, provide a mechanism for the gas phase transport of the cluster-containing product.

Reactions of graphite, ZrI_4, and Zr powder gave crystalline $Zr_6I_{12}C$ powder in fair yields at as low a temperature as 650°C. Reactions of ZrI_4 and a two-fold excess of Zr powder (relative to ZrI_2) were run for one week with paraffin to test the hypothesis that hydrocarbons acted as transport agents. These showed little or no reaction at 350°C, but resulted in black, poorly crystalline powders at 450°C. The X-ray diffraction patterns of this solid showed some ZrI_3, but also included rather broad lines attributed to poorly crystalline $Zr_6I_{12}C$! Increasing the temperature to 550°C resulted in a higher yield (40%) of $Zr_6I_{12}C$, and at 650°C the major products were a combination of $Zr_6I_{14}C$ and poorly crystalline ZrC. Presumably the less reduced cluster phase forms because excess carbon in the system uses zirconium to form the carbide and

therefore acts as an oxidant. Reactions with the identical ZrI_4/Zr ratios but without the added paraffin that were run at 450 and 550°C resulted in the formation of only ZrI_3. The ability of added carbon to affect the reaction at low temperatures may have a relationship to the effect that graphite added as a 'lubricant' to the Zircaloy cladding produces on SCC. One possibility is that the formation of the carbon-containing phases reduces the vapor pressure of ZrI_4 below the critical value[89] at which SCC occurs. Another hypothesis is that the reduced phase that is believed to be involved with the formation of cracks across grains is unstable with respect to the carbon-containing phases when graphite is present in the system. These hypotheses may warrant additional study.

Substitution and Nonstoichiometry

At the outset of this study, one of the hints of something amiss in the '$CsZr_6I_{14}$' phases was the range of lattice parameters found for the products from different reactions. The number and diversity of interstitial atoms that can be included in the centers of the zirconium octahedra in the phases synthesized during this work suggests the possibility of both substitution and nonstoichiometry for these materials.

Although nonstoichiometry has been observed for the potassium-centered clusters, no such nonstoichiometry has been observed for the nonmetal-centered clusters. The lattice parameters that have been obtained from the products of a number of reactions producing $CsZr_6I_{14}C$, for example, match within a few standard deviations. The carbon-

containing clusters are obtained in high yields if stoichiometric quantities of graphite are added. When less than a stoichiometric quantity of carbon is included in the reaction, a correspondingly smaller yield of product is obtained with the lattice parameters of the fully stoichiometric product. Because they were obtained in smaller yield, no such convincing comparison is available for the silicon or aluminum-containing cluster compounds, but the X-ray structures of these phases refined as being fully stoichiometric in the interstitial and no contradictory evidence is currently available.

The alkali metal that occupies the 'cesium' position, however, is clearly nonstoichiometric in the carbon-containing cluster phases. The cell volumes of $Zr_6I_{14}C$, $K_{0.58}Zr_6I_{14}C$, and the material believed to be $KZr_6I_{14}C$ obey Vegard's law. In similar fashion, reactions that were stoichiometrically loaded to form $Cs_{0.5}Zr_6I_{14}C$ produced a large (80%) yield of material that gave a smaller cell volume than the fully stoichiometric $CsZr_6I_{14}C$. No similar data were collected for rubidium salts or for materials with other interstitials, but the cesium position was only partially occupied in both the silicon- and aluminum-centered clusters.

Another factor in the variability of lattice parameters of the '$CsZr_6I_{14}$' phases is isomorphic substitution of the interstitial atoms. Research by Goldschmidt[90] and others has established that the isomorphic substitution can occur in materials where the sizes of the unit cells and the coordinates of generally situated atoms differ but slightly. As noted earlier, the cell volume difference of the smallest to the largest

6-14 phases found in this research is only between 3 and 4%, much less than the 10-15% upper limit established by Goldschmidt.

The diversity of the interstitial atoms found in the centers of these clusters also raises the possibility of heterovalent as well as isovalent isomorphism in these materials. Although not exploited in this research, heterovalent isomorphism is an important technological process in the production of many materials. In these systems, it may be possible to selectively form phases with a variable susceptibility, for example.

This process of isomorphous substitutions presumably is also possible for the alkali metal atoms that occupy the 'cesium' site in the cell, although this too has not been experimentally verified.

In natural substances, isomorphic substitutions are commonplace and give rise to the complexity of many minerals. In the synthesis of 6-14 phases in reactions that contain unknown amounts of a number of probable impurities, substitutions are likely to have a similar effect, giving rise to the range of lattice parameters[2] found for '$CsZr_6I_{14}$'.

FUTURE WORK

The interstitial-containing halide clusters that have been found in the course of this investigation and other recent studies represent the initial examples of what is rapidly becoming a large class of materials. The emphasis of the current research has been primarily synthesis and structural characterization to concretely establish the presence of the interstitial atoms in the centers of these clusters. In this, considerable success has been attained. There are, however, several areas where unanswered questions remain and new questions have been raised. In this section, several suggestions for further study are offered, not as a comprehensive list, but rather as guide for what might be possible.

Much work remains in the synthesis of interesting new interstitial-containing clusters. As noted previously, many of the post-transition elements have orbital energies and radii conducive to inclusion in octahedral clusters, especially clusters that have some flexibility of metal atom positions. The post-transition elements that have not been tried but offer promise as interstitial atoms include Ga, In, Ge, Sn, Pb, P, As, Sb, Bi, S, Se, and Te. The inclusion of some of these atoms into 6-14 phases should certainly be possible with the most likely candidate being phosphorous in the 15-electron $Zr_6I_{14}P$ or the 16-election cluster in the similar phase with an additional cesium atom.

It is somewhat surprising that no 6-15 phases have been found in the course of this research, but perhaps the use of other synthetic routes may give different results. The oxidation of $CsZr_6I_{14}C$ with liquid

iodine at low temperatures may give $CsZr_6I_{15}C$, as was found in the similar oxidation of Ta_6I_{14}.[80]

This research has established the existence of nonmetal-centered clusters that contain 14, 15, or 16 cluster electrons, but the small (0.5 eV) gap between the HOMO and LUMO of the 16-electron clusters may not preclude the formation of clusters with more electrons.

As noted earlier, two unidentified phases were obtained in attempts to form $CsZr_6I_{14}Al$ and $Zr_6I_{12}Al$ and it may be possible to characterize and synthesize these materials in good yield.

There remain several questions about the synthesis and characterization of $CsZr_6I_{14}K$ or the isotypic sodium compound. Reactions have been conducted to give these products and have resulted in a fair yield of gem-shaped cyrstals. However, at the time these crystals were obtained no clear understanding of the role of interstitial atoms was available, making an interpretation of a possible crystal structure difficult. With the completion of the current work, perhaps some study of these compounds would be fruitful.

Very little attention has been given to the gross physical properties of the clusters synthesized in this work or the possible products that might result from their decomposition. For example, it may be possible to obtain ZrC by some low temperature route that involves the formation of a carbon-containing zirconium iodide cluster followed by vacuum decomposition of the cluster.

The solid state NMR results of carbon-containing clusters indicate that perhaps the bonding in these materials is not as simple as would be

indicated by the extended Hückel calculations. The further NMR study of interstitial-containing clusters is made possible by the synthesis of both $CsZr_6I_{14}B$ and $Zr_6I_{12}B$. It may be of interest to determine if the broad resonance seen for $Zr_6I_{12}C$ is related to a previously reported broad ^1H resonance seen for Zr_6Cl_{12} prepared in the presence of hydrogen.[91]

There is also a possibility that transition metals may also be included in zirconium clusters, bonded by the interaction of the t_{2g} d orbitals on the metal and the t_{2g} Zr-Zr cluster orbitals. While this may seem far-fetched, the inclusion of nonmetal interstitials in these clusters was thought equally unlikely before it was demonstrated.

The inclusion of carbon and dicarbon units in rare earth halide clusters has been previously cited. The larger size of the octahedral clusters in rare earth halides, especially iodides, suggests the possibility of including larger nonmetals in the centers of these clusters.

In the course of this research, a phase was prepared by the interaction of Nb_3I_8 and Nb at 850-950°C in a Nb reaction container that had been contaminated with cleaning solution. The phase appears as extremely fine shiny black needles that are difficult to isolate as single crystals. Microprobe analysis of these crystals gave a composition 'Nb_6I_{10}' with only niobium and iodine as elements with an atomic number greater than ten, but further characterization has proven difficult. Judging from past experience, it is likely that this phase is also impurity stabilized. Attempts to form the needles by purposeful addition of

water, Nb_2O_5, and graphite have instead all given the typical cluster Nb_6I_{11}, but other possible interstitials have not been tried. Work to determine the nature of this material may be interesting.

REFERENCES

1. Cox, B.; Wood, J. C. "Corrosion Problems in Energy Conversion and Generation"; C. S. Tedman, Jr., Ed.: Electrochemical Society: New York, 1974; p. 275

2. Guthrie, D. H. Ph.D. Dissertation, Iowa State University, Ames, IA, 1981.

3. Daake, R. L.; Corbett, J. D. Inorg. Chem. 1978, 17, 1192.

4. Corbett, J. D.; Guthrie, D. H. Inorg. Chem. 1982, 21, 1747.

5. Guthrie, D. H.; Meyer, G.; Corbett, J. D. Inorg. Chem. 1981, 20, 1192.

6. Daake, R. L. Ph.D. Dissertation, Iowa State University, Ames, IA, 1976.

7. Corbett, J. D.; Daake, R. L.; Poeppelmeier, K. R.; Guthrie, D. H. J. Am. Chem. Soc. 1978, 100, 652.

8. Guthrie, D. H.; Corbett, J. D. Inorg. Chem. 1982, 21, 3290.

9. Simon, A.; Schnering, H.-G.; Wöhrle, H.; Schäfer, H. Z. Anorg. Allg. Chem. 1965, 339, 155.

10. Bauer, D.; Schnering, H.-G.; Schäfer, H. J. Less-Common Metals 1965, 8, 388.

11. Bauer, D.; von Schnering, H.-G. Z. Anorg. Allg. Chem. 1968, 361, 259.

12. Cotton, F. A.; Haas, T. E. Inorg. Chem. 1964, 3, 10.

13. Robbins, D. J.; Thomson, A. J. J. Chem. Soc., Dalton Trans. 1972, 2350.

14. Mingos, D. M. P. Oxford University, Oxford, England, private communication to J. D. Corbett, 1984.

15. Corbett, J. D.; Poeppelmeier, K. R.; Daake, R. L. Z. Anorg. Allg. Chem. 1982, 491, 51.

16. Simon, A. Angew. Chem., Int. Ed. Engl. 1981, 20, 1.

17. Corbett, J. D. Acc. Chem. Res. 1981, 14, 239.

18. Attributed to F. A. Cotton, Texas A&M, College Station, TX, Chemistry in Britain 1983, 806.

19. Simon, A. Z. Anorg. Allg. Chem. 1967, 355, 311.

20. Imoto, H.; Corbett, J. D. Inorg. Chem. 1980, 10, 1241.

21. Struss, A. W.; Corbett, J. D. Inorg. Chem. 1970, 9, 1373.

22. Seaverson, L. M.; Corbett, J. D. Inorg. Chem 1983, 22, 2789.

23. Warkentin, E.; Masse, R.; Simon, A. Z. Anorg. Allg. Chem. 1982, 491, 323.

24. Warkentin, E.; Simon, A. Rev. Chem. Minerale 1983, 20, 488.

25. Ford, J. E.; Corbett, J. D.; Hwu, S.-J. Inorg. Chem. 1983, 22, 2789.

26. Ziebarth, R. P.; Corbett, J. D., Iowa State University, Ames, IA, unpublished research, 1984.

27. Hwu, S.-J.; Corbett, J. D.; Poeppelmeier, K. R. J. Solid State Chem., accepted, 1984.

28. Holmberg, B.; Dagerhamn, T. Acta Chem. Scand. 1961, 15, 919.

29. Juza, V. R.; Heners, J. Z. Anorg. Allg. Chem. 1964, 332, 159.

30. Daake, R. L., Ames Laboratory, Iowa State University, Ames, IA, unpublished research, 1976.

31. Corbett, J. D. and coworkers, Iowa State University, Ames, IA, unpublished research.

32. Searcy, A. W. "Condensed State Reactions and Phase Equilibria" in Int. Symp. on High Temperature Technology, McGraw-Hill: New York, 1960; p. 336.

33. Corbett, J. D. Inorg. Syn. 1983, 22, 15.

34. Miller, A. E.; Daane, A. H.; Haberman, C. E.; Beaudry, B. J. Rev. Sci. Inst. 1963, 34, 644.

35. Cisar, A. Ph.D. Dissertation, Iowa State University, Ames, IA, 1978.

36. Imoto, H., Ames Laboratory, Iowa State University, Ames, IA, unpublished research, 1978.

37. Takusagawa, F., Ames Laboratory, Iowa State University, Ames, IA, unpublished research, 1981.

38. Garcia, E., Ames Laboratory, Iowa State University, Ames, IA, unpublished research, 1983.

39. Clark, C. M.; Smith, D. K.; Johnson, G. J. "A Fortran IV Program for Calculating X-Ray Powder Diffractions Patterns-Version 5", Department of Geosciences, Pennsylvania State University, University Park, PA, 1973.

40. Ziebarth, R. P., Ames Laboratory, Iowa State University, Ames, IA, unpublished research, 1984.

41. Powder Diffraction File, JCPDS International Centre for Diffraction Data, 1601 Park Lane, Swathmore, PA, 1982.

42. Schroeder, D. R.; Jacobson, R. A. Inorg. Chem. 1973, 21, 210.

43. Jacobson, R. A. Applied Crystallogr. 1976, 9, 115.

44. Jacobson, R. A., Ames Laboratory, Iowa State University, Ames, IA, unpublished research, 1982.

45. Jacobson, R. A., United States AEC Report IS-3469, Iowa State University, Ames, IA, 1974.

46. Karcher, B. A. Ph.D. Dissertation, Iowa State University, Ames, IA, 1981.

47. Smith, J. D., Ames Laboratory, Iowa State University, Ames, IA, unpublished research, 1983.

48. Rogers, J.; Jacobson, R. A., United States AEC Report IS-2155, Iowa State University, Ames, IA, 1967.

49. Helland, B., Ames Laboratory, Iowa State University, Ames, IA, unpublished research, 1981.

50. Lapp, R. L.; Jacobson, R. A., United States AEC Report IS-4708, Iowa State University, Ames, IA, 1979.

51. Powell, D. R.; Jacobson, R. A., United States AEC Report IS-4737, Iowa State University, Ames, IA, 1980.

52. "International Tables for X-Ray Crystallography", Vol. III; Kynoch Press: Birmingham, England, 1968.

53. Johnson, C. K. "ORTEP: A Fortran Thermal-Ellipsoid Plot Program for Crystal Structure Illustrations", ORNL Report 3794, Oak Ridge National Laboratory, Oak Ridge, TN, 1970.

54. Coppens, P.; Hamilton, W. C. Acta Cryst. 1970, A26, 71.

55. Smith, J. D., Ames Laboratory, Iowa State University, Ames, IA, unpublished research, 1983.

56. Jacobson, R. A., Ames Laboratory, Iowa State University, Ames, IA, unpublished research, 1980.

57. Stierman, R. J.; Gschneidner, K. A., Jr.; Tsand T.-W. E.; Schmidt, F. A.; Klavins, P.; Shelton, R. N.; Queen, J.; Legvold, S. J. Magn. Mat. 1983, 36, 249.

58. Gerstein, B.; Chow, C.; Pembleton, R. G.; Wilson, R. C. J. Phys. Chem. 1981, 81, 565.

59. Schaffer, A. M.; Gouterman, M.; Davidson, E. R. Theoret. Chim. Acta (Berl.) 1973, 30, 9.

60. Hoffmann, R. J. Chem. Phys. 1963, 39, 1397.

61. Hinze, J.; Jaffé, H. H. J. Phys. Chem. 1963, 67, 1501.

62. Moore, C. E. "Atomic Energy Levels", Natl. Stand. Ref. Data Ser., Natl. Bur. Stand. (U.S.) 1971, NSRDS-NBS 35.

63. Basch, H.; Gray, H. B. Theort. Chim. Acta (Berl.) 1966, 4, 367.

64. Clementi, E.; Roetti, C. At. Data Nucl. Data Tables 1974, 14, 179.

65. Corbett, J. D. J. Solid State Chem. 1981, 37, 335.

66. Schäfer, H.; von Schnering, H.-G. Angew. Chem. 1964, 76, 883.

67. Garcia, E.; Hwu, S.-J., Ames Laboratory, Iowa State University, Ames, IA, unpublished research, 1984.

68. Converse, J. G.; McCarley, R. E. Inorg. Chem. 1970, 9, 1361.

69. Simon, A.; Schäfer, H.; von Schnering, H.-G. Z. Anorg. Allg. Chem. 1967, 355, 295.

70. Imoto, H.; Simon, A. Inorg. Chem. 1982, 21, 308.

71. Simon, A., Max-Planck-Institut FKF, Stuttgart, FRG, private communication, 1983.

72. Fry, C., Ames Laboratory, Iowa State University, Ames, IA, private communication, 1984.

73. Smith, J. D.; Corbett, J. D. J. Am. Chem. Soc. 1984, 106, 4618.

74. Hwu, S.-J., Ames Laboratory, Iowa State University, Ames, IA, unpublished research, 1984.

75. Ziebarth, R. P., Ames Laboratory, Iowa State University, Ames, IA, unpublished research, 1984.

76. Hansen, R. S., Ames Laboratory, Iowa State University, Ames, IA, private communication, 1984.

77. Shannon, R. D. Acta Cryst., Sect. A, 1976, A32, 751.

78. Guggenberger, L. J.p; Sleight, A. W. Inorg. Chem. 1969, 8, 2041.

79. Koknat, F. W.; McCarley, R. E. Inorg. Chem. 1974, 13, 295.

80. Bauer, D.; Schäfer, H. J. Less-Common Metals 1968, 14, 476.

81. Simon, A.; von Schnering, H.-G.; Schäfer, H. Z. Anorg. Allg. Chem. 1968, 361, 235.

82. Corbett, J. D., Ames Laboratory, Iowa State University, Ames, IA, unpublished research, 1984.

83. Eckerlin, P.; Wölfel, E. Z. Anorg. Allg. Chem. 1955, 280, 321.

84. Simon, A., Max-Planck-Institut FKF, Stuttgart, FRG, private communication, 1983.

85. Hoppe, R. Angew. Chem. 1981, 20, 70.

86. Fenske, R., University of Wisconsin, Madison, WI, private communication, 1984.

87. Cox, B. Reviews on Coatings and Corrosion 1975, 1, 367.

88. Schäfer, H. "Chemical Transport Reactions", Academic Press: New York, 1964; Chapter 3.

89. Hofman, P.; Spino, J. J. Nucl. Mat. 1983, 114, 50.

90. Goldschmidt, V. M. Trans. Faraday Soc. 1929, 25, 253.

91. Imoto, H.; Corbett, J. D.; Cisar, A. Inorg. Chem. 1981, 20, 145.

ACKNOWLEDGEMENTS

'For even as He loves the arrow that flies, so He loves also the bow that is stable.'

Kahlil Gibran

The author wishes to thank Professor John D. Corbett for the support, patience, and guidance given throughout this research.

Special thanks are due Dr. R. A. Jacobson and members of his group, especially J. Richardson and J. Benson, for assistance with diffractometers and crystallographic programs.

The author is indebted to B. Beaudry and co-workers for the use of metal-working facilities, to F. Laabs for electron microprobe analysis, to R. Stierman and K. Gschneidner for the use of the Faraday balance, to E. Dekalb for elemental analysis, to C. Fry and B. Gerstein for the ^{13}C NMR results, to G. Meyer for MAPLE calculations, and to S. Wijeyesekera for the extended Hückel programs.

The discussions, suggestions, and patience of many friends and coworkers are kindly remembered.

The author wishes to extend special thanks to his parents and relatives, who by example have demonstrated the importance of higher education and have provided support to that end.

Finally, the author acknowledges the support, love, patience, and sacrifices contributed by his wife Cheryl Ann.

APPENDIX A. CALCULATED POWDER PATTERNS OF $CsZr_6I_{14}C$, $Zr_6I_{14}C$, AND $Zr_6I_{12}C$

STRONGER LINES IN THE GUINIER POWDER PATTERNS FOR $CsZr_6I_{14}C$, $Zr_6I_{14}C$, AND $Zr_6I_{12}C$[a]

			$CsZr_6I_{14}C$	$Zr_6I_{14}C$				$Zr_6I_{12}C$
h	k	ℓ	I_{calc}	I_{calc}	h	k	ℓ	I_{calc}
1	1	1	19	85	1	0	1	15
3	1	2	11	13	1	1	0	6
4	2	1	35	47	0	0	3	15
0	0	4	35	36	1	3	1	45
0	4	2[b]	81	86	1	3	-2	100
4	2	2	100	95	1	3	4	32
0	4	3	30	34	5	2	0	32
4	2	3	82	100	1	3	-5	11
1	5	2	11	13	5	2	3	10
1	1	5	13	9	2	6	-1	10
4	2	4	17	14	2	6	2	15
4	2	5	22	22	2	6	-4	11
4	6	0	51	45	1	3	7	7
8	0	0	27	25	2	6	5	6
0	4	6	22	23	5	2	6	6
4	2	6	29	24	9	1	2	6
4	6	4	27	23				
8	0	4	13	11				
8	4	2	27	25				
0	0	8	12	9				
8	4	3	10	8				

[a]Cu $K\alpha_1$ radiation, Guinier geometry.

[b]Interference from Si standard.

APPENDIX B. 1. VALENCE ORBITAL IONIZATION ENERGIES AND ZETAS OF ATOMS USED IN EXTENDED HUCKEL CALCULATIONS

2. GEOMETRIES OF CLUSTERS USED FOR EXTENDED HUCKEL CALCULATIONS

1. VALENCE ORBITAL IONIZATION ENERGIES AND ZETAS OF ATOMS USED IN EXTENDED HUCKEL CALCULATIONS

ATOM	NS[a]	EXPS[b]	COULS[c]	NP[d]	EXPP[e]	COULP[f]	ND[g]	EXPD[h]	C2[i]	C1[j]	EXPDA[k]	COULD[l]
Zr	5	1.82	-7.07	5	1.78	- 4.28	4	3.84	0.5798	0.6213	1.505	-8.30
I	5	2.68	-20.84	5	2.32	-11.21						
B	2	1.30	-15.20	2	1.30	- 8.50						
Al	3	1.37	-12.30	3	1.37	- 6.50						
K	4	0.90	- 7.96	4	0.90	- 5.67						
C	2	1.625	-21.50	2	1.625	-11.4						

[a]Principal quantum number of the valence s orbital.
[b]Zeta of the valence s orbital.
[c]s valence orbital ionization energy (eV).
[d]Principal quantum number of the valence p orbitals.
[e]Zeta of the valence p orbitals.
[f]p valence orbital ionization energy (eV).
[g]Principal quantum number of the valence d orbitals.
[h]First zeta of the valence d orbital double zeta expansion.
[i]Coefficient of the first zeta.
[j]Second zeta of the valence d orbital double zeta expansion.
[k]Coefficient of the second zeta.
[l]d valence orbital ionization energy (eV).

2. GEOMETRIES OF CLUSTERS USED FOR EXTENDED HUCKEL CALCULATIONS

CLUSTER	ATOM	x	y	z
$Zr_6I_{12}^{2+}$				
	Zr	1.600	1.600	0.000
	Zr	0.000	0.000	2.254
	I	0.000	3.960	0.000
	I	3.960	0.000	0.000
	I	1.973	1.973	2.843
$Zr_6I_{18}^{4-}$	(d(Zr-I^a) = 3.10 A)			
	Zr	1.600	1.600	0.000
	Zr	0.000	0.000	2.254
	I	0.000	3.960	0.000
	I	3.960	0.000	0.000
	I	1.973	1.973	2.843
	I	0.000	0.000	5.363
	I	3.792	3.792	0.000
$Zr_6I_{18}^{4-}$	(d(Zr-I^a) = 3.30 A)			
	Zr	1.600	1.600	0.000
	Zr	0.000	0.000	2.254
	I	0.000	3.960	0.000
	I	3.960	0.000	0.000
	I	1.973	1.973	2.843
	I	0.000	0.000	5.563
	I	3.933	3.933	0.000
$Zr_6I_{18}C^{4-}$				
	Zr	0.000	0.000	2.254
	Zr	1.648	1.648	0.000
	I	0.000	0.000	5.776
	I	3.900	3.900	0.000
	I	0.000	3.983	0.000
	I	4.050	0.000	0.000
	I	1.973	1.973	2.843
	C	0.000	0.000	0.000

2. Continued

CLUSTER	ATOM	x	y	z
$Zr_6I_{18}B^{5-}$				
	Zr	0.000	0.000	2.335
	Zr	1.701	1.701	0.000
	I	0.000	0.000	5.745
	I	3.946	3.946	0.000
	I	1.999	1.999	2.864
	I	4.079	0.000	0.000
	I	0.000	4.016	0.000
	B	0.000	0.000	0.000
$Zr_6I_{14}Si^{4-}$				
	Zr	0.000	0.000	2.499
	Zr	1.802	1.802	0.000
	I	0.000	0.000	5.767
	I	3.971	3.971	0.000
	I	2.023	2.023	2.877
	I	4.099	0.000	0.000
	I	0.000	4.052	0.000
	Si	0.000	0.000	0.000
$Zr_6I_{14}Al^{5-}$				
	Zr	0.000	0.000	2.337
	Zr	1.707	1.707	0.000
	I	0.000	0.000	5.707
	I	3.904	3.904	0.000
	I	1.972	1.972	2.836
	I	4.050	0.000	0.000
	I	0.000	3.980	0.000
	Al	0.000	0.000	0.000
$Zr_6I_{14}K^{5-}$				
	Zr	0.000	0.000	2.393
	Zr	1.740	1.740	0.000
	I	0.000	0.000	5.798
	I	3.950	3.950	0.000
	I	2.007	2.007	2.877
	I	4.116	0.000	0.000
	I	0.000	4.049	0.000
	K	0.000	0.000	0.000

APPENDIX C. CALCULATED AND OBSERVED STRUCTURE FACTOR AMPLITUDES FOR $Zr_6I_{14}K$

APPENDIX D. CALCULATED AND OBSERVED STRUCTURE FACTOR AMPLITUDES FOR $Zr_6I_{14}K_{0.46}(z)$

APPENDIX E. CALCULATED AND OBSERVED STRUCTURE FACTOR AMPLITUDES FOR $CsZr_6I_{14}B$

L = 0

H	K	FO	FC
0	2	95	100
0	4	30	20
0	6	208	211
0	8	264	270
0	10	209	210
0	12	334	346
0	14	137	142
0	16	36	40
0	18	64	69
2	0	107	108
2	2	79	77
2	4	176	173
2	6	41	47
2	8	77	79
2	10	103	101
2	12	46	50
4	0	190	181
4	2	172	168
4	4	190	188
4	6	989	1007
4	8	213	208
4	10	39	24
4	12	133	147
4	14	227	227
4	16	83	87
4	18	183	184
6	0	92	89
6	2	208	204
6	4	136	133
6	6	56	61
6	8	68	67
6	12	39	67
6	14	97	97
6	16	67	64
8	0	990	1058
8	4	32	16
8	6	117	116
8	8	276	267
8	10	136	148
8	12	473	452
8	14	96	92
10	0	136	131
10	4	147	140
10	6	107	106
10	8	164	159
10	10	132	125
10	16	65	50
12	2	160	160
12	4	129	126
12	6	670	658
12	8	58	64
12	12	90	90
12	14	216	208
14	0	96	97
14	2	171	167
14	4	78	83
14	6	49	53
14	8	81	79
14	12	47	33
16	0	379	371
16	2	47	32
16	8	233	228
16	10	31	36
18	0	66	65
18	4	86	89
18	6	39	41
18	8	109	103
20	0	36	66
20	2	118	121
20	4	63	71

L = 1

H	K	FO	FC
0	2	61	35
0	4	331	346
0	6	87	94
0	8	418	442
0	10	33	38
0	12	243	242
0	16	64	66
1	1	132	135
1	3	136	140
1	5	134	138
1	7	131	134
1	9	34	61
1	11	160	159
1	13	66	68
1	17	42	38
2	2	49	34
2	4	31	31
2	6	108	110
2	8	33	34
2	10	89	93
2	12	38	48
2	16	33	39
3	1	106	108
3	3	136	143
3	5	112	111
3	7	123	123
3	13	90	98
3	17	82	87
4	2	439	448
4	4	79	83
4	6	183	183
4	10	175	178
4	12	45	34
4	14	302	304
4	18	166	174
5	1	195	200
5	3	176	179
5	5	68	71
5	7	170	165
5	13	182	119
5	17	99	104
6	2	131	134
6	4	81	83
6	6	45	40
6	12	97	98
6	16	62	66
7	3	133	134
7	5	32	30
7	7	29	28
7	9	33	38
7	11	129	123
8	4	300	299
8	6	43	48
8	8	377	364
8	12	188	183
8	16	33	42
9	1	100	97
9	3	90	89
9	5	121	121
9	7	139	135
9	9	76	76
9	11	129	126
9	13	51	51
10	4	27	89
10	6	111	111
10	10	115	110
11	1	38	46
11	3	36	36
11	5	103	104
11	9	79	84
11	15	98	96
12	2	318	317
12	6	80	83
12	10	167	159
12	14	219	208
13	1	96	99
13	3	106	104
13	5	43	32
13	7	83	80
13	13	66	72
14	2	100	100
14	4	79	79
14	12	79	80
15	1	35	43
15	3	85	84
15	7	44	51
15	9	88	83
15	11	56	64
16	4	223	221
16	8	231	224
17	3	36	39
17	5	34	33
18	4	33	49
18	6	65	60
19	1	64	71
19	5	62	59
20	2	193	191

L = 2

H	K	FO	FC
0	0	38	10
0	2	75	73
0	4	775	872
0	6	69	70
0	8	439	463
0	10	64	66
0	14	34	38
0	16	387	403
1	1	23	14
1	3	91	96
1	5	269	277
1	9	133	136
1	11	97	100
2	0	32	34
2	2	59	61
2	4	142	139
2	6	77	76
2	10	86	92
2	12	85	90
2	18	48	68
3	1	168	169
3	3	143	140
3	9	48	32
3	11	72	78
3	13	76	78
3	17	45	51
4	0	84	82
4	2	690	758
4	4	82	70
4	6	28	7
4	8	56	39
4	10	634	631
4	12	38	24
4	14	167	169
5	1	207	205
5	3	238	237
5	5	78	70
5	11	145	143
5	13	115	118
5	17	69	75
6	0	39	62
6	2	93	94
6	4	103	104
6	6	49	33
6	10	84	83
6	12	89	87
7	1	74	74
7	3	65	66
7	5	105	103
7	9	31	37
7	13	43	47
8	2	61	63
8	4	682	687
8	6	41	47
8	8	396	385
8	10	43	49
8	14	42	34
8	16	390	343
9	3	97	97
9	5	235	230
9	9	125	120
9	11	103	100
10	4	118	118
10	6	78	74
10	8	34	29
10	10	74	74
10	12	66	72
11	1	44	47
11	5	114	113
11	7	29	29
11	9	86	89
12	0	44	34
12	2	485	496
12	4	36	50
12	8	48	54
12	10	463	445
12	14	134	132
13	1	111	113
13	3	123	120
13	11	83	84
13	13	64	72
14	0	53	54
14	2	80	80
14	4	53	61
14	6	40	39
14	10	57	62
14	12	61	64
15	1	76	77
15	3	120	118
15	11	57	59
16	0	32	28
16	4	413	406
16	8	252	244
17	5	94	91
17	9	48	51
18	4	76	79
18	6	46	48
19	3	55	58
19	5	97	98
20	2	265	266

L = 3

H	K	FO	FC
0	2	48	41
0	4	609	653
0	6	227	233
0	8	514	529
0	10	198	205
0	12	115	115
0	18	55	64
1	1	160	165
1	3	131	136
1	7	44	48
1	9	32	28
1	11	51	53
1	15	113	118
2	2	69	71
2	4	91	91
2	6	69	72
2	8	44	41
3	1	48	47
3	3	27	30
3	5	100	98
3	7	36	39
3	9	137	137
3	11	37	40
3	13	47	32
4	2	684	747
4	4	160	160
4	6	135	134
4	10	230	234
4	12	171	162
4	14	201	203
4	16	96	96
5	3	46	31
5	5	117	116
5	7	91	91
5	9	169	164
6	2	166	165
6	4	55	59
6	10	48	54
6	12	65	69
7	1	46	49
7	3	69	70
7	7	89	88
7	11	58	57
7	13	39	50
7	15	76	74
7	17	49	41
8	4	460	461
8	6	159	152
8	8	439	428
8	10	141	136
8	12	133	128
8	16	37	23
9	1	129	131
9	3	107	108
9	15	98	102
10	4	155	150
10	6	108	105
10	8	36	38
10	10	77	78
10	12	61	71
11	1	62	67
11	5	30	31
11	9	49	52
11	11	50	55
11	13	59	57
12	2	435	435
12	6	134	133
12	10	112	116
12	12	67	73
12	14	168	168
13	5	57	63
13	7	50	34
13	9	108	100
14	2	125	123
14	4	68	71
14	10	59	61
14	12	76	77
15	7	78	77
15	11	35	37
16	2	57	66
16	4	199	198
16	6	42	48
16	8	257	251
17	1	41	48
17	3	54	52
18	4	78	84
18	6	61	63
20	2	185	190

L = 4

H	K	FO	FC
0	0	783	840
0	2	183	185
0	4	224	227
0	8	407	420
0	12	510	521
0	14	98	102
0	16	123	122
1	1	42	47
1	5	95	98
1	11	68	76
2	0	225	227
2	2	105	103
2	4	28	33
2	6	52	52
2	8	127	126
2	14	128	128
2	16	46	55
3	1	61	63
3	3	32	31
3	5	35	34
3	7	44	53
3	9	35	37
3	13	40	35
3	17	38	43
4	0	24	18
4	2	396	406
4	6	711	710
4	8	194	186
4	10	37	31
4	14	280	281
5	1	68	72
5	3	58	58
5	5	70	70
5	7	38	42
5	13	40	32
5	17	45	53
6	0	28	25
6	6	167	163
6	8	224	218
6	10	32	38
6	14	52	62
7	3	44	44
7	5	34	39
7	11	32	30

H	K	FO	FC
15	7	37	38
16	4	161	166

L = 10

H	K	FO	FC
0	0	139	140
0	4	470	467
0	6	55	61
0	8	244	244
0	10	106	110
0	14	34	34
1	5	160	156
1	7	32	38
1	11	31	34
2	0	33	39
2	2	39	37
2	4	142	141
2	10	102	101
2	12	71	72
2	14	48	45
3	1	107	108
3	11	93	95
4	0	47	49
4	2	384	382
4	4	83	91
4	6	57	62
4	8	61	64
4	10	424	418
4	14	89	96
5	1	137	133
5	3	30	33
5	5	39	31
5	11	126	125
6	2	101	109
6	4	109	111
6	6	42	25
6	8	80	86
6	10	60	67
6	12	84	80
7	3	49	49
7	5	84	81
7	7	53	53
8	0	71	78
8	4	399	394
8	8	244	233
8	10	71	79
9	5	150	146
9	7	36	34
10	0	93	97
10	4	133	128
10	6	64	70
10	8	46	50
10	10	105	102
11	1	40	43
11	3	61	55
12	2	304	303
12	4	63	69
12	10	293	289
13	1	89	96
14	0	34	33
14	2	104	103
14	4	68	70
14	8	76	82
15	3	63	63
16	4	231	230

L = 11

H	K	FO	FC
0	2	76	77
0	4	362	356
0	6	114	114
0	8	315	315
0	10	119	125
1	1	66	69
1	3	139	139
1	5	33	35
1	9	42	34
1	11	91	83
1	13	73	73
3	3	123	123
3	5	43	47
3	7	102	101
3	9	70	66
4	2	414	408
4	4	122	119
4	6	35	36
4	10	143	146
4	12	94	98
5	3	142	139
5	7	113	113
5	9	50	57
6	2	60	62
6	4	50	55
6	6	33	35
7	1	40	36
7	3	113	116
7	9	41	18
7	11	72	76
8	2	36	35
8	4	266	263
8	6	62	73
8	8	272	264
8	10	79	83
8	12	32	49
9	1	60	62
9	3	121	119
9	5	46	46
9	9	36	32
9	11	60	63
10	2	43	46
10	4	85	89
10	6	50	34
10	10	44	48
11	1	43	44
11	3	66	68
11	5	40	46
11	7	39	39
11	9	62	58
12	2	282	283
12	6	73	38
13	3	99	103
13	7	71	79
14	2	35	61
14	4	45	64
14	6	41	41
15	3	39	69

L = 12

H	K	FO	FC
0	0	343	338
0	2	37	40
0	4	38	44
0	8	219	215
0	12	283	288
1	1	86	91
1	5	101	102
1	11	121	120
2	0	38	37
2	2	47	50
2	4	40	36
2	8	38	43
3	1	36	37
3	5	81	79
3	7	68	76
4	2	133	132
4	6	435	441
4	12	33	34
5	1	68	71
5	3	42	33
5	5	129	128
5	7	57	61
5	11	36	35
6	2	39	33
6	6	57	64
6	8	50	61
7	1	43	46
7	3	33	32
7	11	42	31
8	0	477	470
8	8	173	172
9	1	82	84
9	5	91	95
10	0	77	82
10	2	32	32
10	4	32	36
11	3	38	40
11	7	73	73
12	2	82	94
12	6	346	341
13	5	88	84

L = 13

H	K	FO	FC
0	4	146	145
0	6	35	66
0	8	168	168
1	1	139	140
1	9	94	96
2	2	53	59
2	6	66	73
2	8	35	37
2	10	37	47
3	1	30	30
3	3	67	67
3	5	56	61
3	7	79	80
4	2	153	152
4	6	64	67
4	10	118	119
5	3	76	77
5	5	91	92
5	7	143	137
5	9	63	60
6	2	93	88
6	6	45	47
7	7	71	74
7	9	44	51
8	2	36	41
8	4	136	139
8	8	147	147
9	1	141	143
10	4	50	54
10	6	66	73
11	1	69	74
12	2	123	129

L = 14

H	K	FO	FC
0	0	172	171
0	2	98	98
0	4	399	383
0	6	69	70
0	8	247	243
1	3	69	71
1	5	112	112
1	7	58	62
2	0	72	77
2	2	45	44
3	1	107	104
3	9	67	68
4	0	48	60
4	2	361	352
4	6	99	98
4	8	139	131
5	1	109	110
5	9	69	68
6	6	70	77
6	8	82	76
7	3	49	56
7	5	101	99
8	0	116	118
8	2	58	63
8	4	338	328
9	3	53	57
9	5	97	101
10	0	126	122
10	2	57	66
11	1	69	74

L = 15

H	K	FO	FC
0	4	77	82
0	8	182	182
1	1	59	55
1	3	49	56
4	2	152	151
4	6	65	70
6	2	40	50
6	4	34	34
7	3	38	26
8	4	79	92
9	1	39	49

L = 16

H	K	FO	FC
0	0	324	313
0	4	64	63
1	1	69	71
1	3	85	82
1	5	84	81
2	0	90	86
3	3	85	87
3	5	58	60
4	0	76	73
4	2	77	83
5	3	139	135
6	0	66	69

APPENDIX F. CALCULATED AND OBSERVED STRUCTURE FACTOR AMPLITUDES FOR $Cs_{0.30(1)}Zr_6I_{14}Si$

L = 0

H	K	FO	FC
0	6	210	234
0	8	197	217
0	10	227	234
0	12	617	652
0	14	144	132
0	18	80	91
2	2	132	150
2	4	200	226
2	6	51	52
2	8	72	87
2	10	139	139
2	12	30	43
4	0	230	245
4	2	133	99
4	4	184	202
4	6	1012	1232
4	8	136	144
4	12	148	150
4	14	206	213
4	16	142	136
4	18	286	236
6	0	86	84
6	2	238	215
6	4	166	170
6	10	87	97
6	12	70	65
6	14	31	55
6	16	78	72
8	0	1213	1284
8	6	148	150
8	8	179	194
8	10	175	186
8	12	509	532
8	14	98	100
10	0	76	84
10	4	174	169
10	6	90	88
10	8	136	139
10	10	186	130
12	0	72	81
12	2	81	81
12	4	137	133
12	6	771	782
12	8	55	66
12	12	76	88
12	14	174	174
14	0	80	86
14	2	178	163
14	4	98	93
14	6	42	46
14	8	49	56
14	10	33	51
14	12	56	56
16	0	678	640
16	6	40	37
16	8	145	143
16	10	105	104
18	0	58	65
18	4	103	100
18	6	58	61
18	8	96	100
20	4	79	76

L = 1

H	K	FO	FC
0	2	63	61
0	4	309	340
0	6	69	81
0	8	393	421
0	10	48	62
0	12	280	284
0	16	90	62
1	1	189	197
1	3	52	64
1	5	59	64
1	7	76	81
1	11	71	78
1	13	104	111
2	2	63	61
2	4	43	53
2	6	59	68
2	8	45	56
2	10	43	38
3	1	48	40
3	3	68	71
3	7	163	175
3	13	46	44
3	17	64	70
4	2	458	446
4	4	82	85
4	6	163	175
4	10	147	158
4	12	58	67
4	14	278	279
4	18	158	160
5	1	117	119
5	3	109	110
5	7	178	183
5	13	53	67
5	17	66	78
6	2	115	118
6	4	34	32
6	6	33	31
6	12	64	71
7	1	97	104
7	3	43	49
7	11	57	63
7	13	97	90
8	4	275	268
8	6	47	52
8	8	337	341
8	12	173	176
8	16	58	57
9	1	124	130
9	3	46	48
9	5	79	81
9	7	90	90
9	9	60	71
9	11	52	62
9	13	79	85
10	4	92	89
10	6	55	60
10	8	44	39
10	10	39	43
11	7	90	94
11	15	48	62
12	2	315	285
12	6	92	98
12	10	123	126
12	12	43	31
12	14	193	197
13	1	76	83
13	3	85	80
13	7	108	106
13	13	48	47
14	2	103	96
14	4	56	52
15	5	59	50
15	9	50	55
16	4	188	174
16	8	206	203
17	5	54	52
17	7	48	46
18	4	58	65
18	6	45	44
19	1	65	73
20	2	156	158

L = 2

H	K	FO	FC
0	0	80	73
0	2	136	138
0	4	889	967
0	6	95	103
0	8	454	477
0	10	80	82
0	14	70	76
0	16	433	405
1	3	113	112
1	5	289	294
1	9	154	157
1	11	54	60
2	0	106	102
2	2	121	129
2	4	156	159
2	6	83	91
2	8	65	63
2	10	98	95
2	12	58	63
3	1	218	205
3	3	166	157
3	11	129	137
3	13	35	34
3	15	30	33
4	0	122	126
4	2	768	812
4	4	113	110
4	6	43	45
4	8	98	101
4	10	627	650
4	12	42	49
4	14	186	186
4	16	49	49
4	18	42	17
5	1	225	227
5	3	237	223
5	5	40	47
5	11	180	180
5	13	61	73
5	15	56	59
5	17	61	62
6	0	97	96
6	2	139	132
6	4	119	116
6	6	76	74
6	8	37	44
6	10	92	96
6	12	56	60
7	1	56	57
7	5	162	163
7	9	81	88
8	0	73	61
8	2	96	97
8	4	720	714
8	6	77	79
8	8	380	382
8	10	51	62
8	14	48	65
8	16	359	344
9	3	116	114
9	5	256	245
9	9	145	143
9	11	65	71
10	0	48	62
10	2	56	68
10	4	131	125
10	6	68	71
10	8	56	57
10	10	53	64
10	12	44	48
10	16	48	36
11	1	83	87
11	5	65	71
11	9	49	65
12	0	70	72
12	2	498	483
12	4	57	61
12	8	59	67
12	10	453	443
12	14	130	135
13	1	140	139
13	3	154	142
13	11	129	132
13	13	47	54
14	0	50	61
14	2	76	89
14	4	66	58
14	6	46	44
14	10	57	70
15	3	66	61
15	11	46	44
16	4	424	391
16	8	228	223
17	3	53	54
17	5	143	134
17	9	73	83
18	4	65	76
19	5	63	73
20	2	238	239

L = 3

H	K	FO	FC
0	2	50	50
0	4	648	718
0	6	173	181
0	8	571	597
0	10	169	167
0	12	138	135
0	16	71	72
0	18	103	94
1	1	92	92
1	3	51	52
1	5	72	72
1	9	47	65
1	15	94	86
2	2	70	76
2	4	71	76
2	6	58	61
2	8	53	58
3	1	43	49
3	3	46	44
3	9	65	77
3	11	60	58
4	2	829	822
4	4	138	135
4	6	119	122
4	10	284	282
4	12	174	165
4	14	283	265
4	16	104	103
5	1	65	61
5	5	64	65
5	7	58	68
5	9	111	105
6	2	136	129
6	12	56	71
7	5	68	64
7	9	57	55
7	15	56	52
7	17	61	43
8	4	528	519
8	6	139	132
8	8	484	476
8	10	125	121
8	12	131	125
9	1	98	95
9	3	53	58
9	5	39	39
9	9	42	41
9	15	79	80
10	4	114	113
10	6	77	77
10	8	46	55
10	10	50	59
11	11	62	64
12	2	486	475
12	4	47	45
12	6	97	97
12	10	184	179
12	12	103	103
12	14	200	195
13	7	61	59
13	9	76	76
14	2	101	103
14	10	43	54
14	12	84	76
15	5	50	41
16	4	266	258
16	6	56	64
16	8	262	272
18	4	63	82
18	6	46	56
20	2	191	220

L = 4

H	K	FO	FC
0	0	903	902
0	2	210	217
0	4	195	220
0	8	407	419
0	12	504	494
0	14	164	147
0	16	80	75
0	18	70	49
1	1	62	64
1	5	40	50
1	11	49	57
2	0	298	278
2	2	121	111
2	6	134	132
2	8	112	115
2	12	47	56
2	14	116	111
3	1	38	38
4	2	420	395
4	4	50	62
4	6	695	699
4	8	212	213
4	10	57	5
4	14	299	282
5	5	64	68
5	7	52	44
6	0	112	110
6	2	44	39
6	6	219	209
6	8	184	167
6	14	60	63
7	1	33	37
8	0	675	691
8	2	152	143
8	4	170	162
8	8	330	316
8	12	436	418
8	14	124	113
8	16	62	56
9	1	52	52
10	0	281	281
10	2	120	118
10	8	59	39
10	12	61	69
10	14	127	120
12	2	234	215
12	6	507	466
12	8	117	113
12	14	180	182
13	5	47	47
14	6	184	175
14	8	149	138
16	0	442	415
16	2	53	51
16	4	68	82
16	6	148	151
18	0	193	185
18	2	67	76
20	2	78	83

L = 5

H	K	FO	FC
0	2	58	60
0	4	484	532
0	6	65	77
0	8	466	452
0	10	98	99
0	12	141	138
0	16	87	87
1	1	265	257
1	3	95	98
1	5	102	104
1	9	176	163
1	13	90	102
1	15	77	89
1	17	71	58
3	3	208	197
3	5	63	78
3	7	170	170
3	11	113	106
3	13	53	49
3	15	82	78
4	2	614	588
4	4	89	95
4	6	112	108

4	10	267	256
4	12	69	74
4	14	239	223
4	16	63	60
5	1	44	45
5	3	193	182
5	5	131	126
5	7	236	245
5	9	51	51
5	11	89	88
5	15	88	85
7	1	108	106
7	3	115	113
7	5	61	69
7	7	73	75
7	9	129	124
7	15	44	49
8	2	36	32
8	4	419	404
8	6	60	57
8	8	386	366
8	10	72	73
8	12	122	123
8	16	63	72
9	1	235	240
9	3	47	60
9	5	79	80
9	9	141	130
9	13	121	118
9	15	91	84
11	3	142	135
11	11	94	90
11	13	64	62
12	2	387	362
12	6	78	82
12	10	167	167
12	14	173	165
13	3	113	108
13	5	92	94
13	7	199	189
15	3	91	94
15	7	84	81
15	9	51	64
16	4	230	214
16	8	205	214
17	1	148	141
17	9	54	66
19	3	82	77

L = 6

H	K	FO	FC
0	0	231	235
0	2	150	144
0	4	721	824
0	8	434	429
0	14	153	138
0	16	363	333
1	3	140	145
1	7	86	87
1	9	111	106
1	11	64	58
2	0	169	159
2	2	97	94
2	4	65	70
2	6	91	98
2	8	74	76
2	12	55	50
2	14	61	50
3	1	32	15
3	3	138	136
3	13	90	86
4	0	59	57
4	2	728	699
4	6	145	144
4	8	184	170
4	10	607	572
4	14	172	169
5	3	188	179
5	5	54	59
5	9	67	72
5	13	111	108
6	0	103	100
6	2	79	75
6	4	44	52
6	6	125	119
6	8	90	90
6	10	52	56
7	3	32	34
7	7	60	57
7	9	58	61
8	0	183	177
8	2	109	103
8	4	664	651
8	8	368	343
8	14	111	113
9	3	137	134
9	7	69	80
9	9	97	96
9	11	64	69
9	13	46	50
10	0	151	145
10	2	72	74
10	4	57	60
10	12	55	50
12	0	57	54
12	2	477	444
12	6	84	91
12	8	110	105
12	10	424	404
13	3	126	117
13	5	55	45
13	9	51	51
14	2	39	44
14	6	91	93
14	8	66	70
16	0	94	94
16	2	44	42
16	4	393	372
16	8	188	191
17	3	68	67
18	0	91	93

L = 7

H	K	FO	FC
0	4	145	147
0	6	103	110
0	8	286	283
0	10	81	90
0	12	170	158
0	14	49	49
1	1	108	103
1	3	79	77
1	9	41	50
1	13	102	97
2	2	94	93
2	4	72	74
2	6	80	82
2	8	87	92
2	10	48	40
2	12	60	59
3	3	55	59
3	7	119	118
4	2	245	227
4	4	72	77
4	6	107	110
4	10	82	79
4	12	107	104
4	14	238	234
5	3	89	91
5	7	122	118
6	2	159	155
6	8	44	54
6	12	96	94
6	16	70	57
7	1	68	73
7	3	51	49
7	13	88	86
8	4	140	139
8	6	76	80
8	8	251	238
8	10	60	63
8	12	120	122
9	1	80	84
9	3	73	74
9	9	54	63
9	13	77	73
10	4	119	116
10	6	76	88
10	8	94	94
10	10	74	72
11	7	66	77
12	2	187	175
12	6	67	59
12	10	70	77
12	12	67	57
13	3	80	76
13	7	78	76
14	2	138	134
14	4	46	48
15	5	49	49
16	4	103	112
16	8	148	152
17	3	52	53
18	4	85	88

L = 8

H	K	FO	FC
0	0	1093	1043
0	6	158	172
0	8	131	142
0	10	115	114
0	12	493	464
0	14	76	78
1	1	133	140
1	3	97	98
1	5	129	134
1	9	175	169
1	11	53	57
2	0	56	55
2	2	77	77
2	4	100	99
2	6	88	76
2	8	71	77
2	10	66	63
2	12	60	43
3	1	88	86
3	3	154	149
3	5	128	129
3	7	72	81
3	11	68	69
3	13	66	49
3	15	88	91
4	0	199	183
4	2	80	80
4	4	78	73
4	6	777	790
4	8	83	89
4	12	107	105
4	14	142	144
5	1	106	102
5	3	195	183
5	5	108	110
5	7	73	80
5	11	97	86
5	13	54	52
5	15	105	102
6	0	108	105
6	2	129	126
6	4	72	75
6	12	46	53
6	14	52	61
7	1	134	128
7	5	78	86
7	9	116	117
7	11	60	66
8	0	857	819
8	6	118	122
8	8	125	130
8	10	85	92
8	12	417	387
8	14	59	59
9	1	111	107
9	3	99	99
9	5	122	123
9	9	157	157
10	4	81	87
10	6	88	87
10	8	112	110
10	10	54	66
11	1	42	43
11	3	58	66
11	5	109	111
12	0	84	84
12	2	63	69
12	4	44	55
12	6	520	523
13	1	73	77
13	3	141	135
13	5	72	77
13	11	63	67
14	0	92	91
14	2	111	110
15	1	93	87
16	0	450	449
16	8	87	101
17	1	69	67
17	3	68	58
17	5	64	77

L = 9

H	K	FO	FC
0	4	279	278
0	8	293	300
0	12	170	162
1	1	83	83
1	7	81	89
1	11	62	63
1	15	62	60
3	1	42	51
3	7	79	87
4	2	354	337
4	6	121	126
4	10	146	143
4	14	189	176
5	1	115	106
5	7	82	95
5	9	68	72
5	13	76	76
7	9	42	43
8	4	235	234
8	8	255	251
8	12	135	135
9	1	70	65
9	5	63	63
9	7	93	99
12	2	244	237
12	6	79	85
12	10	103	107
13	1	83	82
16	4	142	149

L = 10

H	K	FO	FC
0	0	107	98
0	4	448	441
0	8	237	252
0	10	109	110
1	5	228	228
1	7	97	89
1	9	57	65
2	0	44	39
2	2	94	89
2	4	161	159
2	10	125	119
2	14	40	28
3	1	182	171
3	11	146	142
4	2	394	371
4	4	96	97
4	6	50	62
4	10	382	366
4	14	115	116
5	1	211	197
5	3	78	83
5	11	182	173
6	2	120	120
6	4	123	123
6	10	104	113
7	5	148	148
7	7	54	72
8	0	67	69
8	4	370	365
8	8	204	218
8	10	80	89
9	5	213	212
9	7	72	81
9	9	65	70
10	0	46	59
10	2	39	38
10	4	141	142
10	8	56	49
10	10	84	93
11	1	94	94
11	11	53	69
12	2	271	265
12	4	55	68
12	10	239	260
13	1	145	147
13	3	66	68
14	2	78	102
14	4	61	71
16	4	207	221

L = 11

H	K	FO	FC
0	2	80	84
0	4	395	367
0	6	93	96
0	8	338	333
0	10	128	121
1	1	71	75
1	3	114	109
1	7	47	43
1	13	84	87
3	1	45	46
3	3	74	75
3	7	102	106
3	9	72	66
4	2	435	417
4	4	119	118
4	10	184	174
4	12	108	101
5	3	94	92
5	7	84	95
5	9	69	80
6	2	44	41
7	1	70	73
7	3	73	73
8	2	56	54
8	4	300	292
8	6	65	74
8	8	274	278
8	10	77	91
9	3	108	105
10	4	53	61
11	7	82	89
12	2	281	277
12	4	50	56
13	3	72	79

L = 12

H	K	FO	FC
0	0	472	433
0	2	56	58
0	4	71	81
0	8	207	213
0	12	276	269
1	1	87	86
1	5	61	72
1	11	91	91
2	0	139	134
2	6	71	80
3	5	72	77
3	7	52	65
4	2	180	172
4	6	371	368
4	8	71	70
5	1	63	53
5	5	104	102
5	7	51	63
6	0	67	63
6	6	117	120

[illegible]

APPENDIX G. CALCULATED AND OBSERVED STRUCTURE FACTOR AMPLITUDES FOR $Cs_{0.66(1)}Zr_6I_{14}Al$

L = 0

H	K	FO	FC
0	2	83	79
0	6	220	229
0	8	280	279
0	10	227	229
0	12	609	597
0	14	160	154
2	0	101	85
2	2	93	98
2	4	191	195
2	6	67	59
2	8	83	88
2	10	120	118
4	0	149	202
4	2	148	153
4	4	194	203
4	6	1088	1138
4	8	201	205
4	12	171	165
4	14	259	252
4	16	114	108
6	2	194	208
6	4	144	152
6	14	107	91
8	0	1195	1190
8	6	126	134
8	8	263	268
8	10	164	165
8	12	494	491
8	14	122	105
10	0	129	136
10	4	140	146
10	6	110	113
10	8	140	151
10	10	144	135
12	2	143	141
12	4	137	132
12	6	701	700
12	12	117	106
14	0	125	101
14	2	168	162
14	4	80	88
16	0	385	391
16	8	216	214
18	4	101	89

L = 1

H	K	FO	FC
0	4	354	346
0	6	91	86
0	8	463	462
0	12	273	275
1	1	197	175
1	3	96	101
1	5	96	98
1	7	125	129
1	11	124	139
1	13	82	93
2	2	62	57
2	6	87	99
2	10	72	79
3	1	69	70
3	3	98	96
3	5	67	69
3	7	156	163
3	13	97	98
4	2	480	499
4	4	64	81
4	6	191	198
4	10	163	167
4	14	316	322
5	1	160	164
5	3	139	143
5	7	176	187
5	13	110	109
6	2	117	186
6	4	66	67
6	12	84	92
7	3	79	96
7	11	102	105
8	4	282	290
8	8	357	373
8	12	208	207
9	1	114	117
9	3	63	66
9	5	97	100
9	7	109	117
9	11	105	108
10	4	79	85
10	6	106	100
10	10	102	95
11	1	63	63
12	2	304	310
12	6	90	97
12	10	140	144
13	1	81	85
13	3	97	88
13	7	96	91
14	2	95	93
15	3	73	57
15	9	92	100
16	4	202	205
16	8	225	222

L = 2

H	K	FO	FC
0	2	106	98
0	4	1019	971
0	6	76	79
0	8	470	470
0	14	78	82
0	16	449	452
1	3	96	95
1	5	293	289
1	9	139	142
1	11	103	98
2	0	61	56
2	2	88	86
2	4	143	148
2	6	83	85
2	10	112	101
2	12	81	91
3	1	190	181
3	3	145	146
3	11	101	95
3	13	79	76
4	0	79	96
4	2	800	810
4	4	79	88
4	8	88	83
4	10	662	690
4	14	151	164
5	1	213	213
5	3	230	235
5	5	78	73
5	11	146	156
5	13	107	113
6	0	75	72
6	2	105	104
6	4	112	116
6	6	65	63
6	10	86	85
7	1	68	70
7	5	112	120
7	9	72	69
8	2	81	78
8	4	699	730
8	8	370	384
9	3	83	97
9	5	224	236
9	9	129	126
9	11	111	100
10	4	111	116
10	6	76	75
10	10	76	83
11	5	107	103
12	2	479	496
12	10	462	470
13	1	120	119
13	3	124	124
13	11	111	98
14	2	77	77
15	1	82	71
15	3	102	102
16	4	392	405
16	8	241	232
17	5	108	100

L = 3

H	K	FO	FC
0	4	731	696
0	6	244	237
0	8	389	374
0	10	210	212
0	12	136	141
1	1	130	127
1	3	105	103
1	5	60	60
1	9	63	58
1	15	134	118
2	2	74	72
2	4	83	84
2	6	75	74
3	5	67	74
3	9	119	120
4	2	809	814
4	4	159	161
4	6	145	148
4	10	238	243
4	12	179	182
4	14	235	233
4	16	94	112
5	5	88	94
5	7	67	69
5	9	141	147
6	2	157	159
6	4	60	56
7	7	72	55
8	4	469	480
8	6	154	156
8	8	443	459
8	10	144	145
8	12	136	146
9	1	118	110
9	3	87	86
10	4	133	140
10	6	95	102
10	10	75	80
12	2	439	433
12	6	143	136
12	10	133	126
12	12	91	88
13	9	94	91
14	2	125	118
16	4	204	209
16	8	273	264
18	4	79	81

L = 4

H	K	FO	FC
0	0	975	933
0	2	209	199
0	4	228	219
0	8	483	453
0	12	557	552
0	14	105	110
0	16	139	134
1	1	58	57
1	5	88	86
1	11	81	80
2	0	257	248
2	2	111	111
2	6	80	88
2	8	131	130
2	14	131	136
3	1	50	57
3	7	72	59
4	2	420	416
4	6	739	736
4	8	197	194
4	14	313	321
5	1	60	64
5	5	77	75
6	0	55	58
6	6	173	175
6	8	212	216
6	14	77	67
7	3	55	42
8	0	738	749
8	2	121	114
8	4	156	161
8	8	312	325
8	12	455	467
8	14	83	72
9	5	69	69
10	0	270	271
10	2	132	134
11	7	69	51
12	2	212	205
12	6	542	548
14	6	147	148
14	8	169	172
14	10	84	42
16	0	499	478
16	4	79	82
18	0	170	163
18	2	91	79

L = 5

H	K	FO	FC
0	4	523	507
0	6	73	72
0	8	477	456
0	10	108	104
0	12	175	180
0	16	92	73
1	1	299	292
1	5	101	100
1	9	153	156
1	15	167	152
3	3	166	170
3	5	88	75
3	7	155	156
3	9	88	96
3	11	104	109
4	2	572	567
4	4	88	88
4	6	138	135
4	10	235	240
4	14	237	238
5	3	160	167
5	5	136	125
5	7	232	232
5	9	148	143
5	11	84	75
5	15	80	95
6	6	38	48
7	1	92	94
7	3	80	78
7	7	139	141
7	9	96	87
8	4	376	382
8	8	359	370
8	12	154	160
9	1	258	257
9	5	73	75
9	9	116	120
9	13	78	77
11	1	117	113
11	3	104	102
11	11	117	111
12	2	343	348
12	6	92	103
12	10	157	154
13	3	91	88
13	5	83	80
13	7	169	173
13	9	80	79
15	3	81	81
15	7	134	138
16	4	202	199
17	1	110	120

L = 6

H	K	FO	FC
0	0	266	265
0	2	163	156
0	4	900	880
0	8	444	438
0	14	169	165
1	3	151	147
1	7	92	102
1	9	101	103
1	11	76	78
2	0	182	172
2	2	77	79
2	6	98	82
2	8	62	65
3	3	130	136
3	13	89	86
4	2	755	739
4	6	136	133
4	8	217	219
4	10	596	599
4	14	166	160
5	3	191	192
5	5	74	76
5	9	64	70
5	13	123	123
6	0	72	72
6	6	126	129
6	8	112	115
7	7	63	56
8	0	185	180
8	2	103	102
8	4	694	702
8	8	337	335
9	3	119	130
9	7	84	93
9	11	80	80
10	0	180	180
10	2	81	85
11	5	64	55
11	11	84	68
12	0	75	70
12	2	477	456
12	8	105	120
12	10	427	440
13	3	102	107
14	6	91	106
14	8	96	96
16	4	401	405

L = 7

H	K	FO	FC
0	4	160	160
0	6	134	129
0	8	368	357
0	10	104	98
0	12	223	221
1	3	106	92
1	7	59	60
1	13	108	98
2	2	79	84
2	4	62	60
2	6	113	116
2	8	62	65
2	10	92	87
2	12	74	51
3	7	72	75
3	9	91	92
4	2	261	259
4	4	83	93
4	6	138	137
4	10	111	96
4	12	107	92
4	14	309	312
5	1	58	55
5	3	83	76
5	7	63	68
5	9	80	87
6	2	164	169
6	4	66	64
6	12	118	120
7	11	68	47
7	13	100	95
8	4	172	175
8	6	76	77
8	8	297	299
8	12	149	156
9	3	79	80
10	4	118	122

H	K	FO	FC
10	6	121	131
10	10	110	115
12	2	224	222
12	10	117	108
14	2	138	135
16	4	163	162

L = 8

H	K	FO	FC
0	0	1090	1050
0	6	169	169
0	8	205	194
0	10	124	113
0	12	486	479
0	14	84	88
1	1	145	146
1	3	82	88
1	5	159	158
1	9	177	174
2	2	58	59
2	4	75	73
2	6	78	76
2	8	97	94
3	1	83	86
3	3	154	153
3	5	130	130
3	7	80	77
3	13	76	84
4	0	172	170
4	2	128	128
4	4	68	71
4	6	813	807
4	8	108	101
4	12	109	112
4	14	187	188
5	1	109	108
5	3	212	212
5	5	85	86
5	7	93	86
5	11	91	83
5	13	104	104
6	0	113	117
6	2	123	124
7	1	143	149
7	5	71	75
7	9	98	110
8	0	834	827
8	6	120	115
8	8	185	185
8	10	83	83
8	12	396	401
9	1	119	108
9	3	89	96
9	5	136	140
9	9	130	160
10	4	66	69
10	6	95	98
10	8	133	130
11	5	142	142
11	7	74	40
11	9	72	47
12	2	108	113
12	6	532	531
13	1	74	71
13	3	145	141
13	5	73	71
14	0	90	101
14	2	102	110
15	1	112	107
16	0	466	446

L = 9

H	K	FO	FC
0	4	346	341
0	8	361	343
0	10	88	84
0	12	195	194
1	1	88	88
1	5	83	83
1	7	142	141
1	11	91	105
3	1	93	85
3	7	77	86
3	13	106	98
4	2	424	419
4	6	177	161
4	10	150	150
5	1	162	155
5	7	112	111
5	9	82	82
5	13	121	117
7	9	88	88
7	11	81	73
8	4	274	277
8	8	288	287
9	1	67	69
9	5	82	84
9	7	143	133
9	11	83	90
12	2	293	286
12	6	116	117
13	1	98	92

L = 10

H	K	FO	FC
0	0	136	140
0	4	309	313
0	8	869	867
0	10	122	125
1	5	195	199
1	7	85	78
2	0	65	64
2	4	165	166
2	10	134	127
2	12	72	73
3	1	139	140
3	11	130	132
4	2	420	414
4	4	101	108
4	6	73	64
4	10	438	447
5	1	171	166
5	5	66	56
5	11	159	164
6	2	120	124
6	4	141	137
6	8	70	68
6	10	76	88
7	5	113	116
8	0	79	80
8	4	415	425
8	8	243	249
8	10	101	91
9	5	182	183
9	7	81	72
10	0	89	94
10	4	154	144
10	6	71	58
11	1	70	69
12	2	322	317
13	1	129	121
14	2	111	110

L = 11

H	K	FO	FC
0	2	86	90
0	4	399	394
0	6	131	127
0	8	364	364
0	10	141	144
1	1	94	87
1	3	129	141
1	11	95	88
3	3	114	115
3	7	118	129
4	2	450	456
4	4	135	134
4	10	163	163
5	3	137	135
5	7	135	130
7	3	106	114
8	4	291	296
8	8	301	305
9	1	72	75
9	3	122	123
10	4	74	86
11	3	76	89
12	2	292	287

L = 12

H	K	FO	FC
0	0	378	382
0	4	70	57
0	8	261	298
1	1	105	107
1	5	113	108
2	0	91	94
2	6	67	63
3	5	94	94
3	7	86	92
4	2	177	181
4	6	454	477
5	1	74	79
5	5	133	140
5	7	75	76
6	6	104	97
6	8	71	74
8	0	507	501
9	1	88	95
9	5	101	99
10	0	118	115

L = 13

H	K	FO	FC
0	4	174	175
0	8	195	196
1	1	149	153
1	9	132	133
2	2	88	84
2	6	86	81
3	3	105	108
3	7	99	94
4	2	178	179
4	6	100	73
5	3	108	110
5	5	99	98
5	7	155	161
6	2	99	103
6	6	81	58
8	2	74	62
8	4	152	162
9	1	166	162

L = 14

H	K	FO	FC
0	0	180	187
0	2	111	112
0	4	421	448
0	6	77	78
1	3	77	101
1	5	128	129
1	7	73	77
3	1	125	122
4	2	379	400
4	6	115	110
5	1	128	127
7	3	76	79